Norwegian University
of Life Sciences

Master's Thesis 2020 30 ECTS
Faculty of Science and Technology

The Galvanostatic Intermittent Titration Technique for Silicon-Based Li-ion Battery Anodes: Theory and Experimental Validation

Vilde Stueland Nysted
Environmental Physics and Renewable Energy

Acknowledgements

With this master's thesis I complete my Master of Science in Environmental Physics and Renewable Energy at NMBU.

I had a summer job at the Institute for Energy Technology (IFE) in 2018 and was lucky enough to be invited back to write my master's thesis in collaboration with IFE. I am very grateful for this opportunity, and I have learned a lot about batteries through this process.

I want to give a huge thank you to Asbjørn Ulvestad, my supervisor at IFE, for much support, great advice, answering my questions and giving feedback on my writing. Another big thank you to my supervisor at NMBU, Espen Olsen, for encouragement and feedback. Additionally, I want to thank Jan Petter Mæhlen at IFE for help with the use of the Python library Cellpy, general programming advice and help with the interpretation of my results. I also want to thank Marius Nagell, lab engineer at IFE, for lab training and allowing me access to the battery labs.

Lastly I want to thank my friends and family for all the support and encouragement I have received during my studies and while writing this thesis. An especially big thank you goes to my friends Inger, for a thorough read through, and Maylinn, for many motivation quotes.

Vilde Stueland Nysted

Ås, 02.06.2020

Sammendrag

Litium-ion-batterier er det foretrukne batteriet for en rekke anvendelser, og markedet for litium-ion-batterier er stadig i vekst. Gode kinetiske egenskaper er viktig for mange anvendelser, slik som elektriske kjøretøy, lagring i kraftnett og bærbar elektronikk. Galvanostatisk intermitterende titrering (GITT) er en teknikk som brukes til å beregne diffusjonskonstanter for litium i elektrodematerialer. Tre eksperimentparametre, pulstid, pausetid og strømrate, må bestemmes for å gjennomføre et GITT eksperiment. I denne oppgaven undersøkes innflytelsen av disse parameterne på de beregnede diffusjonskoeffisientene.

Innflytelsen av eksperimentparameterne ble studert i et hovedeksperiment hvor en serie GITT opp-/utladninssykler ble gjennomført, med en pulstid som ble doblet hver iterasjon. Eksperimentet ble gjennomført med tre strømrater, C/10, C/5 og C/2, på forskjellige batterier. Cellene brukt i eksperimentet var halvceller med tynnfilmer av silisium som arbeidselektrode. Tynnfilmene hadde tykkelsene 60 nm og 80 nm. Totalt ble 18 celler brukt, 9 av hver tykkelse. Et tilleggseksperiment ble gjennomført på to av cellene, en av hver tykkelse, for å teste innflytelsen av en lengre pausetid.

Dataene fra GITT eksperimentene ble analysert ved hjelp av programmeringsspråket Python. Diffusjonskoeffisientene beregnet gjennom GITT eksperimentene varierte signifikant med valg av parameterverdier. Den største endringen i resultat ble sett i det andre eksperimentet med lenger pausetid. En tilstrekkelig lang pausetid ble derfor ansett som viktig for å oppnå gode resultater ved bruk av GITT.

Gyldigheten til to forenklinger som ble gjort under utledningen av GITT ble også undersøkt for ulike pulstider. Forenklingene er gyldige for ulike pulstider avhengig av strømraten som blir brukt. Ved en lavere strømrate kan lengre pulstider benyttes. For cellene som ble brukt i denne oppgaven ble en pulstid på 8 - 64 s ansett som et godt valg, ettersom forenklingene er gyldige i dette området og for mye støy ved lave pulstider unngås.

Abstract

Lithium ion batteries (LIBs) are the battery of choice for a number of applications, and the LIB market is growing rapidly. Good kinetic abilities is important for many applications, such as electric vehicles, grid storage and portable electronics. The galvanostatic intermittent titration technique (GITT), is a method used to determine the diffusion constant of Li in electrode materials. Three experimental parameters, pulse time, current rate and relaxation time, need to be chosen for GITT experiments. In this study, the influence of these parameters on the calculated diffusion coefficients are explored.

The effect of these parameters were studied in a main experiment where a series of GITT charge/discharge cycles were conducted with the pulse length being doubled in each iteration. The experiment was run with three current rates, C/10, C/5 and C/2, on different batteries. The cells used in the experiment were half cells with silicon thin films as working electrodes. The thin films had a thickness of 60 nm and 80 nm. A total of 18 cells where used, 9 with each thin film thickness. A secondary experiment was performed on two of the cells, one of each thickness, to test the influence of a longer relaxation time.

The data resulting from the GITT experiments was analysed using the programming language Python. The diffusion coefficients determined by GITT experiments were found to vary significantly with choice of parameter values. The largest change in results was observed in the second experiment with longer relaxation time. A sufficiently long relaxation time was therefore deemed important to achieve good results with GITT.

The validity of two simplifications made during in the derivation of the GITT method were tested for different pulse lengths. The pulse lengths where these simplifications are valid depend on the current rate utilized. A lower current rate allows for longer pulse times. For the cells used in this thesis a pulse length between 8 - 64 s at a current rate of C/10 were deemed a good choice, as the simplifications are valid in this range and too much noise at low pulse lengths is avoided.

Contents

List of Figures

List of Tables

Abbreviations

EV electric vehicle

GITT galvanostatic intermittent titration technique

IEA The International Energy Agency

LIB lithium-ion battery

LTO lithium titanium oxide

SEI Solid Electrolyte Interface

SOC state of charge

Chapter 1

Introduction

1.1 Background

The rising levels of CO_2 in the atmosphere since the industrial revolution have led to a warming of the climate [1]. The changing climate has negative consequences such as rising ocean levels, ocean acidification and an increase in extreme weather conditions such as droughts, floods, heat waves and wildfires. To limit the impact of climate change the Paris Agreement was adopted at the climate conference in Paris in 2015 [2]. The goal of the agreement is to keep the global temperature increase well below 2 °C and preferably limit it to 1.5°C. To reach this target a drastic decrease in global CO_2 emissions is necessary.

Batteries play an important role in several decarbonizing efforts, from grid storage to electrification of the transport sector [3]. Widespread integration of renewable energy technologies, e.g. wind and solar power, is an important step towards decarbonisation of the power generation [4]. Due to the intermittent nature of these renewables, widespread integration into the power grid benefits greatly from energy storage. The energy storage should handle both short drops or spikes in power lasting seconds or minutes and longer fluctuations in power production of hours and days. To achieve this an energy storage technology with high power and energy and a short response time is needed [5]. According to The International Energy Agency (IEA) the transport sector was responsible for 24% of the global CO_2 emissions in 2016 [6]. Electrification of the transport sector is thus another important step to decrease CO_2 emissions.

The high energy and power density of lithium-ion batteries (LIBs) make them the battery of choice for EVs [7] and grid storage [8]. The sale of electric vehicles has increased significantly in recent years and in 2018 the number of electric cars globally was above 5.1 million. The use of LIBs for grid storage has also increased in recent years [8] and can be expected to increase further in the coming years [3]. Though not relevant for the decarbonizing efforts, LIBs are the most used battery for portable electronics, and this is a large part of the LIB market. Figure 1.1 shows the development of the Li-ion battery market from 2010 - 2015 and expected market developments towards 2030.

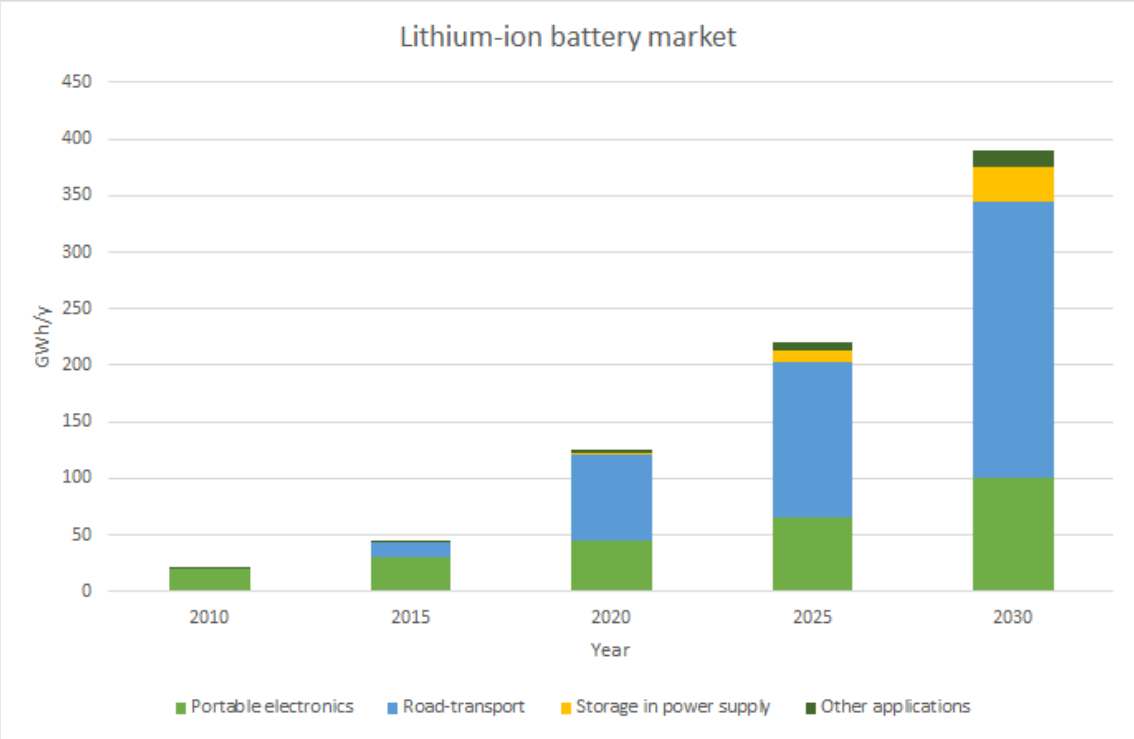

Figure 1.1: Evolution of LIB market development in recent years and the expected market development from 2020 until 2030. The data is from [3]

1.2 Aim of This Work

Good kinetic properties are important for all the mentioned LIB applications. To further increase the popularity of electric vehicles, improvements should be made to the charging time [9, 10]. Faster charging would make long trips more feasible and lead to more flexibility [11]. For grid storage fast kinetics is important for handling quick changes in power output [5]. With regard to portable electronics good kinetic properties are important to meet the consumers expectations of short recharge times [3].

In 1977 Weppner and Huggins [12] introduced the galvanostatic intermittent titration technique (GITT). The method obtains kinetic properties of solid mixed-conducting electrodes [12], mainly focused on determining the diffusion constant of Li in the electrode. Since diffusion of Li in the electrode material often is the rate-limiting factor [7], GITT is a useful tool.

The GITT test procedure consists of applying a series of short current pulses to a half cell and letting the cell relax between each pulse. Some experimental parameters, i.e. the pulse time, the pause time and the current rate, must be chosen when performing GITT experiments. The main parameters are the pulse time, the pause time and the current rate. The parameters used in literature vary widely, e.g. pulse lengths ranging from seconds to 1 h are observed [12–21]. The main tasks in this work are therefore to implement the GITT technique as a Python script and analyse experimental data with the goal of determining the impact of chosen experimental parameters on the result. This will be done through experiments with different pulse times, current rates and pause times on half cells with a silicon working electrode.

Chapter 2

Theory

2.1 A Brief History of Batteries

A battery is a device that can store chemical energy and convert it to electrical energy through an electrochemical reaction [22, 23]. Batteries can be divided into two main categories; primary and secondary batteries. Primary batteries can only be discharged once and are then discarded. Secondary batteries can be recharged by sending a current through the battery so that the chemicals are restored to their original condition [22, 24].

The first battery was described in 1800 by Alessandro Volta, Professor of Natural Philosophy at the University of Pavia in Italy, in a study published by the Royal Society of London. The experiment he did consisted of stacking metal discs of two different types, where the two different metals were separated by a cloth saturated with an alkaline solution. When the ends of the pile were connected by a conductor, a current was produced. This first primary battery is called the voltaic pile [22, 23].

One of the earliest primary batteries in common use was the Leclanché cell, invented by the French chemist Georges Leclanché in 1866. It consisted of a zinc rod as the negative electrode and a carbon rod surrounded by manganese dioxide (MnO_2) as the positive electrode. The electrolyte was a solution of ammonium chloride (NH_4Cl) and zinc chloride ($ZnCl_2$). The cell delivers a voltage of 1.5 V [22]. Since this early battery there have been many new developments in the battery world. In the 1970s a big improvement in the battery voltage was made with the introduction of lithium primary batteries with a potential of 3 V [23].

The first secondary battery was the lead-acid battery. It was invented by the French physicist Gaston Planté in 1859. The anode consists of lead peroxide (PbO_2) and the cathode of lead. The electrolyte is a weak sulfuric acid. The lead-acid battery has a voltage of 2 V and is still commonly used as car batteries [23, 25].

The first secondary lithium ion battery was commercialized by Sony in 1991. It had a specific energy of 80 Wh/kg and an energy density of 200 Wh/l [26]. Since then there have been many improvements made and the energy density has surpassed other rechargeable batteries like lead-acid, nickel-cadmium and nickel metal hydride, as illustrated in Figure 2.1

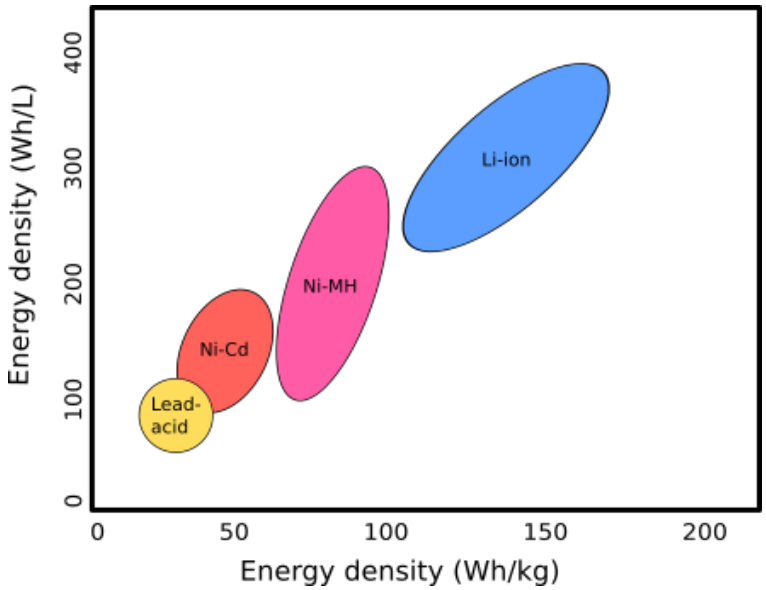

Figure 2.1: Energy density and specific energy for different types of rechargeable batteries. Ni-Cd and Ni-MH correspond to nickel-cadmium and nickel metal hydride batteries respectively. Illustration adapted from [27]

2.2 Electrochemical Cells

2.2.1 Difference Between Cell and Battery

An electrochemical cell is the basic electrochemical unit able to convert chemical energy to electrical energy. A battery is one or more cells connected either in series or parallel to reach a desired operating voltage or current for the intended application. The term battery is usually the one used for products sold to a user, while the term cell is used to describe the chemistry and inner workings of the battery [24].

2.2.2 Components in an Electrochemical Cell

An electrochemical cell consists of three main parts (see Figure 2.2):

1. *The negative electrode* - During discharge the negative electrode is oxidized, which means that it gives up electrons to the external circuit. The negative electrode is then called the anode. The negative electrode should be a good reducing agent, and often metals like zinc or lithium are chosen [24].

2. *The positive electrode* - During discharge the positive electrode is reduced, which means that it takes up electrons from the external circuit. The positive electrode is then called the cathode. The positive electrode should be a good oxidizing agent and metallic oxides are often used [24].

3. *The electrolyte* surrounds the negative and the positive electrode. It is an ionic conductor and provides a way for ions to be transferred between the anode and the cathode. The electrolyte should not be electronically conductive to avoid an internal short-circuit of the cell. Other important properties include low reactivity with electrode materials, good safety, low cost, a wide electro-

chemical window and stability over a broad range of operating temperatures [22, 24].

In addition to these three components, the cell needs a separator. It physically separates the anode and the cathode to prevent short-circuiting. It is usually porous so that the electrolyte can fill the pores and ions can be transported through the pores. Lastly the cell needs some form of housing or container to keep everything in place and prevent leaks. The housing can have different shapes depending on the intended use of the cell [22, 24].

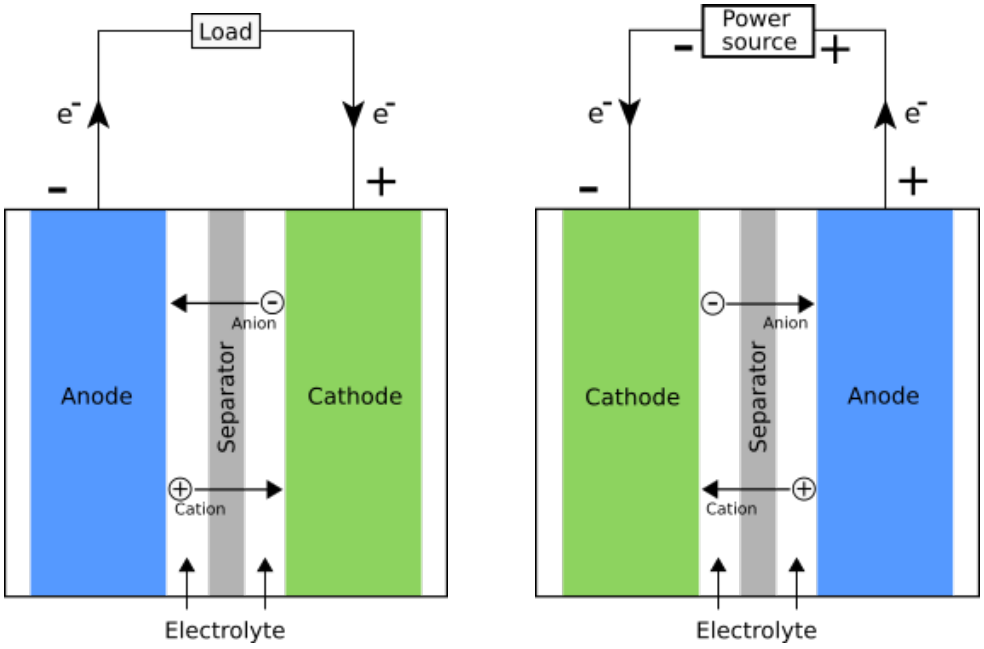

(a) Discharge *(b) Charge*

Figure 2.2: Working principle of an electrolytic cell during discharge and charge. Illustration adapted from [22, 23]

2.2.3 Operation of an Electrochemical Cell

When the cell is discharged there is an oxidation happening at the anode. During oxidation the anode releases electrons. These electrons flow from the anode to the cathode through an external circuit with a load where they do useful work. At the cathode the electrons are taken up and a reduction takes place. A flow of ions through the electrolyte completes the electric circuit. Positive ions (cations) flow from the anode to the cathode and negative ions (anions) from the cathode to the anode, as illustrated in Figure 2.2. The difference in electrode potential between the electrodes works as a driving force, moving the electrons through the external circuit [22, 24].

The oxidation reaction that takes place at the anode can be described as

$$M \longrightarrow M^{n+} + ne^{-}, \tag{2.1}$$

where M an oxidizable species, typically a metal, and e^{-} is an electron.

The reduction reaction that takes place at the cathode can be described as

$$X + ne^- \longrightarrow X^{n-}, \tag{2.2}$$

where X is an oxidizing agent (a material that oxidizes another material and is itself reduced) and e^- is an electron.

When charging a cell the flow of electrons is reversed. Now the oxidation happens at the positive electrode and the reduction happens at the negative electrode. Thus the negative electrode is the cathode and the positive electrode is the anode [22, 24]. Discharge is considered the standard mode of operation for a battery and the anode and cathode are generally named thereafter [22].

2.2.4 Full Cell vs Half Cell

Both full cells and half cells can be used in electrochemical experiments, depending on what the purpose of the experiment is [23]. A full cell is a complete battery with relevant electrochemical reactions at both the anode and the cathode. It can be used to measure performance of the whole battery, or with the addition of a reference electrode it can make individual measurements at the cathode and anode [23]. A half cell consists of the material undergoing testing as the working electrode and uses the counter electrode as a reference electrode. Half cells are useful for examining one specific electrode material since the counter electrode typically has a constant electrode potential and the change in cell potential during cycling is caused by the working electrode [28].

The cells used in this thesis are half cells with a silicon based working electrode and lithium as the counter electrode. Any electrode material that can be used in a lithium-ion battery (LIB) has a higher electrode potential than lithium. In the half cell, the working electrode is therefore the cathode and the lithium counter electrode the anode. This is regardless of whether the electrode material is intended to function as an anode or a cathode in a full lithium ion cell. Discharge of the half cell thus means lithiation of the working electrode and charge of the half cell means delithiation of the working electrode [28].

2.2.5 Battery Characteristics

Voltage

The voltage of an electrochemical cell is the potential difference between the electrodes [22]. The standard cell voltage depends on the type of electrode material used in the cell and can be calculated from the standard electrode potentials [24]. The open-circuit voltage is the potential between the electrodes when no current is going through the cell [22].

The actual working voltage when a current flows through the cell is lower than the open-circuit voltage. This is due to polarization losses at the electrodes and ohmic losses in the cell components [22]. The polarization losses have two components:

1. The activation polarization comes from kinetic limitations related to the electrochemical reactions happening at the electrode surface [22, 29].

2. The concentration polarization comes from differences in reactant and product concentrations at the electrode surface or in the bulk material. This can be caused by slow diffusion in the bulk material or mass transfer in the electrolyte or across the electrode-electrolyte interface [22, 29].

The voltage drop due to ohmic losses is often called the IR drop. The internal resistance in the cell is the sum of the resistance in all the components in the cell. The voltage drop caused by the internal resistance is proportional to the current through the cell, according to Ohm's law [29]. Figure 2.3 illustrates how the voltage drop increases with increasing current.

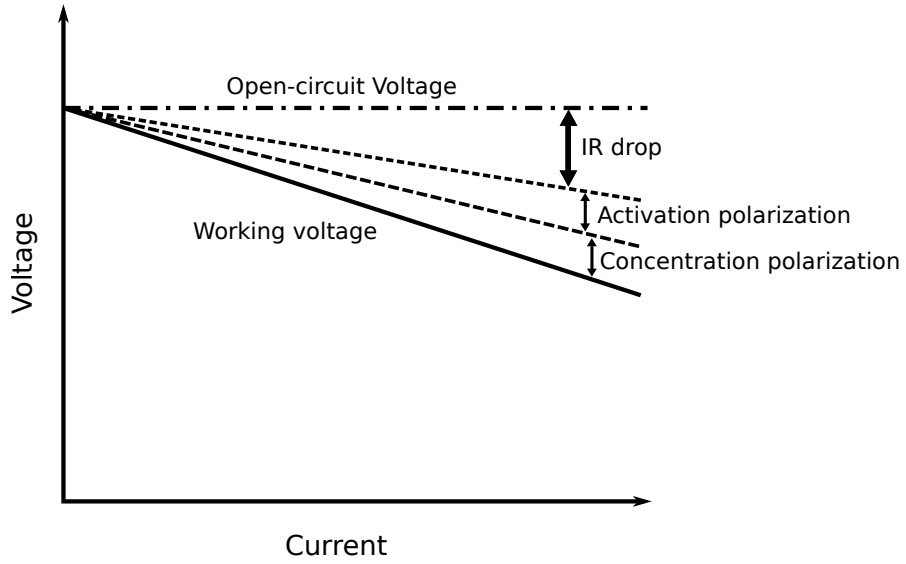

Figure 2.3: Illustration of voltage loss due to polarization and IR drop. The illustration was adapted from [29].

Capacity

The formula for calculating the theoretical specific capacity of the active materials in a cell is given by

$$Cap = \frac{nF}{M} \tag{2.3}$$

where n is the number of moles of electrons being transferred for each mole of reactant, F is the Faraday constant and M is the molar mass of the reactants [28].

Several factors influence the actual capacity of a cell, e.g. the temperature, the age of the cell and the current rate employed [22]. The specific capacity of the whole cell is also much lower than the theoretical specific capacity due to the added mass of the other cell components.

The capacity is often expressed in ampere-hours. This is the product of a current and the number of hours a battery can be discharged at that current, before it reaches the defined cut-off voltage [22].

C-rate

The C-rate is a way of expressing the current rate normalized to the capacity of a battery. This is useful for comparing current rates between batteries with different

capacities. 1C is the current rate which charges or discharges the battery fully in 1 hour. At C/5 the battery would be charged/discharged in 5 hours and at 5C in 0.2 hours.

State of Charge

The state of charge (SOC) of a battery is the battery capacity at a specific time given as a fraction of the total capacity of the battery [22].

Energy

The energy content of a cell can be expressed in watt-hours by multiplying the capacity by the voltage. To allow comparison between batteries the energy is often expressed as a ratio of its size or weight. The specific energy is the energy per unit mass of the battery (Wh/kg) and the energy density is the energy per unit volume of the battery (Wh/l) [22].

Cycle Life

The cycle life of a battery is the number of charge/discharge cycles a battery can go through before it no longer meets some chosen performance criteria [22]. One such criteria is the number of cycles before the battery capacity reaches a certain percentage of the initial capacity. 80% of the initial capacity is a common limit to use.

Self-discharge

Self-discharge is the loss of energy stored in the battery under open-circuit conditions due to unwanted chemical reactions in the cell or short-circuits. The mechanisms this happens through and the rate of self-discharge depend on the battery chemistry. The rate of self discharge varies much between different battery types. Lithium ion batteries have a fairly low self discharge of 2 - 8 % each month [30].

2.3 Li-ion Battery

Two properties of lithium make it very attractive as an anode material; it is the lightest metal with an atomic mass of 6,94 u and it has the lowest standard reduction potential of 3,045V [22]. The first property makes it useful for producing lightweight batteries and it has a high specific capacity (capacity per unit mass). The low standard reduction potential leads to a high working voltage for the cell. Together the high capacity and high voltage result in a high specific energy [22, 23].

Due to the great properties of lithium, the first rechargeable lithium batteries focused on using lithium metal as the anode material. In 1977 Exxon commercialized a battery with lithium metal as the anode and an intercalation cathode of TiS_2. These batteries quickly developed a problem with dendrite growth at the anode during cycling [31]. During recharging the lithium in the positive electrode must go through the electrolyte and get electroplated onto the negative electrode [22]. Electroplating is the process of using an electric current to coat something with a metal [32]. This

electroplating of lithium often leads to a non-uniform distribution, resulting in some of the lithium losing electrical contact with the electrode or the growth of dendrites [22]. These dendrites could grow long enough to reach the cathode, which may lead to short circuit and fire. After this, several other lithium metal batteries have failed and due to safety issues they have still not reached widespread commercialization. A lot of different anode materials were tested before carbon-based materials became the most promising. Carbon has a relatively high capacity (372 mAh/g), a low potential vs lithium and the lithiation and delithiation has good cycleability [33]. The first lithium ion batteries were commercialised by Sony in 1991 and used a carbon intercalation anode [31].

Lithium ion batteries use intercalation of lithium into both the anode and the cathode material. During cycling, lithium ions (Li^+) move back and forth between the positive and the negative electrode [30]. Due to the lack of lithium metal, li-ion batteries are safer and have a longer cycle life than rechargeable lithium metal batteries.

Some advantages of lithium ion batteries mentioned by Erlich [30] are

- High operation voltage (2.5 – 4.2 V)
- High specific energy and energy density
- Capable of rapid recharging
- Can discharge at high rate and high power
- Long lifetime (> 1000 cycles)
- Long shelf life
- Low self-discharge (2 – 8 % per month)
- Can operate in a wide window of temperatures (-20 °C – 60 °C)

2.3.1 The Intercalation Process

Intercalation is insertion or removal of small atoms or molecules into a host structure that happens without significant changes to the host structure. This is a reversible process and the guests tend to be ions [34]. In the case of lithium ion batteries, Li^+ is the guest being inserted into the host materials in the cathode and the anode. During discharge, lithium ions are removed from the negative electrode material and inserted into the positive electrode material, the opposite happens during charge (see Figure 2.4). For an example cell based on a lithium metal oxide cathode and a carbonaceous anode, the reactions happening at the electrodes can be described by

$$\text{Positive:} \qquad \mathrm{Li_{1-x}MO_2 + xLi^+ + xe^-} \underset{charge}{\overset{discharge}{\rightleftharpoons}} \mathrm{LiMO_2} \tag{2.4}$$

$$\text{Negative:} \qquad \mathrm{Li_xC} \underset{charge}{\overset{discharge}{\rightleftharpoons}} \mathrm{C + xLi^+ + xe^-} \tag{2.5}$$

$$\text{Total:} \qquad \mathrm{Li_xC + Li_{1-x}MO_2} \underset{charge}{\overset{discharge}{\rightleftharpoons}} \mathrm{LiMO_2 + C,} \tag{2.6}$$

where M is a metal, e.g. Co, and x can be between 0 and 1 [30].

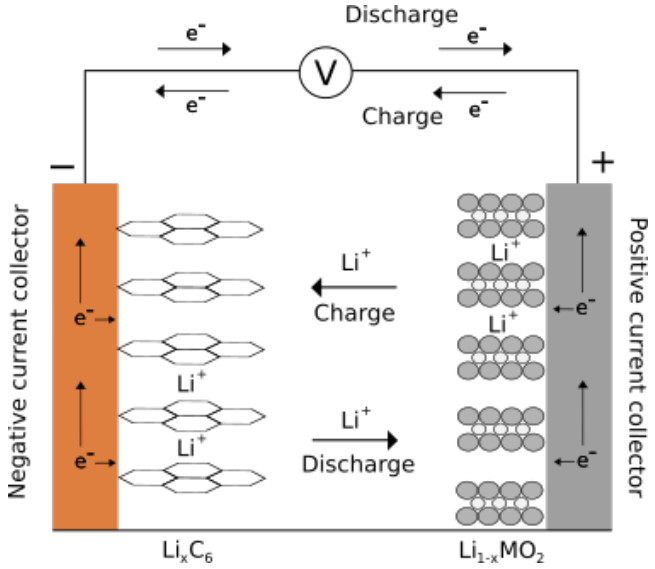

Figure 2.4: Working principle of Lithium ion cell with intercalation electrodes. The illustration was adapted from [30]

2.3.2 Electrode Materials

A material must have certain qualities to be a good electrode material. It must be able to take up a large amount of lithium to ensure a high capacity. To achieve a long cycle life with a small loss of capacity in each cycle, lithium should be inserted and removed reversibly without major structural changes to the electrode material. The material should have a high lithium ion diffusivity and a good electronic conductivity to ensure good rate capabilities. Additionally, a good electrode material should be readily available, environmentally friendly and have a low cost [30].

There are three main types of electrode materials that can be used in LIBs; intercalation materials, alloying materials and conversion materials [35]. Intercalation materials are the most used today and their working principle were described in Section 2.3.1. Two examples of intercalation electrode materials are graphite and lithium cobalt oxide ($LiCoO_2$) [7]. Conversion electrodes go through a redox reaction where chemical bonds are broken and recombined. This means the crystal structure changes during lithiation/delithiation [7]. Some materials that could be promising conversion cathode materials are transition metal fluorides (e.g. FeF_2) and chalcogens or halogens, of which sulfur (S) is an attractive candidate [7, 36]. Possible conversion anode materials are transition metal oxides and sulfides (e.g. Fe_3O_4 and FeS_2) [36, 37]. An alloy is a metallic substance that consists of two or more elements [38]. In alloying materials Li forms an alloy with the electrode material during lithiation [7]. Silicon as an alloying anode material has received much attention due to its high capacity, abundance and low cost [7].

Cathode Materials

Positive electrode materials should have a high discharge potential versus Li/Li^+ to give the cell a high voltage and high energy density. The positive electrode

material in Li-ion batteries is usually a metal oxide. The first Li-ion batteries used a $LiCoO_2$ cathode [30]. Recently, complex metal oxides with alloys of nickel, cobalt and manganese (NMC) or nickel, cobalt and aluminium (NCA) have been much used in batteries for EVs [39].

Anode Materials

The ideal negative electrode material for lithium batteries would be lithium metal. Due to safety issues related to dendrite growth during recharging of lithium metal batteries the focus shifted towards using intercalation materials instead [30]. A good negative electrode material has a low discharge potential versus Li/Li^+ so that the cell still has a high voltage. The most used anode material is carbon, often in the form of graphite [39]. Another widely used material is lithium titanium oxide (LTO) which has a good thermal stability, high rate and high cycle life, but has a lower capacity and a higher discharge potential versus Li/Li^+ compared to carbon [7]. Alloying anode materials have been getting a lot of attention recently due to their high capacity, but they generally have significant degradation issues related to the large changes in volume during cycling.

Electrolyte

Lithium is highly reactive with water, so an aqueous electrolyte cannot be used in Li-ion batteries. Some non-aqueous electrolytes that can be used instead are solutions of lithium salts in polar organic/inorganic liquids and ionically conducting polymers or ceramics. Polar organic liquids are generally the most used [22]. Most LIBs use $LiPF_6$ as its salt due to the high conductivity and good safety it provides [30].

2.3.3 Solid Electrolyte Interface Layer

The electrolyte used in LIBs should be thermodynamically stable at both the anodic and cathodic potential, i.e. near 0 V to 4.2 V vs lithium [30], to avoid reacting with the electrodes. The typical electrolytes used in LIBs are not stable at the low operating voltage at the negative electrodes [40]. During the first charge of the cell the electrolyte is reduced and starts to decompose on the negative electrode surface to form a passive layer called the Solid Electrolyte Interface (SEI) [41]. SEI formation is an irreversible process with lithium being incorporated into the passivation layer leading to a significant capacity loss, mainly in the first charge/discharge cycle [30]. The SEI stops further degradation of the electrolyte by blocking the transport of electrons and electrolyte molecules through it [40, 41]. Since the electrolyte molecules cannot get to the active material surface they can no longer react with the lithium ions and electrons there. The SEI allows further charging/discharging of the battery since the SEI is permeable to lithium ions [40].

A stable SEI is important to achieve a long cycle life for a battery [41, 42]. Continuing growth of SEI and the consequent loss of lithium is the most common reason for capacity fade in successful LIBs [40]. This is especially problematic for electrode materials that undergo a significant volume change during charge/discharge. Volume changes can cause the SEI to break, and thus re-expose the electrode active

material to the electrolyte. New SEI will form in the areas where the electrode has become exposed and the SEI grows ticker each charge/discharge cycle [42]. The presence of a stable SEI is also important for the safety of the battery [41].

The SEI is composed of a number of organic and inorganic decomposition products created in the reduction of the electrolyte [41]. The exact composition of the SEI depends on several factors including the electrolyte composition, the type of active material and electrochemical conditions, e.g. the mode of cycling. Some reported components of SEI include LiF, Li_2O, Li_2CO_3, polycarbonates and polyolephines [33, 41].

2.3.4 Silicon as Anode Material

Silicon (Si) has received much attention in recent years as a potential anode material in LIBs due to its high theoretical capacity [43]. Its theoretical capacity of 3579 mAh/g, for the fully lithiated state $Li_{3.75}Si$ at room temperature, is almost 10 times as high as the theoretical capacity of graphite (372 mAh/g) [44]. At high temperatures the theoretical capacity of Si increases to 4200 mAh/g corresponding to the formation of $Li_{22}Si_5$. Si anodes have a relatively low working potential of $\sim$ 0.4 V vs Li/Li^+, slightly higher than the working potential of graphite anodes at $\sim$ 0.05 V vs Li/Li^+ [43]. Additional benefits of Si as anode material include its abundance in the earth's crust, low cost, chemical stability, non-toxicity and an already well-developed infrastructure for manufacturing due to the semiconductor industry [7, 45, 46].

Challenges for Silicon Anodes

One major challenge in the commercialization of Si anodes is the large volume changes of more than 300% during lithiation and delithiation [35]. The large volume change results in a poor capacity retention. This means that the capacity typically fades rapidly during cycling, in some cases the reversible capacity of the Si anode drops by 70% after few cycles [46].

Wu and Cui [46] discussed the fundamental material challenges related to the large volume change of Si anodes in a review article. They outlined three main material challenges to using silicon as an anode material.

1. *Material pulverization* (Figure 2.5 a)). The large volume change of over 300% during lithiation/delithiation generates very high stress [35, 46]. The high stress can result in cracking and pulverization of the Si electrode, which in turn can lead to loss of electrical contact with the current collector or the conductive additive, eventually resulting in capacity fading [43, 46]. This mechanism is likely the cause of most of the capacity fade in Si anodes, particularly for Si films, bulk Si and large particles of Si [46].

2. *Morphology and volume change of the whole electrode* (Figure 2.5 b)). Lithiation/delithiation will cause volume and morphology change at the electrode level, not just in individual Si particles. As the Si particles expand during lithiation they can affect each other and when the Si particles contract during delithiation they might not go back to their initial morphology. During contraction some particles might loose electrical contact with their surroundings.

The total electrode volume also changes during lithiation/delithiation and can cause electrode peel-off and failure [46].

3. *Unstable solid electrolyte interphase* (Figure 2.5 c)). As mentioned in Section 2.3.3, a large volume change during cycling makes it hard to form a stable SEI. The SEI formed when the Si anode is in its expanded (lithiated) state can break when the particles contract during delithiation. The broken SEI re-exposes some areas of the electrode surface to the electrolyte and new SEI is formed in those areas. If this continues over several cycles the SEI will keep growing thicker and thicker [46]. The continued growth of SEI degrades the battery performance through consumption of lithium ions and electrolyte when growing the SEI, weaker electrical contact between the current collector and the anode material due to insulation from the SEI, longer diffusion length for Li through the thicker SEI and degradation of the electrode material due to mechanical stress from the SEI [42].

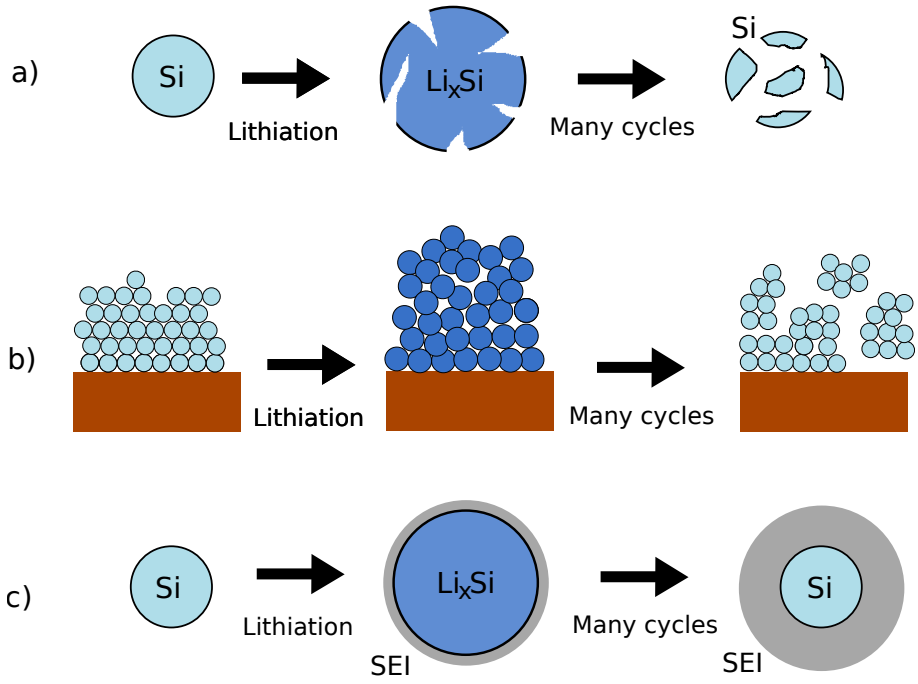

Figure 2.5: Illustration of the material challenges related to the large volume change in Si anodes; a) material pulverization, b) morphology and volume change of the whole electrode, c) unstable solid electrolyte interphase. Illustration adapted from [46]

2.3.5 Phase Transformation

Silicon used as anode material can be either crystalline silicon (c-Si) or amorphous silicon (a-Si). During first lithiation of c-Si a crystalline to amorphous phase transition happens, converting the c-Si into a-Li_xSi phases [35]. In consecutive cycles the now amorphous Si goes through Li_xSi phase transformations. Ogata et al. [47] did a study on these phase transformations in nano-structured silicon anodes. They identified four processes happening from the 2nd cycle during discharge. The first discharge process is a gradual lithiation of the starting a-Si phase to form a $Li_{\sim 2.0}Si$ phase. This happens around 300 - 250 mV. The second process happens at 100 mV

and is a change from the $Li_{\sim 2.0}Si$ phase to a $Li_{\sim 3.5}Si$ phase. At 50 mV a third process takes place, where the amorphous Li_xSi phase recrystallizes to form c-$Li_{\sim 3.75}Si$. With further cycling a fourth process is seen at 30 mV, where an over-lithiated phase, c-$Li_{\sim 3.75+\delta}Si$ (δ = 0.2 - 0.3) is formed [47]. During charge, at least four processes were observed, happening at 170 mV, $\sim$ 270 - 300 mV, 430 mV and 500 mV [47].

2.4 Diffusion

Diffusion is transport of materials caused by atomic motion. It is caused by atoms or molecules jumping from one site to another. This can only happen if the atom has an adjacent empty cite and it has enough energy to overcome any energy barriers in between. When atoms of one substance diffuse into another it is called interdiffusion or impurity diffusion. Diffusion can also happen in only one substance if atoms of the same type are changing position, that is called self-diffusion [38, 48].

2.4.1 Vacancy Diffusion

If there is a vacancy in the lattice structure, an atom can move from its normal position in the lattice into the adjacent vacant position. This is illustrated in Figure 2.6. A flow of atoms in one direction causes a flow of vacancies in the other direction. The activation energy for this jump is the energy needed for the diffusing atom to distort the neighbouring atomic structure and force its way through. This is the main diffusion mechanism for self-diffusion at elevated temperatures. The amount of vacancy diffusion is a function of the number of vacancies in the structure. At higher temperatures, metals have a higher number of vacancies and the energy of the diffusion atoms are higher, so more diffusion occurs [38, 48].

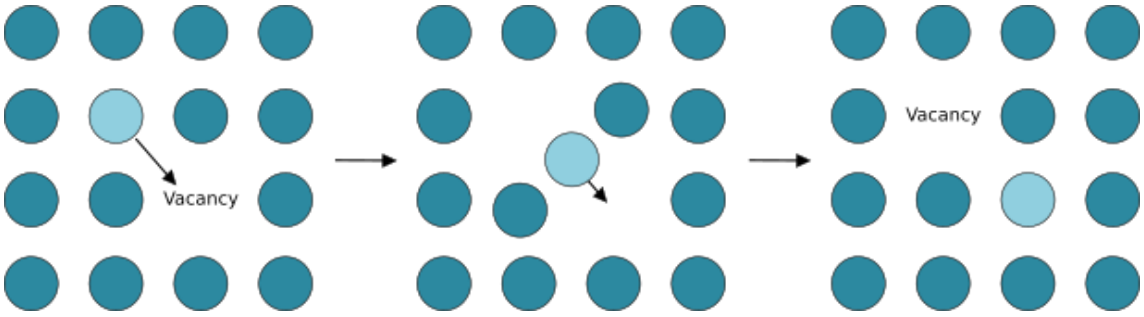

Figure 2.6: Illustration of vacancy diffusion. Illustration adapted from [48]

2.4.2 Interstitial Diffusion

Small atoms, like hydrogen, carbon or lithium, can reside in between the larger atoms in a metal lattice. The cites these small atoms occupy are called interstitial lattice sites. Interstitial diffusion happens by migration of atoms from one interstitial site to an empty neighboring one. This is illustrated in Figure 2.7. Due to a much higher number of vacant interstitial sites compared to vacant sites in the lattice, the diffusivity of an interstitial atom is much larger than for an atom in a lattice site. Additionally, the interstitial atoms are smaller and more mobile, generally leading to faster diffusion [38, 48].

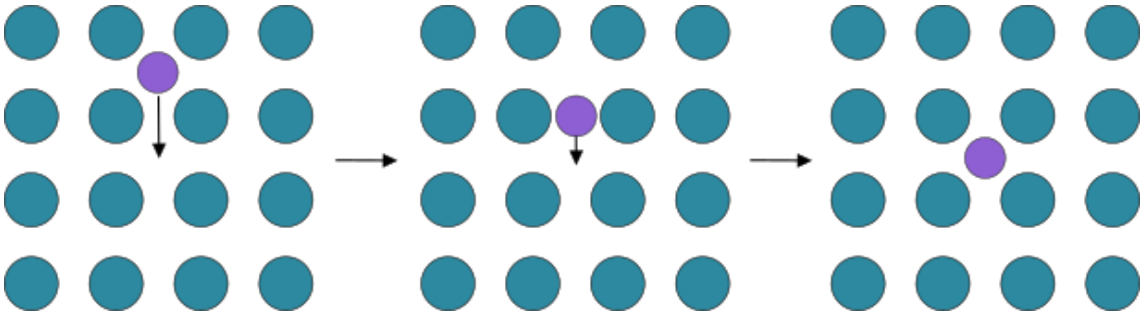

Figure 2.7: Illustration of interstitial diffusion. Illustration adapted from [48]

2.4.3 Fick's Laws

The diffusion flux, J, is a measure for how fast diffusion happens, or the rate of mass transfer [38]. It is given by

$$J = \frac{M}{At}, \tag{2.7}$$

where M is the mass of the atoms diffusing through the cross-section of area A during the diffusion time t [38].

For a steady-state diffusion (constant diffusion flux over time) in one direction (x) the diffusion flux, J, can be described by Fick's first law

$$J = -D\frac{dc}{dx}, \tag{2.8}$$

where D is a proportionality constant called the diffusion coefficient and $\frac{dc}{dx}$ is the concentration gradient. In this case the driving force of the diffusion is the concentration gradient [38].

Most of the time, the diffusion flux and concentration gradient in a solid vary with time, so the diffusion is not steady-state. In these cases Fick's first law is not very useful and Fick's second law is used instead [38]. Fick's second law is given by

$$\frac{\partial c}{\partial t} = \frac{\partial}{\partial x}\left(D\frac{\partial c}{\partial x}\right), \tag{2.9}$$

where c is the concentration and D is the diffusion coefficient. If the diffusion coefficient is constant with regard to x this expression can be simplified to

$$\frac{\partial c}{\partial t} = D\frac{\partial^2 c}{\partial x^2}, \tag{2.10}$$

This is a partial differential equation, and it can be solved by defining boundary and initial conditions that are meaningful for the situation at hand [38].

2.4.4 Influence of Temperature on Diffusion

As mentioned in Section 2.4.1 the temperature greatly influences the rate of diffusion in a material. The temperature dependence of the diffusion coefficient can be expressed by the Arrhenius equation as [38, 49]

$$D = D_0 \exp\left\{-\frac{Q_d}{RT}\right\}, \tag{2.11}$$

where D_0 is a constant pre-exponential factor (m^2/s), Q_d is the activation energy needed for the diffusion process (J/mol or eV/atom), R is the universal gas constant (J/mol·K) or (eV/atom·K) and T is the absolute temperature (K).

Another form of equation (2.11) can be found by taking the natural logarithm on both sides, yielding

$$\ln D = \ln D_0 - \frac{Q_d}{R}\left(\frac{1}{T}\right). \tag{2.12}$$

Plotting $\ln D$ versus $\frac{1}{T}$ should result in a straight line, since D_0, Q_d and R are constants. This can be used to experimentally determine the values of Q_d and D_0.

2.5 Galvanostatic Intermittent Titration Technique

In 1977 Weppner and Huggins [12] proposed a method of determining the diffusion coefficient of lithium ions into the electrode materials in lithium ion batteries. The technique is called galvanostatic intermittent titration technique (GITT). It looks at a case where the rate is limited by transport in the bulk of the electrode [12].

Usually, in a GITT test, a half cell is used, with metallic lithium as the counter and reference electrode and the material to be tested as the working electrode [19]. A schematic illustration of half cells used for GITT experiments in this thesis is shown in Figure 2.8. It is assumed that the concentration of all species is homogeneous before the start of the test, corresponding to an equilibrium voltage, E_0 of the cell [12].

In the GITT procedure a series of short current pulses are applied to a cell, each pulse followed by a relaxation period with no current going through the cell. During charge, the applied current is positive and during discharge it is negative [19].

At the start of a positive current pulse there is a sudden rise in cell potential corresponding to the IR drop due to the internal resistance of the cell components. If the current pulse is negative, the cell potential will fall with a value corresponding to the IR drop [19]. This IR drop shifts the voltage curve upwards or downwards with a constant value without changing the shape of the voltage versus time curve [12].

During the current pulse the relationship between the applied current and the transport of the mobile ionic species (here lithium ions) close to the electrode-electrolyte interface (at x = 0 in Figure 2.8) is given by

$$I = -SzqD\left.\frac{\partial c}{\partial x}\right|_{x=0}, \tag{2.13}$$

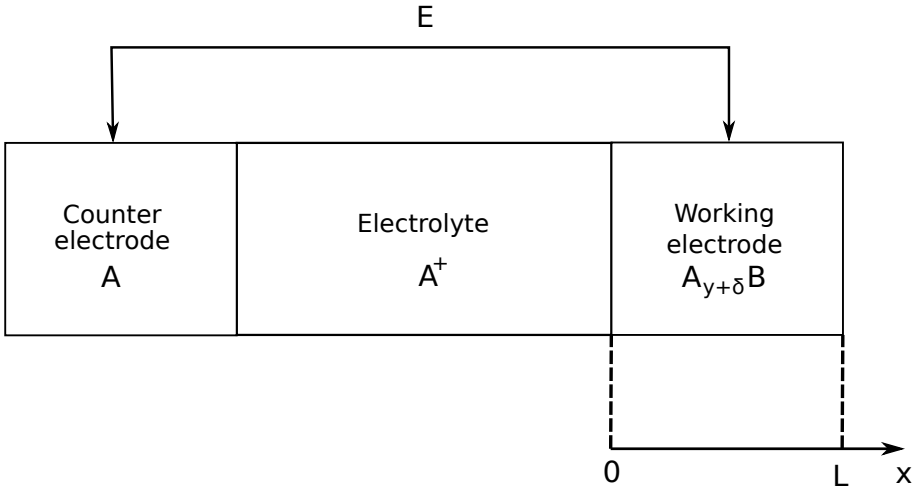

Figure 2.8: Schematic illustration of a half cell used in GITT experiments. The electrode-electrolyte interface is at $x = 0$ and the electrode has a thickness L. Illustration adapted from [12].

where I is the applied current, S is the surface area of the electrode-electrolyte interface, z is the charge number of the mobile ionic species, q is the elementary charge, D is the diffusion coefficient and $\frac{\partial c}{\partial x}$ is the concentration gradient in the x-direction [12].

According to equation (2.13) a constant applied current in the current pulse will produce a constant concentration gradient, since all other variables are constants. The cell voltage increases (during positive current) or decreases (during negative current) to maintain this concentration gradient [12].

Each current pulse is followed by a relaxation period without any current. Again, the cell potential will suddenly decrease (positive current) or increase (negative current) with a value corresponding to the IR drop. After the sudden initial change in potential, the potential continues to slowly decrease/increase until a new equilibrium voltage is obtained [19]. In the relaxation period, lithium ions will diffuse into the electrode material and the electrode composition goes toward being homogeneous. The new voltage is a result of the change in stoichiometry $\Delta\delta$ that results from the added lithium ions into the electrode material [12]. This change in stoichiometry is given by

$$\Delta\delta = \frac{I_0 \tau M}{zmF}, \tag{2.14}$$

where I_0 is the constant pulse current, τ is the time the current is applied, M is the molar mass, z is the charge number, m is the mass and F is Faraday's constant.

To find the voltage E as a function of time it is necessary to know the time dependence of the concentration at the interface (x = 0) [12]. This can be found by Fick's second law, given in equation (2.10), with initial and boundary conditions

$$c(x, t = 0) = c_0 \qquad (0 \leqslant x \leqslant L) \tag{2.15}$$

$$-D\frac{\partial c}{\partial x}\bigg|_{x=0} = \frac{I_0}{Sz_iq} \qquad (t \geqslant 0) \tag{2.16}$$

$$\frac{\partial c}{\partial x}\bigg|_{x=L} = 0 \qquad (t \geqslant 0), \tag{2.17}$$

where c is the concentration, I_0 is the constant pulse current applied to the battery, S is the interface area between the active material and the electrolyte, z is the valence of the diffusion species, q is the elementary charge and D is the diffusion coefficient [12]. The initial condition (eq. (2.15)) is based on the assumption that the cell is in equilibrium at the beginning of a current pulse with a homogeneous concentration of c_0 throughout the electrode. The first boundary condition (eq. (2.16)) gives an expression for the concentration gradient at the electrode-electrolyte interface (at x = 0 in Figure 2.8) and comes from equation (2.13). The second boundary condition (eq. (2.17)) is based on the assumption that the right hand boundary of the electrode (at x = L in Figure 2.8) is impermeable.

Weppner and Huggins [12] give the solution of equation (2.10) with the initial and boundary conditions in eq. (2.15) - (2.17) at x = 0 as

$$c(x = 0, t) = c_0 + \frac{2I_0\sqrt{t}}{Szq\sqrt{D}} \sum_{n=0}^{\infty} \left(ierfc\left[\frac{nL}{\sqrt{D}t}\right] + ierf\left[\frac{(n+1L}{\sqrt{(D)}t}\right]\right), \tag{2.18}$$

with ierfc(λ) = $[\pi^{-1/2}\exp\{-\lambda^2\}] - \lambda + [\lambda\mathrm{erf}(\lambda)]$. When $t << L^2/D$ this can be simplified to [12]

$$\frac{\mathrm{d}c(x = 0, t)}{\mathrm{d}\sqrt{t}} = \frac{2I_0}{Szq\sqrt{D}\pi} \qquad \left(t << \frac{L^2}{D}\right), \tag{2.19}$$

where all the variables are defined as in equations (2.15) - (2.17).

If the change in the molar volume of the electrode caused by the change in electrode composition during charge/discharge is small enough to be neglected, the relationship between the change in concentration and the change in stoichiometry is given by

$$\mathrm{d}c = \frac{N_A}{V_M}\mathrm{d}\delta, \tag{2.20}$$

where N_A is Avogadro's number and V_M is the molar volume [12]. Inserting this relation into eq. (2.19), expanding by $\mathrm{d}E$ and solving for the diffusion coefficient gives

$$D = \frac{4}{\pi}\left(\frac{V_M}{SFz}\right)^2 \left[I_0\left(\frac{\frac{\mathrm{d}E}{\mathrm{d}\delta}}{\frac{\mathrm{d}E}{\mathrm{d}\sqrt{t}}}\right)\right]^2 \qquad \left(\tau << \frac{L^2}{D}\right), \tag{2.21}$$

where F is Faraday's constant, $F = qN_A$. E as a function of δ can be found by plotting the open circuit voltages, or the voltage at the end of the relaxation steps, against the change in composition calculated from equation (2.14). $\mathrm{d}E/\mathrm{d}\delta$ is the slope of this curve [12].

It is possible to simplify equation (2.21). If both the pulse time and current are small enough, the change in equilibrium voltage during each titration step is small. Then $\mathrm{d}E/\mathrm{d}\delta$ can be assumed constant within the current pulse and can be simplified to $\Delta E_s/\Delta\delta$ [12]. Performing this simplification and substituting $\Delta\delta$ according to equation (2.14) gives a new expression for the diffusion coefficient:

$$D = \frac{4}{\pi}\left(\frac{n_m V_m}{S}\right)^2 \left(\frac{\Delta E_s}{\tau\left(\frac{dE}{d\sqrt{t}}\right)}\right)^2 \qquad \left(\tau << \frac{L^2}{D}\right). \tag{2.22}$$

τ is the pulse time, n_m is the number of moles of the electrode, V_m is the molar volume of the electrode, S is the contact area between the electrode and the electrolyte and ΔE_s is the change in open circuit voltage from the end of one relaxation period to the next.

Another simplification can be made to this expression if the curve of E vs $\sqrt{t}$ is approximately linear during the current pulse [12]. $\mathrm{d}E/\mathrm{d}\sqrt{t}$ can then be substituted by $\Delta E/\Delta\sqrt{t}$. $\Delta\sqrt{t}$ is the square root of the pulse time, $\sqrt{\tau}$. Substituting this into equation (2.21) gives

$$D = \frac{4\tau}{\pi}\left(\frac{V_M I_0}{SFz}\right)^2 \left(\frac{\frac{dE}{d\delta}}{\Delta E_t}\right)^2. \tag{2.23}$$

ΔE_t is the change in voltage during one current pulse and all other variables are defined as in equation (2.21).

Joining the two simplifications from eq. (2.22) and eq. (2.23) together into one equation gives the equation usually employed when doing doing GITT experiments, given as

$$D = \frac{4}{\pi\tau}\left(\frac{n_m V_m}{S}\right)^2 \left(\frac{\Delta E_s}{\Delta E_t}\right)^2 \qquad \left(\tau << \frac{L^2}{D}\right), \tag{2.24}$$

where all variables are defined as in equations (2.21) - (2.23). Figure 2.9 shows a single GITT step with these variables drawn in.

For a thin film electrode, this expression can be simplified further. The number of moles, n_m, and the molar volume, V_m, of the electrode multiplied is equal to the volume of the electrode. Due to the simple geometry of a thin film the volume equals the surface area times the thickness of the thin film: $V = Sh$. Substituting this into equation (2.22) gives

$$D = \frac{4}{\pi\tau}h^2\left(\frac{\Delta E_s}{\Delta E_t}\right)^2 \qquad \left(\tau << \frac{L^2}{D}\right), \tag{2.25}$$

where all variables are defined as in equation (2.22).

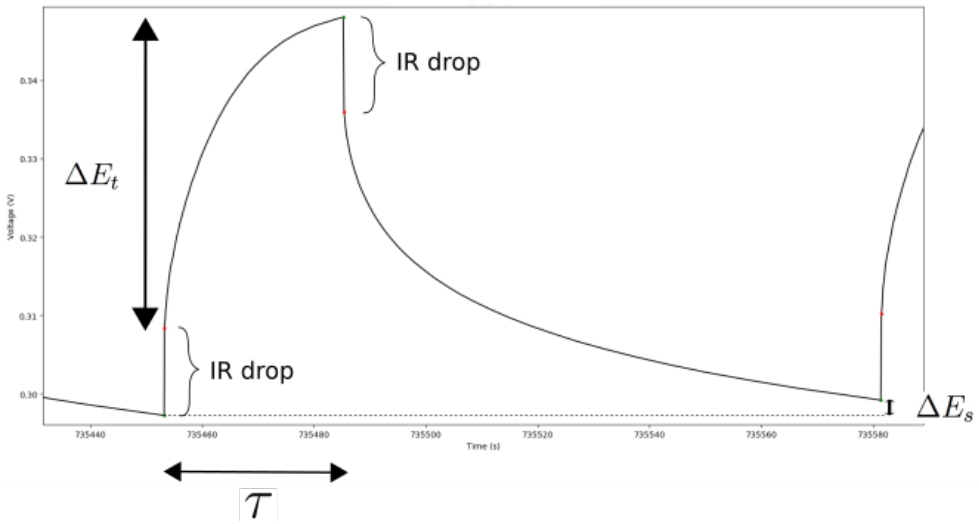

Figure 2.9: Illustration of a single GITT step with parameters used for calculating the diffusion coefficient drawn in. ΔE_s is the change in open circuit voltage of the cell for this pulse, ΔE_t is the change in voltage during the pulse and τ is the time duration of one pulse.

Chapter 3

Method

3.1 Thin Film Creation

The silicon thin films were created through Plasma Enhanced Chemical Vapor Deposition (PECVD) at the Institute for Energy Technology (IFE) as part of an ongoing research project. Chemical vapor deposition (CVD) is a group of processes often used for deposition of thin films of materials. The deposition occurs by decomposition of one or more precursor gases to form solid material on the surface of a substrate. The process if often thermally driven, with the substrates heated to a temperature high enough to decompose the precursors [50, 51]. The PECVD technique uses plasma instead of heat to achieve decomposition. One advantage of PECVD is that the process occurs at low temperatures (often from near room temperature to around 350 °C) [52].

The instrument used for PECVD deposition in work was an Oxford PlasmaLab 133, which has a parallel-plate design. The schematics of a typical parallel-plate PECVD reactor can be seen in Figure 3.1. The reactor has two electrodes, where the anode is heated and holds the substrate and the cathode is often also used as a gas injection system, called the showerhead. All these components are inside a vacuum chamber.

The silicon thin film electrodes were made by depositing films onto copper foil substrates. The copper foil works as the current collector when the electrode is used in an electrochemical cell. The precursor used to make silicon was pure silane (SiH_4) plasma. The substrate temperature was 400 °C, which is low enough to make the thin film amorphous. Remaining parameters for PECVD were a flow rate for silane of 25 sccm, a chamber pressure of 200 mTorr and a plasma power of 40 W.

Thin films electrodes are a good choice for doing GITT experiments due to their simple geometry. To calculate D from GITT (equation (2.22) the surface area S of the electrode is needed. For a thin film electrode it is easy to calculate S from the electrode diameter, d. An additional reason for choosing thin films is that the GITT theory assumes dense planar electrodes and one-dimensional diffusion [13]. For the experiments in this thesis Si thin films of two thicknesses were used; 60 nm and 80 nm.

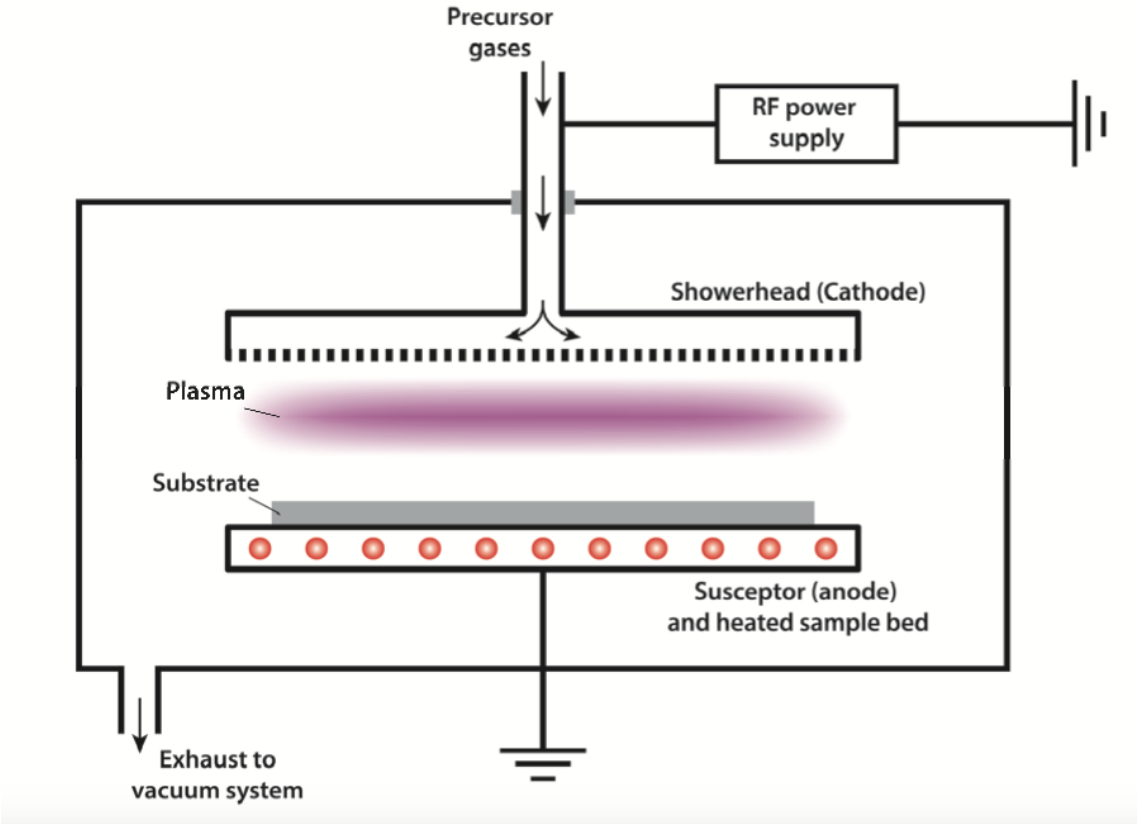

Figure 3.1: Schematic of a PECVD reactor of the parallel-plate type. Illustration by Asbjørn Ulvestad [28], used with permission.

3.2 Cell Assembly

For the experiments in this thesis, half cells with Si thin films as the working electrode and lithium as the counter electrode were used. Using a lithium foil disk as the counter electrode has the advantage of providing an excess of lithium. The cell capacity thus depends on the capacity of the silicon working electrode. Additionally, the lithium metal electrode has a constant potential. This means that the changes in cell potential in the half cell only depends on the working electrode.

Electrodes with a 15 mm diameter were punched from the electrode sheets with a Hohsen punch. The electrodes were then moved into an argon filled glove-box with < 0.1 ppm H_2O and < 0.1 ppm O_2 for cell assembly. The cells used were 2032 coin cells (20 mm diameter and 3.2 mm thickness). The cells were assembled according to the following procedure:

- Added 5 µl of electrolyte to the bottom of the stainless steel coin cell bottom to help the electrode stay in place during assembly.
- Placed the working electrode centered in the cell bottom with the copper side down.
- Added 15 µl of electrolyte.
- Added a Celgard 2400 separator with 18 mm diameter. This separator is a porous monolayer polypropylene membrane with thickness 25 µm.

- Inserted a polyethylene gasket.
- Applied another 15 µl of electrolyte.
- Inserted the Li foil counter electrode (99.99 %, LinYi Gelon LIB Co., 15 mm in diameter and 0.250 mm thick). Prior to insertion the lithium was scraped with a scalpel to remove any oxide formed on the surface.
- Added a 1 mm thick stainless steel spacer.
- Added a stainless steel wave washer spring.
- Added the stainless steel cap.
- Sealed the cell with a crimping machine for coin cells.

A total of 18 cells were made, 9 with an Si thin film of thickness 60 nm and 9 with 80 nm.

The electrolyte used was called "S1" and was a custom mixture from Solvionics. This consisted of 1.2 M $LiPF_6$ in 3:7 ethylene carbonate:ethyl methyl carbonate (EC:EMC), with 10 wt % of fluoroethylene carbonate (FEC) and 2 wt % of vinylene carbonate (VC) as additives.

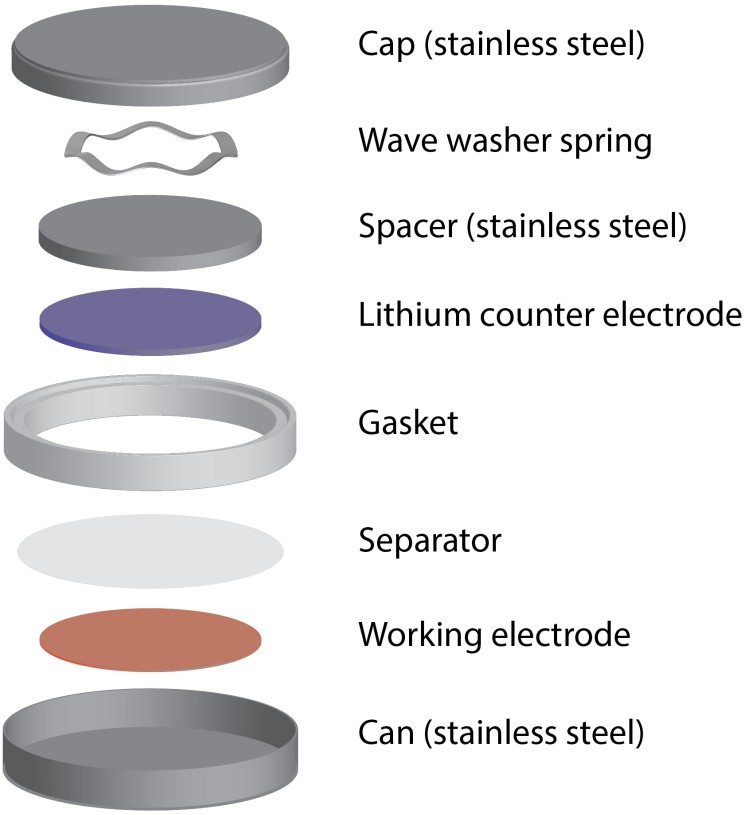

Figure 3.2: Illustration of the coin cell components used in this thesis and their order of assembly in the half cells. Illustration by Asbjørn Ulvestad [28], used with permission.

3.3 GITT Cycling

The half cells were cycled in an Arbin BT2000 potentiostat/galvanostat battery tester. All tests were performed in a temperature controlled environment at 25 °C. The first charge/discharge cycles generally involve reactions that primarily happen at the start of cycling. One example is the formation of SEI which leads to irreversible capacity loss [53]. To allow these reactions to happen fully, the first cycles are usually formation cycles at a low current. In this experiment, all the cells went trough three formation cycles at C/20 before moving on to the actual GITT cycling.

One GITT cycle consists of a constant current pulse of predetermined length directly followed by a relaxation period with no current running through the cell, also with a predetermined length. This combination of pulse and relaxation are repeated until the cell reaches the cut off voltage. The cut off voltage was 0.05 V for lithiation and 1 V for delithiation. When a cell had gone through one discharge and charge cycle the pulse time and relaxation time was changed and a new GITT cycle started. Figure 3.3 shows an example of how the voltage in a GITT cycle typically changes with time.

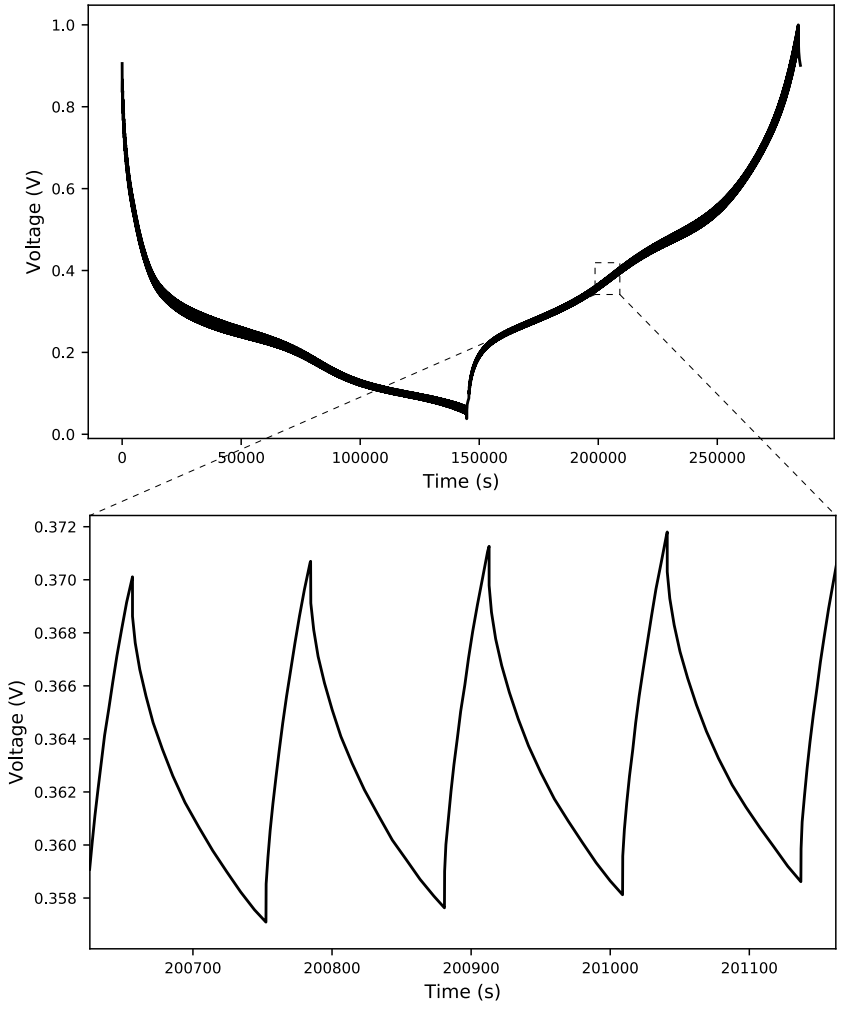

Figure 3.3: The voltage as a function of time for one GITT cycle. By zooming in on one small part of the graph (lower picture) the individual GITT pulses are visible.

To test the influence of different pulse lengths τ, 10 consecutive GITT cycles with different pulse lengths were run. The pulse length started at 2 s in the first cycle and was doubled after each cycle. Due to the time available for the experiment the relaxation time could not be long enough for the cell to entirely reach equilibrium as this can take several hours or days per pulse. To allow the cells a good amount of relaxation between pulses while still keeping the experiment within a reasonable time the relaxation time was chosen to always be 3 times the pulse length. Table 3.1 contains a list of all the pulse and relaxation times used.

Table 3.1: List of pulse times and the corresponding relaxation times for GITT cycles.

GITT cycle number	Pulse time [s]	Relaxation time [s]
4	2	6
5	4	12
6	8	24
7	16	48
8	32	96
9	64	192
10	128	384
11	256	768
12	512	1536
13	1024	3072

Since the current rate also might influence the result of the GITT tests, three different current rates were tested, specifically C/2, C/5 and C/10. The currents were tested on different batteries instead of consecutively due to the possibility that the current rate in one cycle might influence the cell behavior in the next cycle. If the current rate is too high for diffusion to keep up, the surface content of Li could be lower than the Li content in the bulk. The surface composition of the electrode decides the cell voltage, meaning that the charge/discharge would end when the the surface content of Li corresponds to the cut off voltage. The electrode would then not be able to delithiate fully and the next cycle would start with some Li already in the electrode.

For each of the two Si thin film thicknesses (60 nm and 80 nm), there were nine individual cells. To ensure experimental robustness, three parallel cells run the same experiment and with the same same current rate. The experimental set up is summarized in table 3.2. All the cell names with corresponding current rates and thin film thicknesses can be found in Appendix A.

Table 3.2: Set up for GITT experiment summarized. For each of the two thin film thicknesses three current rates are tested on three parallel cells each. On each cell ten consecutive GITT experiments are run, with increasing pulse and relaxation time each cycle (see table 3.1).

L [nm]	I [c-rate]	Number of parallels
60	C/10	3
60	C/5	3
60	C/2	3
80	C/10	3
80	C/5	3
80	C/2	3

3.3.1 GITT Experiment With Longer Relaxation Time

To test the effect that a very long relaxation time had on the result of GITT tests, a new experiment was done on two of the cells, TFSi_60_2 and TFSi_80_2. In this experiment the cells were discharged/charged until they reach around 0.25 SOC. Then the cell was allowed to relax for 5 hours before one GITT step with a 16 s pulse and 5 h relaxation after was performed. This was repeated at 0.5 and 0.75 SOC.

3.4 Data Analysis

3.4.1 Data From Battery Tester

The battery tester records the voltage over the cell, the time elapsed and the current through the cell. From these data other parameters can be calculated, like capacity, energy and power. For GITT calculations, the necessary data is the voltage at specific points in the current pulse and relaxation period and the time elapsed for each pulse.

The cycling program is divided into different steps which all have a step number recorded by the battery tester. For instance all the discharge GITT pulse steps may have the step number 10. Since all equal steps will have the same step number this information can be used to identify which steps are GITT steps and extract the correct voltages from the data.

3.4.2 Cellpy

The data from the battery tester was imported into Python [54] (version 3.7.6) with the help of the Python library Cellpy [55], created by Jan Petter Mæhlen at IFE for handling battery data. Cellpy allows for the data to be imported into a Pandas DataFrame and automatically calculates parameters like charge and discharge capacity and energy. The Cellpy library has a method for creating a step table or a DataFrame where each row has information from one cycling step. The step table contains information like the first and last voltage of a step, the time at the beginning and end of a step and the type of step (e.g. discharge, charge or rest). The

variables needed for GITT calculations are easily extracted from the step table. A python function for extracting relevant data from a step table and doing calculating diffusion coefficients based on equation (2.25) was made. This function can be found in Appendix B.

3.4.3 Data Points With Wrong Step Number

When importing the data into python some of the data point in the DataFrame had the wrong step index. An example can be seen in Figure 3.4, where the last data point in one of the relaxation period has gotten the step index 10, belonging to a current pulse, instead of the step index 11 for a relaxation period. That this step number is wrong is evident from the fact that the current is 0 as it should be in the relaxation step and that the step time marks it as the end of a step and not the beginning of a new one.

Data_Point	Test_Time	Step_Time	DateTime	Step_Index	Cycle_Index	s_FC_Data	Current	Voltage
19932	485674	0.0099	2020-03-04 07:05:30	11	4	0	0	0.459383
19933	485674	0.3508	2020-03-04 07:05:30	11	4	0	0	0.4604
19934	485675	1.154	2020-03-04 07:05:31	11	4	0	0	0.461401
19935	485677	2.6404	2020-03-04 07:05:32	11	4	0	0	0.462407
19936	485679	4.9597	2020-03-04 07:05:35	11	4	0	0	0.463408
19937	485680	6.0017	2020-03-04 07:05:35	10	4	0	0	0.463759
19938	485680	0.0067	2020-03-04 07:05:35	10	4	0	-8.83039e-06	0.460599
19939	485680	0.1324	2020-03-04 07:05:36	10	4	0	-8.82696e-06	0.459581
19940	485681	0.3644	2020-03-04 07:05:36	10	4	0	-8.8252e-06	0.458556
19941	485681	0.7732	2020-03-04 07:05:37	10	4	0	-8.82393e-06	0.457541
19942	485681	1.2869	2020-03-04 07:05:37	10	4	0	-8.82304e-06	0.456541
19943	485682	1.9276	2020-03-04 07:05:38	10	4	0	-8.82035e-06	0.455532
19944	485682	2.0017	2020-03-04 07:05:38	10	4	0	-8.8199e-06	0.455491

Figure 3.4: Example of a data point that has the wrong step number. The data point with a step index marked in blue is wrongly classified as a pulse step (with step index 10) while it should be classified as a relaxation step (with step index 11).

To fix this problem all data points with a step index of 10 and a current of 0 had their step index set to 11. Similarly all data points with a step index of 11 and a current different from 0 had their step index set to 10. The step indices 10 for pulse step and 11 for relaxation step are only correct for lithiation. For delithiation the corresponding step indices are 15 for a pulse step and 16 for a relaxation step. The process for fixing wrong step indices for delithiation is the same as for lithiation, only with other step indices.

3.4.4 Outliers

When plotting the calculated diffusion coefficients, some outliers where observed for the cycles with shortest pulse lengths. An example is shown in Figure 3.5. From

looking at the GITT pulses these outliers came from it can be seen that they come from pulses where a data point has been lost at the end of the relaxation period or in some cases the start or end of the pulse period. Figure 3.6 shows an example where one of the relaxation periods is missing a data point at the end, making it shorter than the other relaxation periods. This means that the difference between the end of this relaxation period and the last one is larger than it should have been, which in turn influences the calculation of the diffusion coefficient. A similar problem is shown in Figure 3.7. Here the pulse step is missing a data point at the start, so the voltage change during the pulse is smaller than other nearby pulses which should be comparable.

Two methods for dealing with these outliers were used. One method was to remove the calculated diffusion coefficients if the length of a pulse or relaxation step was shorter than it should be. Another method was to apply a median filter to the data before further plotting. A median filter replaces each data point with the median of all the data points within a chosen filter size [56]. The median of a set of values is defined as the value in the center after sorting the values from lowest to highest. If there is an even number of values in the set the median is the mean of the two values in the center [56]. To implement the median filter in python the funtion `median_filter` from `scipy.ndimage` was used.

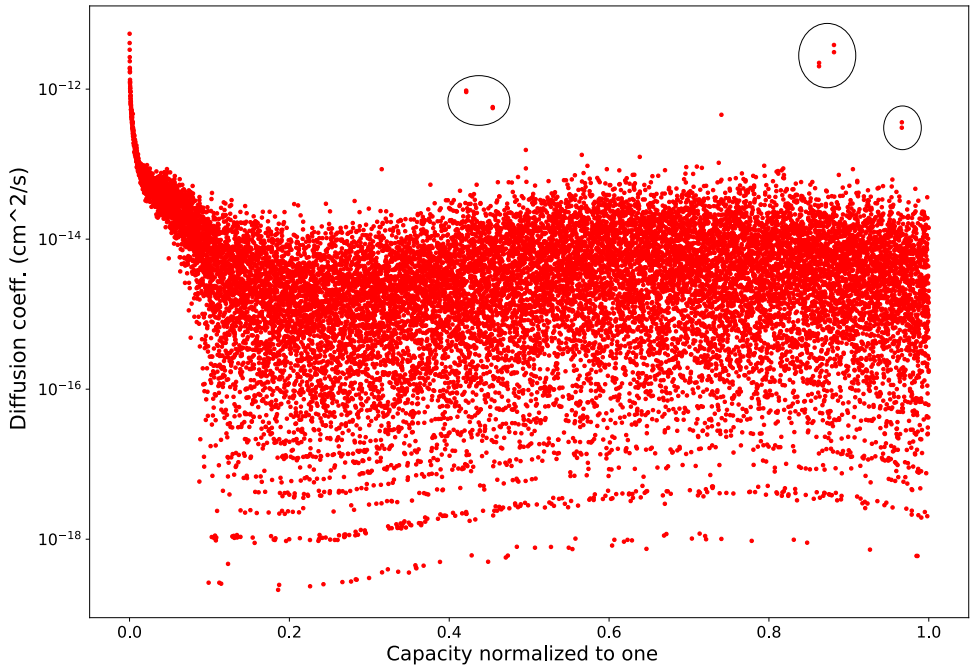

Figure 3.5: Plot of calculated diffusion coefficients for cycle 4 (pulse length 2 s). The black circles mark outliers.

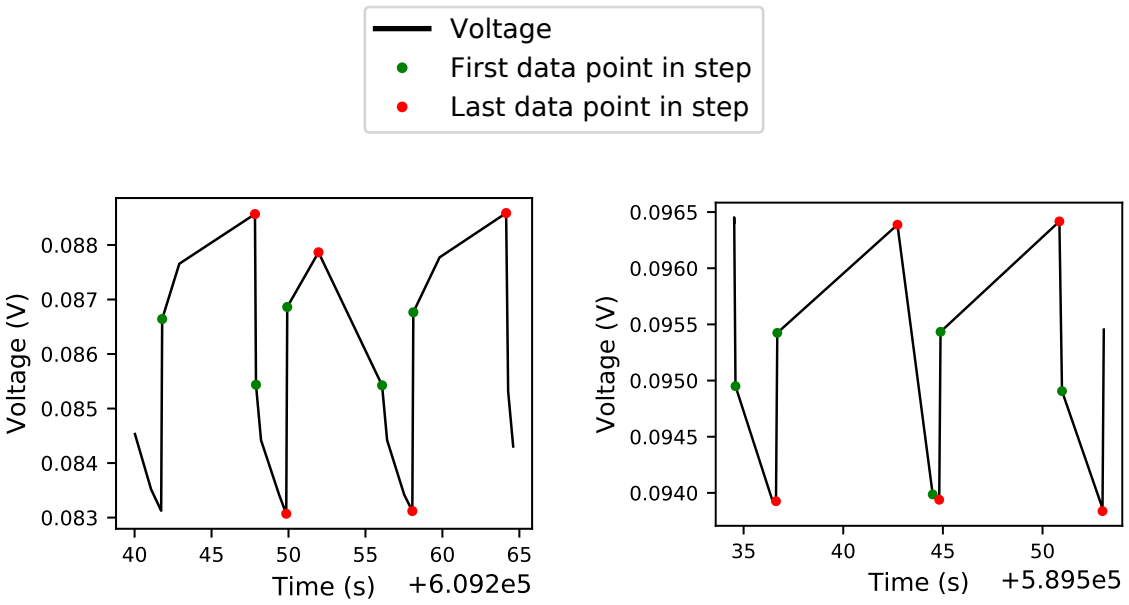

Figure 3.6: Example of relaxation period with a missing data point at the end. The relaxation step in the middle is visibly shorter than the two on the sides

Figure 3.7: Example of pulse period with a missing data point at the start. The pulse in the middle of the figure only has two data points very close to each other.

3.4.5 Smoothing and Interpolation

As can be seen in Figure 3.5, there is a lot of variation in the calculated diffusion coefficients, with values ranging over several orders of magnitude from 10^{-11} to 10^{-18}. This is especially true for short pulse lengths. To make the plots easier to read and get a better idea of how the calculated diffusion coefficients change due to the different pulse lengths the data was smoothed using a Gaussian filter. A Gaussian filter replaces each data point with the weighted mean of the data points within a certain filter size. The data point at the center gets the highest weight, and the data points receive less and less weight with increasing distance from the center [56]. The weight function is used a Gaussian function in one dimension, which can be expressed as

$$G_\sigma(x) = \exp\left\{-\frac{x^2}{2\sigma^2}\right\}, \tag{3.1}$$

where σ is the standard deviation and x is the distance from the center [56].

In Python the Gaussian filter is applied by using the `gaussian_filter1d` method from `scipy.ndimage`.

For both the Gaussian filter and the median filter mentioned previously it is necessary to decide how to handle the edge cases. The python methods in scipy.ndimage have different modes that can be chosen. For smoothing the GITT data the mode 'nearest' was used. In this mode the data set is expanded by repeating the end data points. For example: (a a a a | a b c d | d d d d), where a b c d represent the original data points.

Interpolation was used to increase the number of data points in each cycle data set so that all the cycles had the same number of data points, in order to facilitate equal degree of smoothing in datasets with different data point density. The desired number of data points was chosen by finding the cycle with the highest number of data points and choosing a number above that. The interpolation was done with the python method `interp1d` from `scipy.interpolate`.

A python function to automatically increase the sample size by interpolation followed by application of a median filter, a Gaussian filter or both was created, see Appendix B. Figure 3.8 shows some examples where this function was used to smooth the data from cycle 4 (pulse length 2 s) in cell TFSi_60_2.

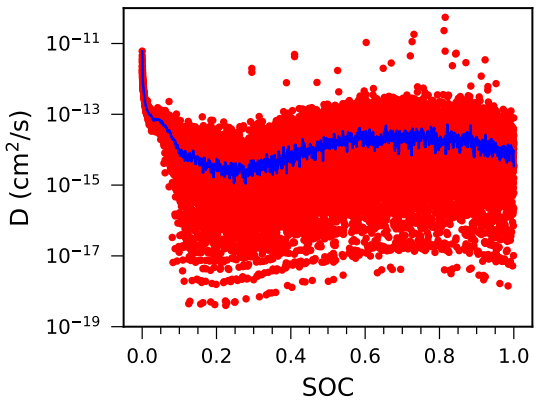

(a) Median filter, size 50

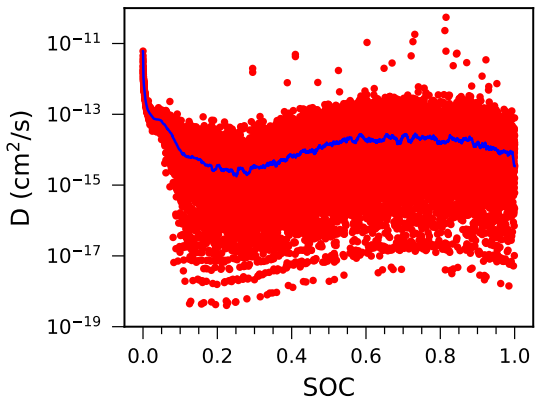

(b) Median filter, size 50

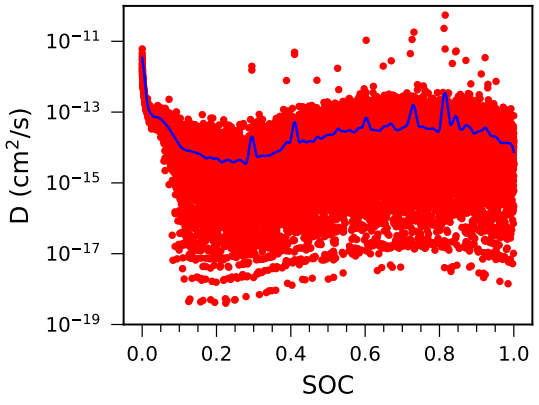

(c) Gaussian filter, σ = 100

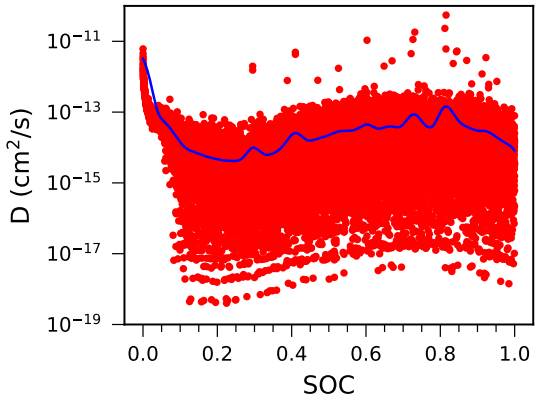

(d) Gaussian filter, σ = 300

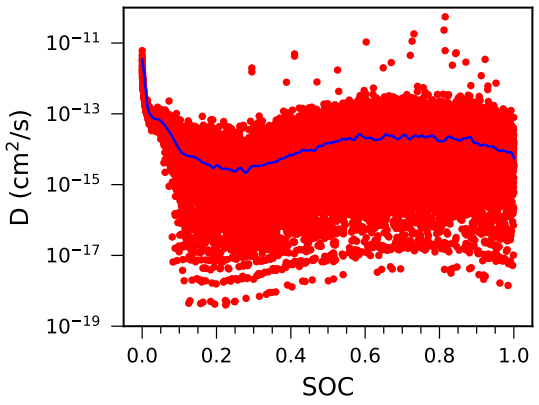

(e) Median and Gaussian filter, size 50, σ = 100

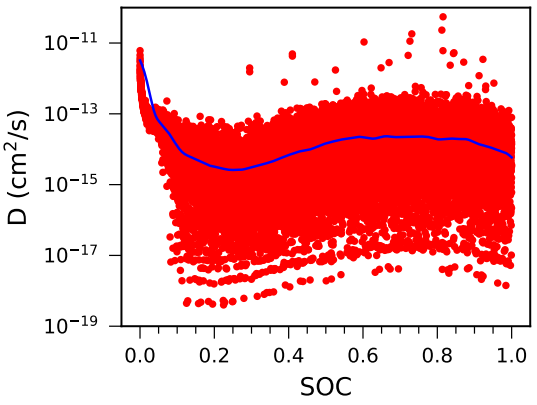

(f) Median and Gaussian filter, size 50, σ = 300

Figure 3.8: Examples of diffusion coefficients with different smoothing methods. The number of data points were increased from 18391 up to 20000 by interpolation. The smoothed diffusion coefficients (blue line) are plotted together with the original data (red dots). The data is from a cell with h = 60 nm and current rate C/10, and a cycle with pulse length 2 s.

3.4.6 Validating Simplifications

As explained in Section 2.5, the simplification used in the derivation of the GITT equations where $\frac{dE}{d\sqrt{t}}$ is assumed equal to $\frac{\Delta E_t}{\Delta\sqrt{t}}$ is valid if the curve of E vs $\sqrt{t}$ is approximately linear over the duration of the current pulse. To check this, a plot of the voltage as a function of $\sqrt{t}$ for one current pulse was made at 3 points along the charge and discharge curve, with a state of charge approximately equal to 0.25, 0.5 and 0.75. This was done for all pulse lengths on one cell of each current rate. The linear portion of the E vs $\sqrt{t}$ plot was determined by visual inspection and a linear regression performed on this linear portion. The linear regression was performed with the Python function `polyfit` from `numpy.polynomial.polynomial`. Diffusion coefficients were calculated for these current pulses both with equation (2.25) and by using the slope of the linear fit in equation (2.22).

The simplification from $\frac{dE}{d\delta}$ to $\frac{\Delta E_s}{\Delta\delta}$ is valid when the change in equilibrium voltage over one GITT step is small enough that $\frac{dE}{d\delta}$ can be considered constant. One way to check this is to plot the $\frac{dE}{d\delta}$ curve and check how linear it is within the δ change in one pulse. The stoichiometry, δ, and the state of charge (SOC) are related by

$$\delta = x_{max} * SOC \tag{3.2}$$

where x_{max} is the maximum value of x in Li_xSi obtained during lithiation of the electrode. For a completely lithiated cell x_{max} is 3.75. The slopes of the E vs δ curve and the E vs SOC curve are related by

$$\frac{dE}{d\delta} = \frac{1}{x_{max}} \frac{dE}{dSOC} \tag{3.3}$$

The E vs δ curve and the E vs SOC curve only differ by a constant. The two curves thus have the same curvature and it does not matter which of the curves are plotted to check for linearity. The E vs SOC curve was chosen since it is easier to find from the data available in the step table.

The $\frac{dE}{d\delta}$ to $\frac{\Delta E_s}{\Delta\delta}$ simplification can also be tested with another method. This method is similar to the one used when checking the $\frac{dE}{d\sqrt{t}}$ to $\frac{\Delta E_t}{\Delta\sqrt{t}}$ simplification. The diffusion coefficients are calculated both with and without the simplification and the results compared. A function of the E vs SOC curve was found by fitting a ninth degree polynomial to the end of relaxation voltage versus SOC curve. This was done using the `curve_fit` function from `scipy.optimize`. The polynomial was then converted into a symbolic function and differentiated using the python library `SymPy`, to give a function for $\frac{dE}{dSOC}$. The value for $\frac{dE}{d\delta}$ to use in eq. (2.23) could then be found by evaluating $\frac{dE}{dSOC}$ at the average SOC in each GITT pulse and utilizing eq. (3.3).

Another possible method of finding the E vs SOC curve is to use the parameterization of the equilibrium potential as a function of SOC formulated by Sethuraman et al. [44]. Sethuraman et al. gives the potential as a function of SOC as

$$U = -4.76z^6 + 9.34z^5 - 1.8z^4 - 7.13z^3 + 5.8z^2 - 1.94z + 0.62, \quad (0 \leq z \leq 1) \quad (3.4)$$

where z is the state of charge. This function could be used to calculate diffusion coefficients without the $\frac{dE}{d\delta}$ to $\frac{\Delta E_s}{\Delta\delta}$ simplification with the same approach as in the previous paragraph.

3.5 Battery Tester Precision

The Arbin battery tester used in this work has a voltage measurement precision of < 100 ppm. The voltage range is -5 to 5 V. < 100 ppm out of the 10 V voltage range gives a precision of < 1 mV. The measurement resolution is < 10 µV. The product specifications of the Arbin battery tester used can be found in Appendix C.

Chapter 4

Results

4.1 Diffusion Coefficients as Function of SOC

Diffusion coefficients from GITT experiments were calculated as described in Section 3.4.2. The calculated diffusion coefficients over all pulse lengths for the cell TF_60_2 ($h = 60$ nm and current rate C/10) are shown in Figure 4.1.

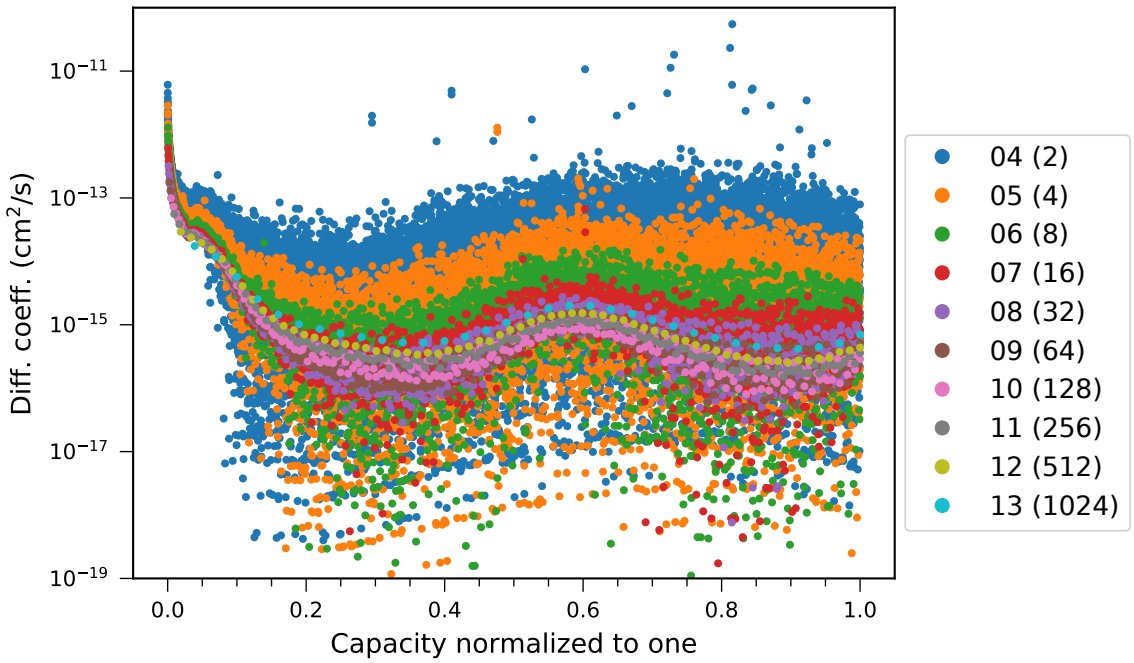

Figure 4.1: Plot of diffusion coefficients as a function of normalized capacity for a cell with $h = 60$ nm and current rate C/10. The legend show the cycle number first and the pulse length in parenthesis.

The diffusion coefficients in Figure 4.1 contain much noise, especially for low pulse lengths. This makes comparison of the results between different pulse lengths difficult. For easier comparison the data was smoothed according to Section 3.4.5 before further plotting. For all the GITT cycles the number of data points was increased to 20000 before a median filter with size 50 was applied to remove outliers followed by a Gaussian filter with sigma = 300 to smooth the curve. The discharge plots for

one representative cell of each of the C-rates for both 60 nm and 80 nm thin films are shown in Figure 4.2. Corresponding plots during charge are shown in Figure 4.3. Equivalent plots for all cells can be found in Appendix D.

These plots show that the diffusion coefficients vary according to the state of charge. The diffusion coefficient is high at the start of lithiation and drops as the electrode is lithiated until around 0.3 - 0.4 SOC. The diffusion coefficients then increase until around 0.6 SOC, before they start to decrease again. This pattern can be seen for lithiation in all the cells. The D(SOC) curves for delithiation have a slightly different shape compared to lithiation, but they show a similar trend.

Figures 4.2 and 4.3 also show a variation in diffusion coefficients as a function of the pulse lengths. The diffusion coefficients start by decreasing as the pulse length increases, they then reach a turning point and from there on increase with increasing pulse lengths. This turning point falls at a different pulse length for the different current rates.

The plots in 4.2 and 4.3 compare the diffusion coefficient curves over different pulse lengths. Similar plots comparing the curves over different currents can be found in Appendix E.

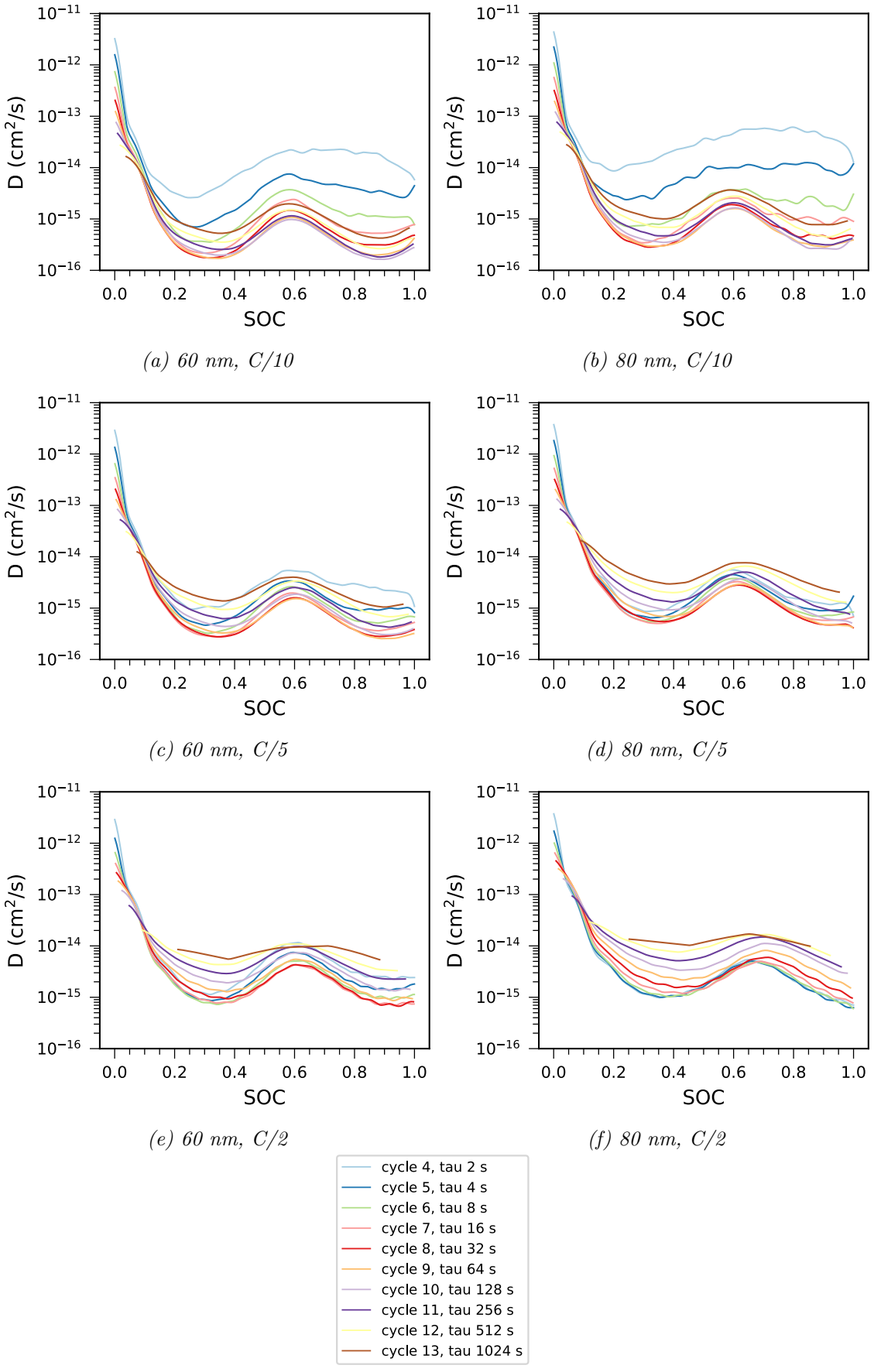

(a) 60 nm, C/10

(b) 80 nm, C/10

(c) 60 nm, C/5

(d) 80 nm, C/5

(e) 60 nm, C/2

(f) 80 nm, C/2

Figure 4.2: Plots of calculated diffusion coefficients versus state of charge during discharge. a), c) and e) are 60 nm thin films. b), d) and f) are 80 nm thin films. One cell with each current rate is shown, with the current rate increasing downward.

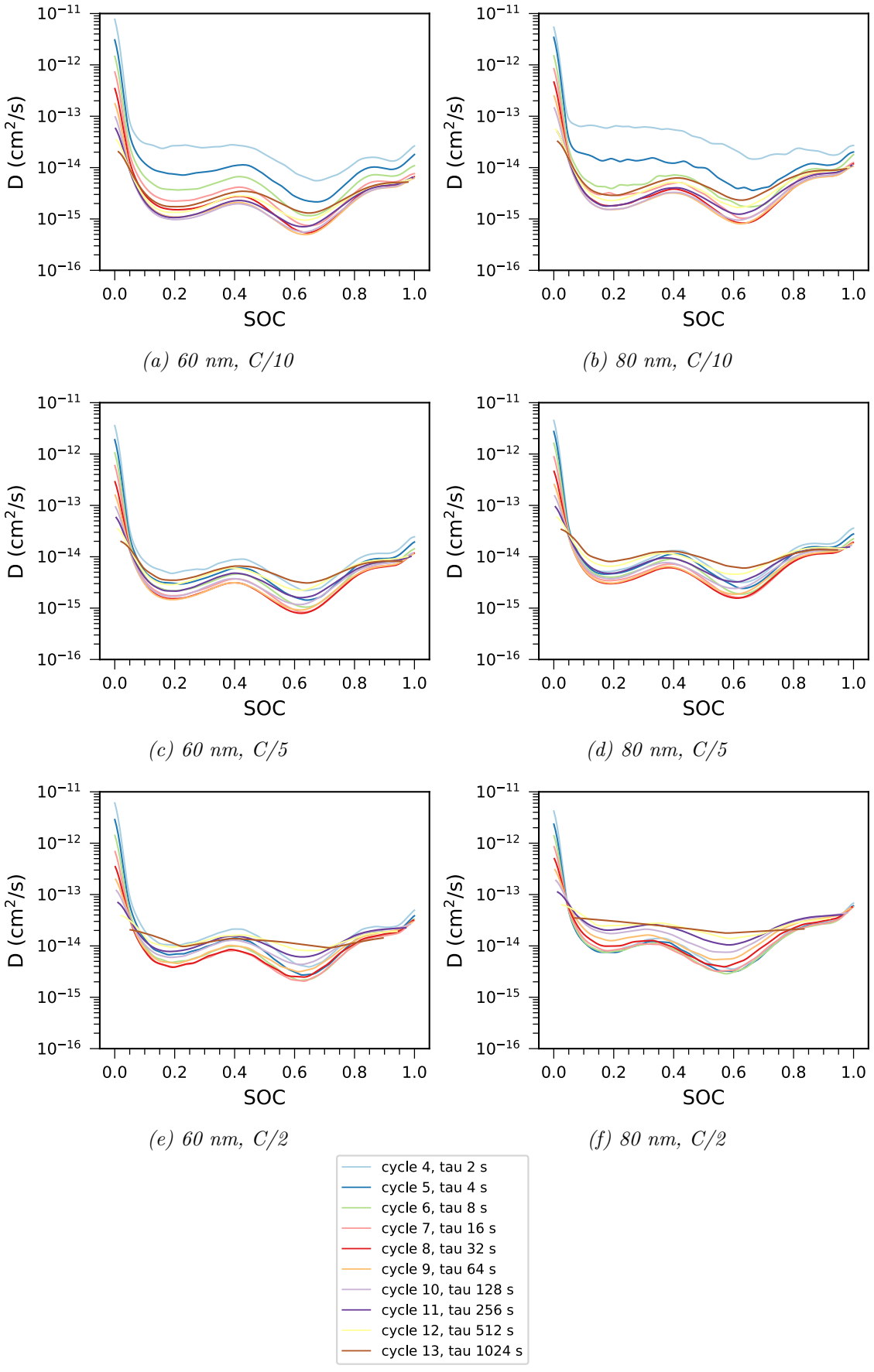

(a) 60 nm, C/10

(b) 80 nm, C/10

(c) 60 nm, C/5

(d) 80 nm, C/5

(e) 60 nm, C/2

(f) 80 nm, C/2

Figure 4.3: Plots of calculated diffusion coefficients versus state of charge during discharge. a), c) and e) are 60 nm thin films. b), d) and f) are 80 nm thin films. One cell with each current rate is shown, with the current rate increasing downward.

4.2 Median of Diffusion Coefficients

Figure 4.2 and 4.3 in Section 4.1 show that the calculated diffusion coefficients vary with both pulse length and current rates, but the relationship between these variables is not very clear in those figures. Plots with the median of all the calculated diffusion coefficients for different pulse lengths from one SOC to another were made to better compare how the diffusion coefficients change with both the GITT pulse length and the current rate. These plots have the pulse length on the x-axis and the median of the diffusion coefficients on the y-axis. The median was chosen above the mean for these plots to minimize the effect from outliers on the result. A base two logarithmic axis was chosen for the x-axis, since the pulse times used were different powers of two. A logarithmic axis was used on the y-axis to better show the variation in diffusion coefficients over several orders of magnitude. The different current rates are plotted in different colors, with each cell being a different shade of that color. Blue shades are C/10, green shades are C/5 and orange shades are C/2.

Because the diffusion coefficients vary substantially with the state of charge, the median values were calculated within small state of charge windows with a width of 0.1 SOC. Figure 4.4 display the medians during discharge for both 60 nm and 80 nm thin films in the SOC windows 0.2 - 0.3, 0.45 - 0.55 and 0.7 to 0.8. Corresponding plots during charge at the same SOC windows can be found in Figure 4.5. Corresponding plots for SOC windows not included in this Section can be found in Appendix F.

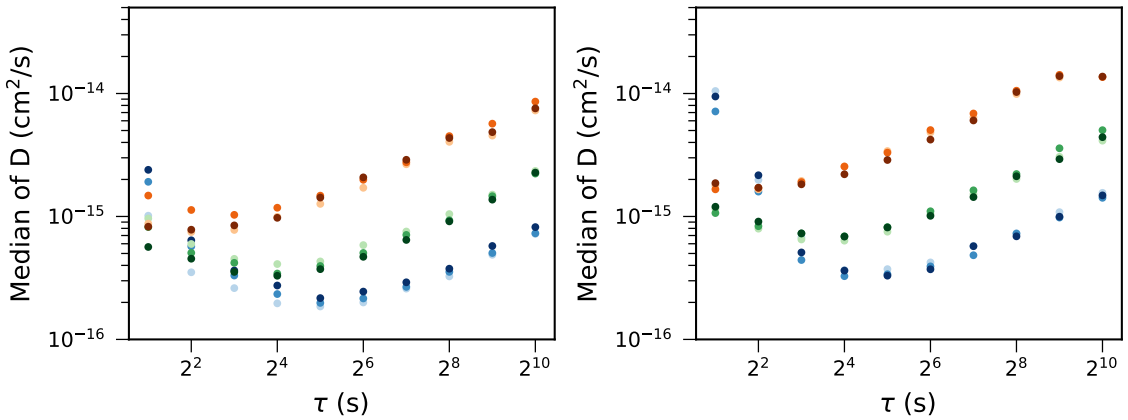

(a) 60 nm, discharge, 0.2 - 0.3 SOC

(b) 80 nm, discharge, 0.2 - 0.3 SOC

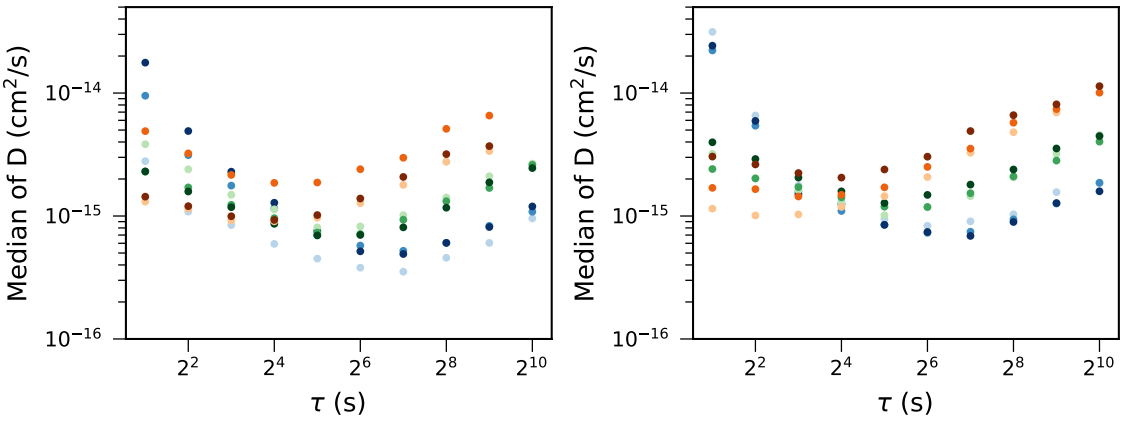

(c) 60 nm, discharge, 0.45 - 0.55 SOC

(d) 80 nm, discharge, 0.45 - 0.55 SOC

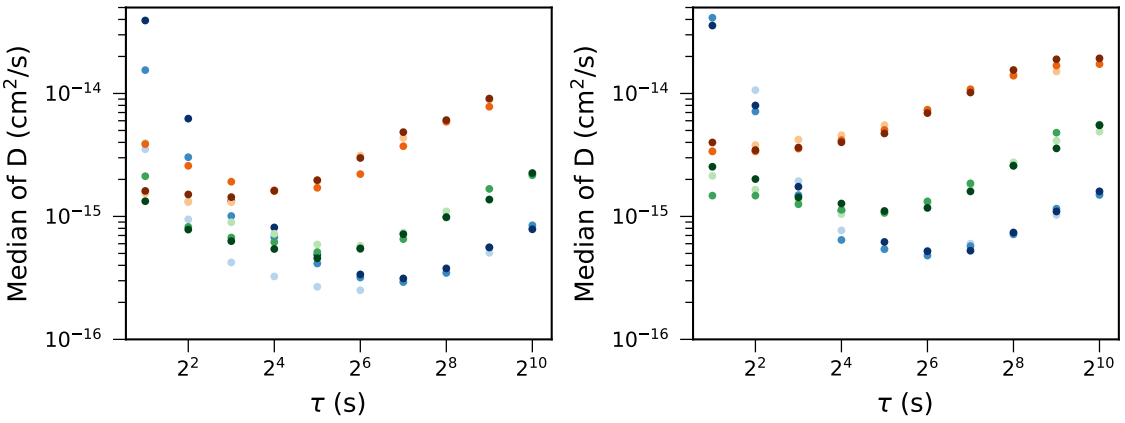

(e) 60 nm, discharge, 0.7 - 0.8 SOC

(f) 80 nm, discharge, 0.7 - 0.8 SOC

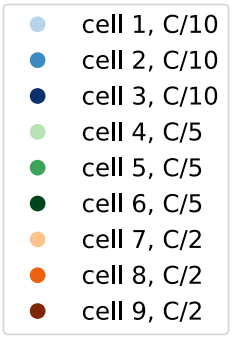

Figure 4.4: Median values of D within given SOC windows as a function of pulse length during discharge. The different current rates are plotted in different colors, with the different cells at the same current rate have varying shades of that color, as given by the legend.

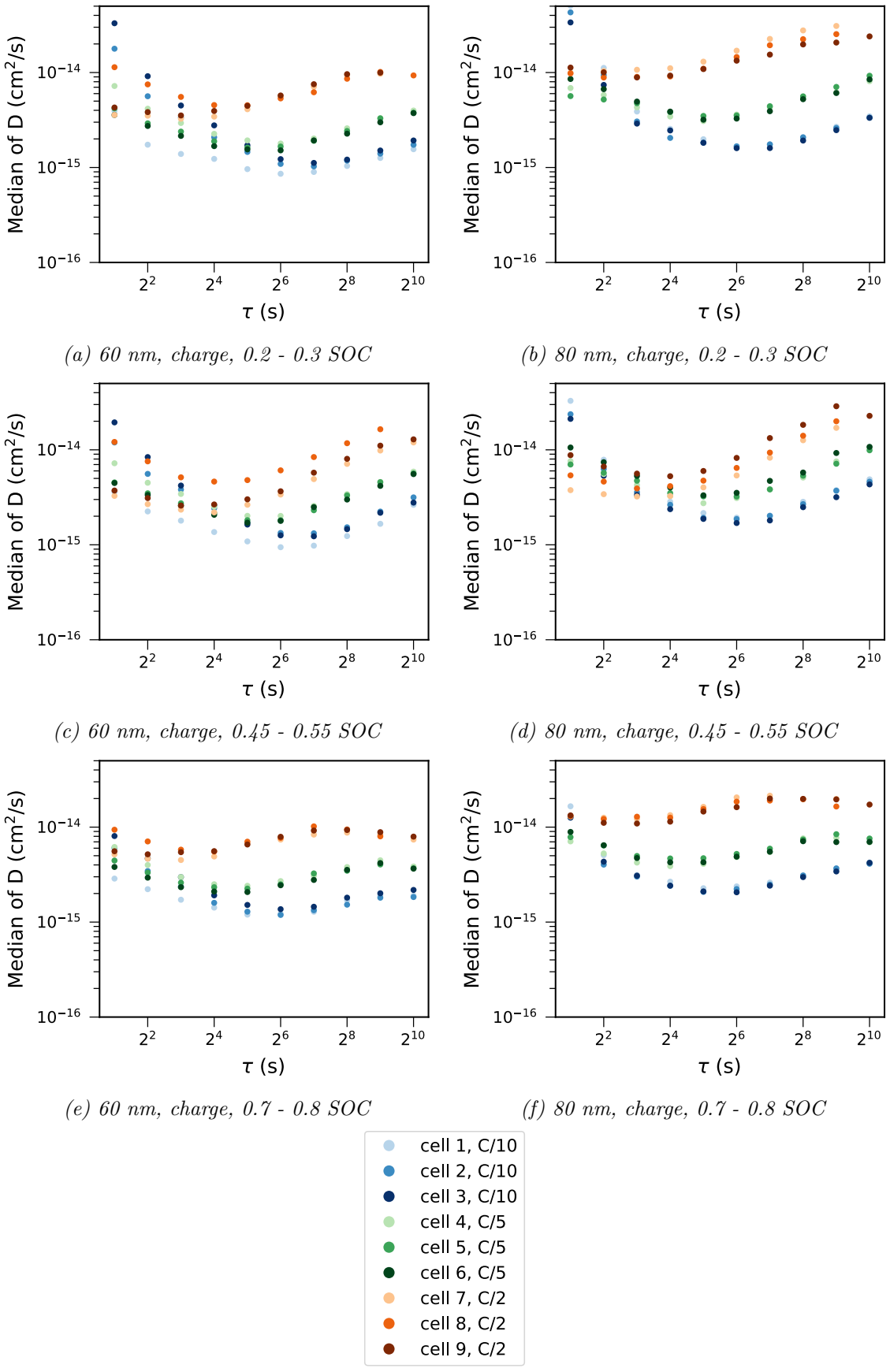

(a) 60 nm, charge, 0.2 - 0.3 SOC

(b) 80 nm, charge, 0.2 - 0.3 SOC

(c) 60 nm, charge, 0.45 - 0.55 SOC

(d) 80 nm, charge, 0.45 - 0.55 SOC

(e) 60 nm, charge, 0.7 - 0.8 SOC

(f) 80 nm, charge, 0.7 - 0.8 SOC

Figure 4.5: Median values of D within given SOC windows as a function of pulse length during charge. The different current rates are plotted in different colors, with the different cells at the same current rate have varying shades of that color, as given by the legend.

4.3 Checking $\frac{dE}{d\sqrt{t}}$ to $\frac{\Delta E}{\Delta\sqrt{t}}$ Simplification

Plots of the voltage as a function of $\sqrt{t}$ were made for selected pulses, to test the validity of the simplification $\frac{dE}{d\sqrt{t}}$ to $\frac{\Delta E}{\Delta\sqrt{t}}$ going form eq. (2.22) to eq. (2.25), as explained in Section 3.4.6. The linear area of the graph was found by visual inspection, and a linear function was fitted to this area. Four examples of such linear fits at different pulse lengths (for the cell TFSi_80_2 and at approximately 0.5 SOC) are shown in f Figure 4.8. These linear fits are compared with the values given by $\frac{\Delta E}{\Delta\sqrt{t}}$, which are represented by the green lines. The remaining linear fits at 0.5 SOC for the same cell can be found in Appendix G. The linear fits were only made for 6 cells, one of each current rate and thin film thickness, due to the time consuming nature of finding the linear area by visual inspection.

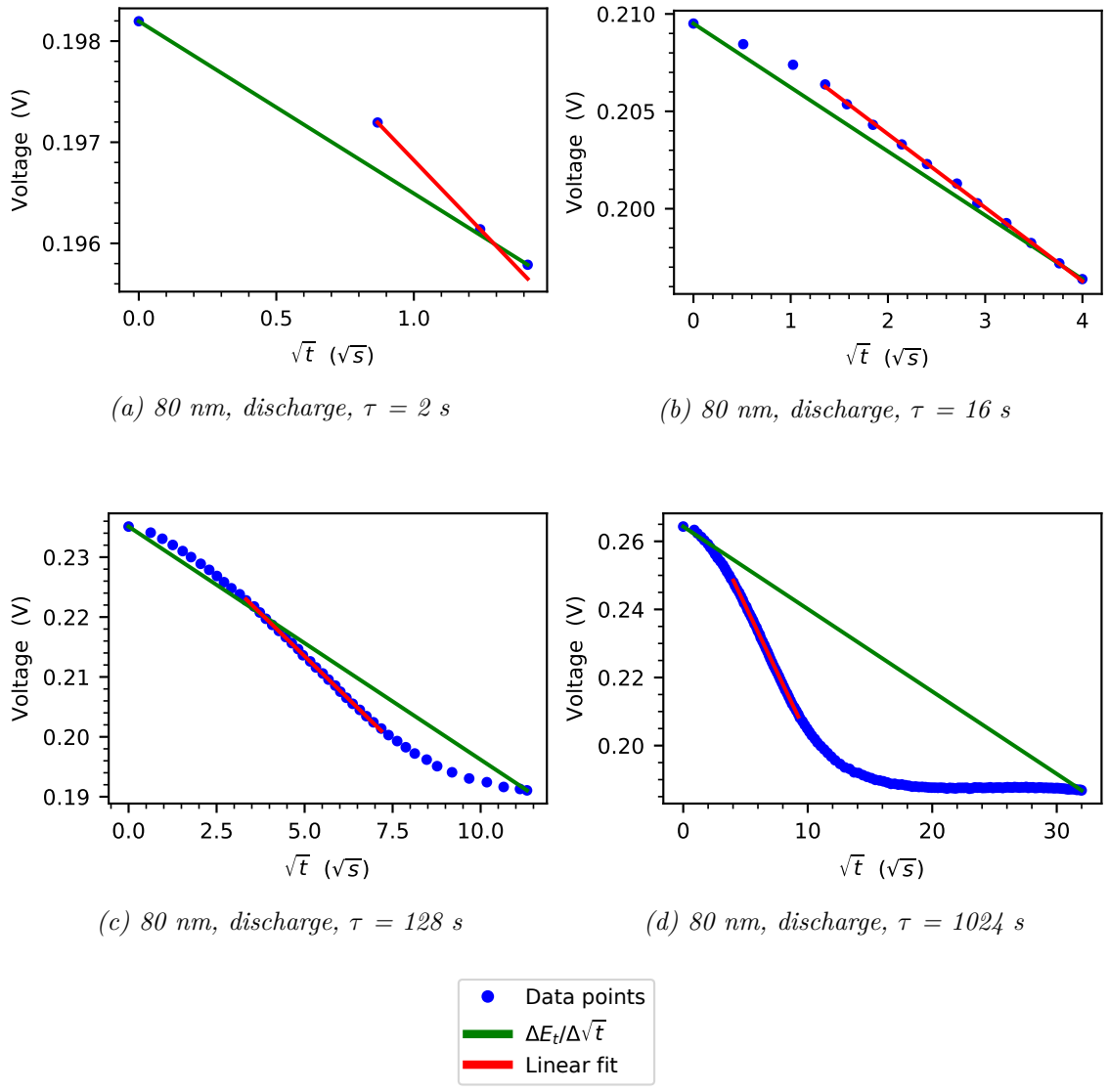

(a) 80 nm, discharge, τ = 2 s

(b) 80 nm, discharge, τ = 16 s

(c) 80 nm, discharge, τ = 128 s

(d) 80 nm, discharge, τ = 1024 s

Figure 4.6: Linear fit of the linear area on the $E(\sqrt{t})$ curve, compared with $\frac{\Delta E}{\Delta\sqrt{t}}$. Four different pulse lengths are shown, all with a current rate C/10.

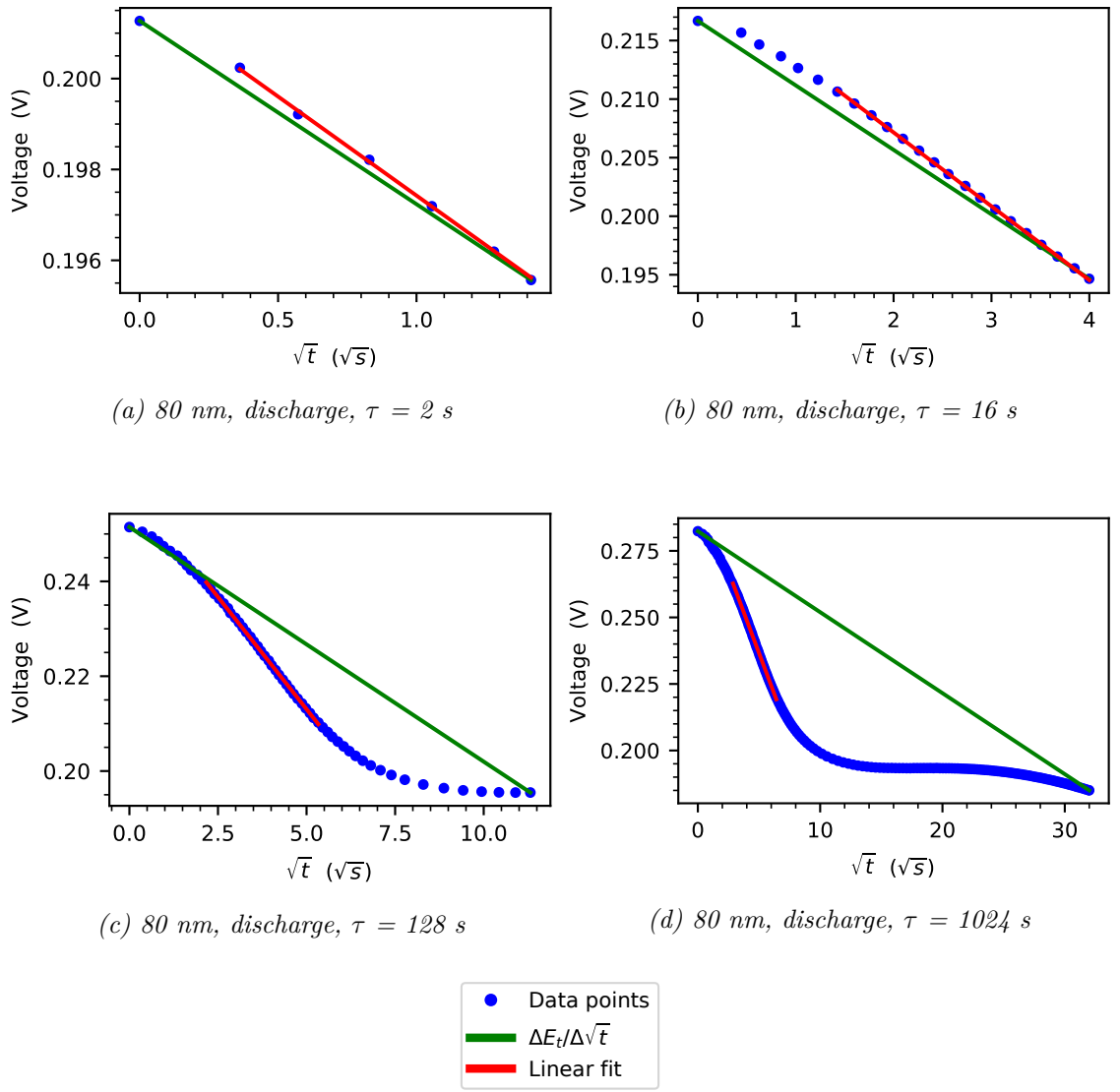

(a) 80 nm, discharge, τ = 2 s

(b) 80 nm, discharge, τ = 16 s

(c) 80 nm, discharge, τ = 128 s

(d) 80 nm, discharge, τ = 1024 s

Figure 4.7: Linear fit of the linear area on the E versus square root of t curve for four different pulse lengths with current rate C/5.

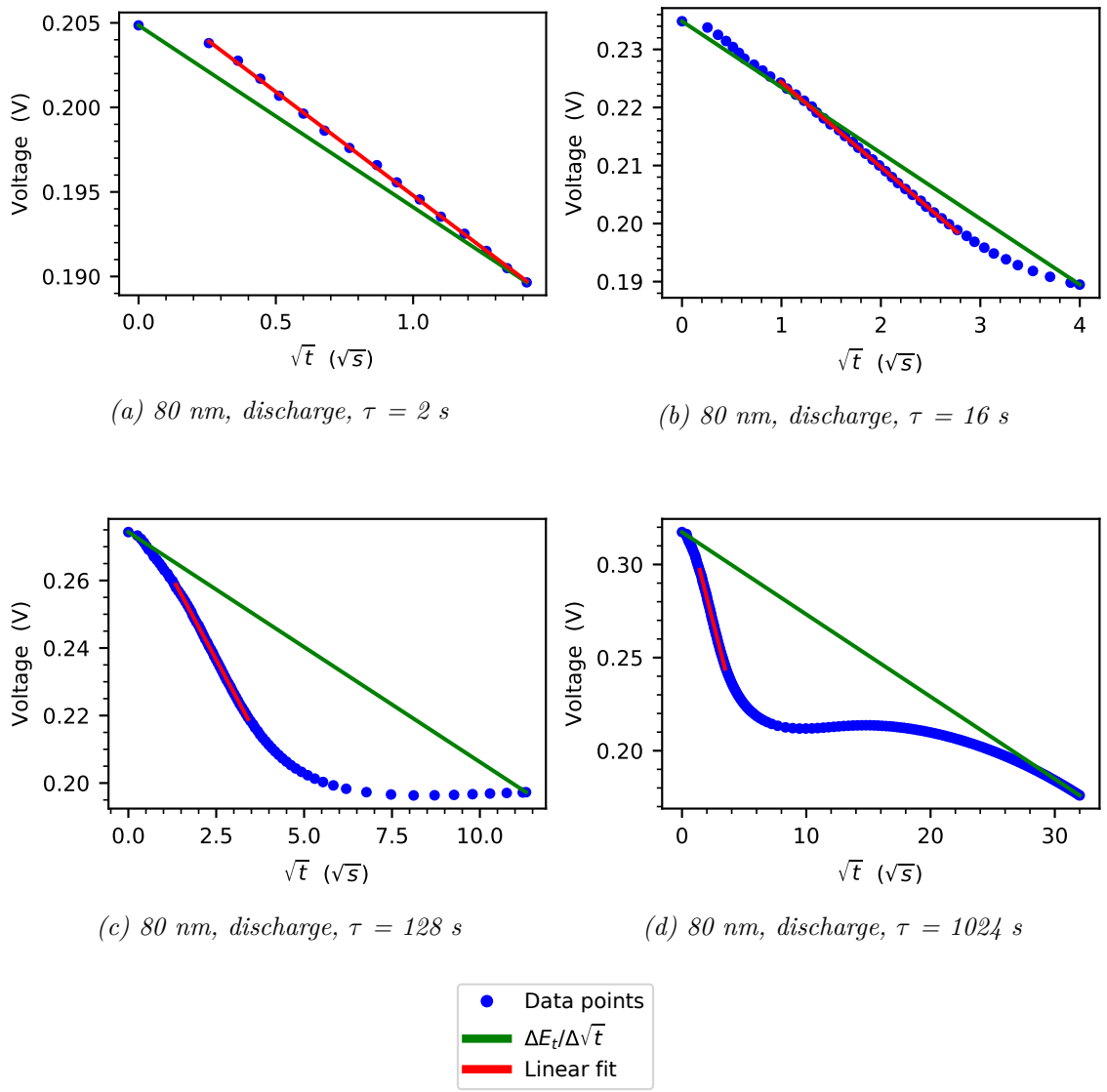

(a) 80 nm, discharge, τ = 2 s

(b) 80 nm, discharge, τ = 16 s

(c) 80 nm, discharge, τ = 128 s

(d) 80 nm, discharge, τ = 1024 s

Figure 4.8: Linear fit of the linear area on the E versus square root of t curve for four different pulse lengths with current rate C/2.

Diffusion coefficients were calculated for the selected pulses using the regular GITT equation (eq. (2.25)) and using the slope of the fitted linear equation for $\frac{dE}{d\sqrt{t}}$ in eq. (2.22). The resulting D values were plotted together in Appendix H with the pulse length along the x axis to compare the two methods. To get a clearer picture of the error in using the $\frac{\Delta E}{\Delta\sqrt{t}}$, the difference between the diffusion coefficients calculated from the eq. (2.25) and eq. (2.22) was found. This was done for all three different current rates (C/10, C/5 and C/2), and the results plotted together in Figure 4.9.

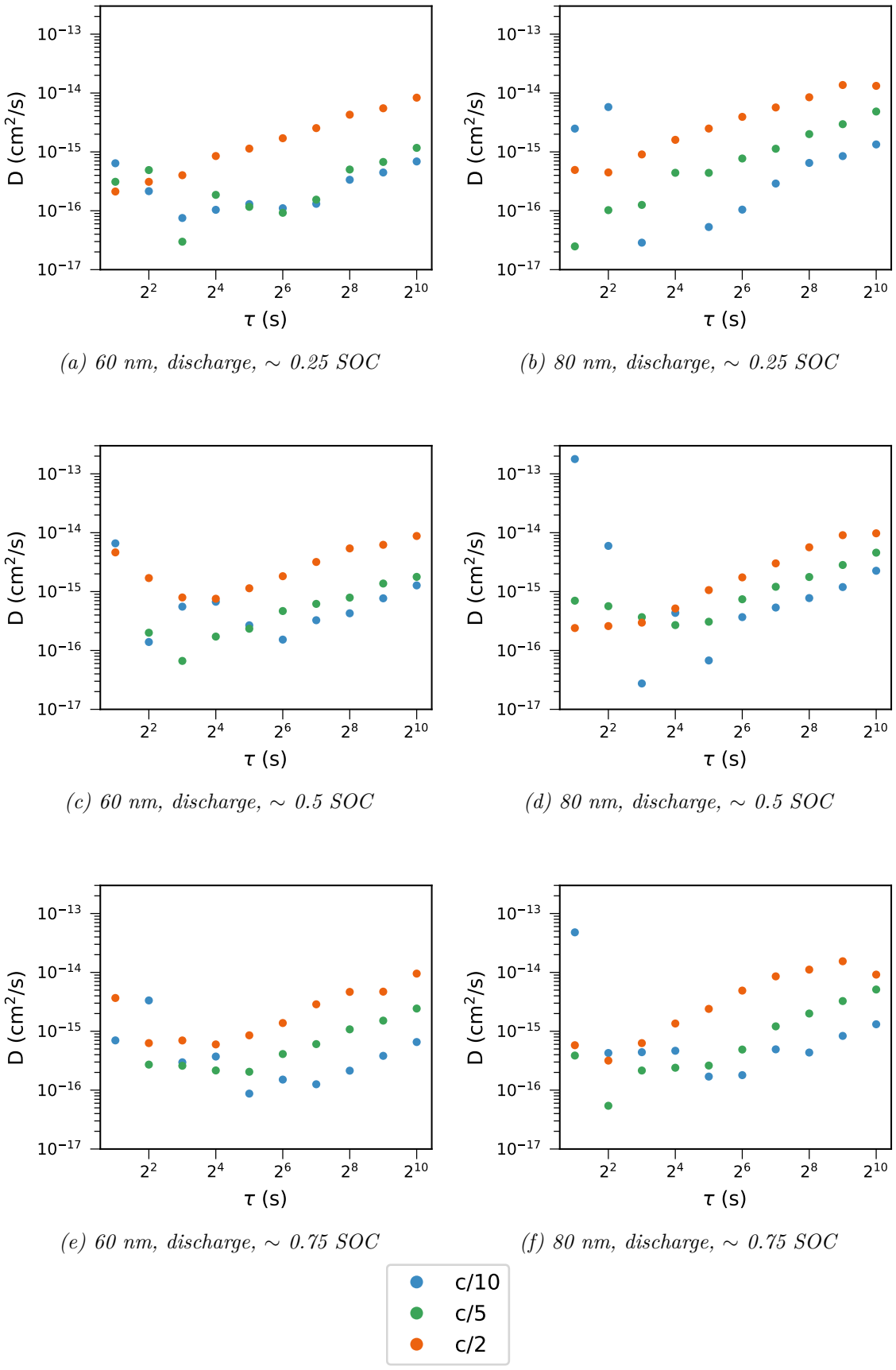

(a) 60 nm, discharge, ∼ 0.25 SOC

(b) 80 nm, discharge, ∼ 0.25 SOC

(c) 60 nm, discharge, ∼ 0.5 SOC

(d) 80 nm, discharge, ∼ 0.5 SOC

(e) 60 nm, discharge, ∼ 0.75 SOC

(f) 80 nm, discharge, ∼ 0.75 SOC

Figure 4.9: Difference between linear fit and regular GITT.

4.4 Checking $\frac{dE}{d\delta}$ to $\frac{\Delta E}{\Delta \delta}$ Simplification

To test the validity of the simplification of $\frac{dE}{d\delta}$ to $\frac{\Delta E}{\Delta \delta}$ a polynomial was fitted to the OCV curve created by plotting all the end of relaxation period voltages against the normalized capacities. A ninth degree polynomial was chosen to give the best fit. The polynomial fit was found in Python with the help of the `curve_fit` function from `scipy.optimize`. An example of such a fitted curve is shown in Figure 4.10.

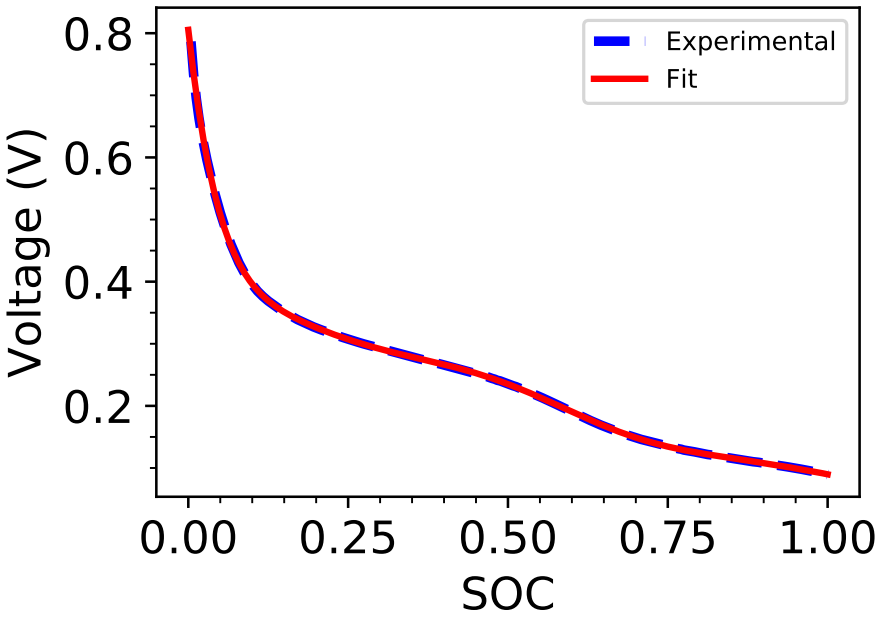

Figure 4.10: A ninth degree polynomial function fitted to the end of relaxation period voltages versus normalized capacity curve. This example if from a cell with 80 nm thin film and current rate C/10. The plotted cycle had pulse length 128 s and pause length 384 s.

The estimated coefficients for the polynomial fit were used to make a symbolic function in python with the help of the python package SymPy [57]. The symbolic function was then differentiated to find the $\frac{dE}{d\delta}$ curve. The slope of the E versus δ curve for one particular GITT current pulse was found by evaluating $\frac{dE}{d\delta}$ at the average SOC in that current pulse. The slope thus estimated was used to calculate diffusion coefficients with the help of equation (2.23). The current used in the calculations was the average current in the GITT step. For V_m, the molar volume of Si (12.06 cm^3/mol [58]) was used and, seeing as the electrode is a thin film, the surface area of the electrode was calculated as $S = \pi r^2$, where r is the electrode radius (r = 0.75 cm). The diffusion coefficients calculated from eq. (2.23) were then plotted together with the diffusion coefficients calculated from the simplified GITT equation, eq. (2.25). The results of this for the four pulse lengths 2, 16, 128 and 1024 s for the cell TFSi_80_2 are shown in Figure 4.11.

The difference between the median of the diffusion coefficients calculated with eq. (2.23) and eq. (2.25) were plotted, see Figure 4.12. This was done at different SOC windows as the diffusion coefficients vary with SOC. Plots showing the median D values from both methods together were also made, these can be seen in Appendix

I.

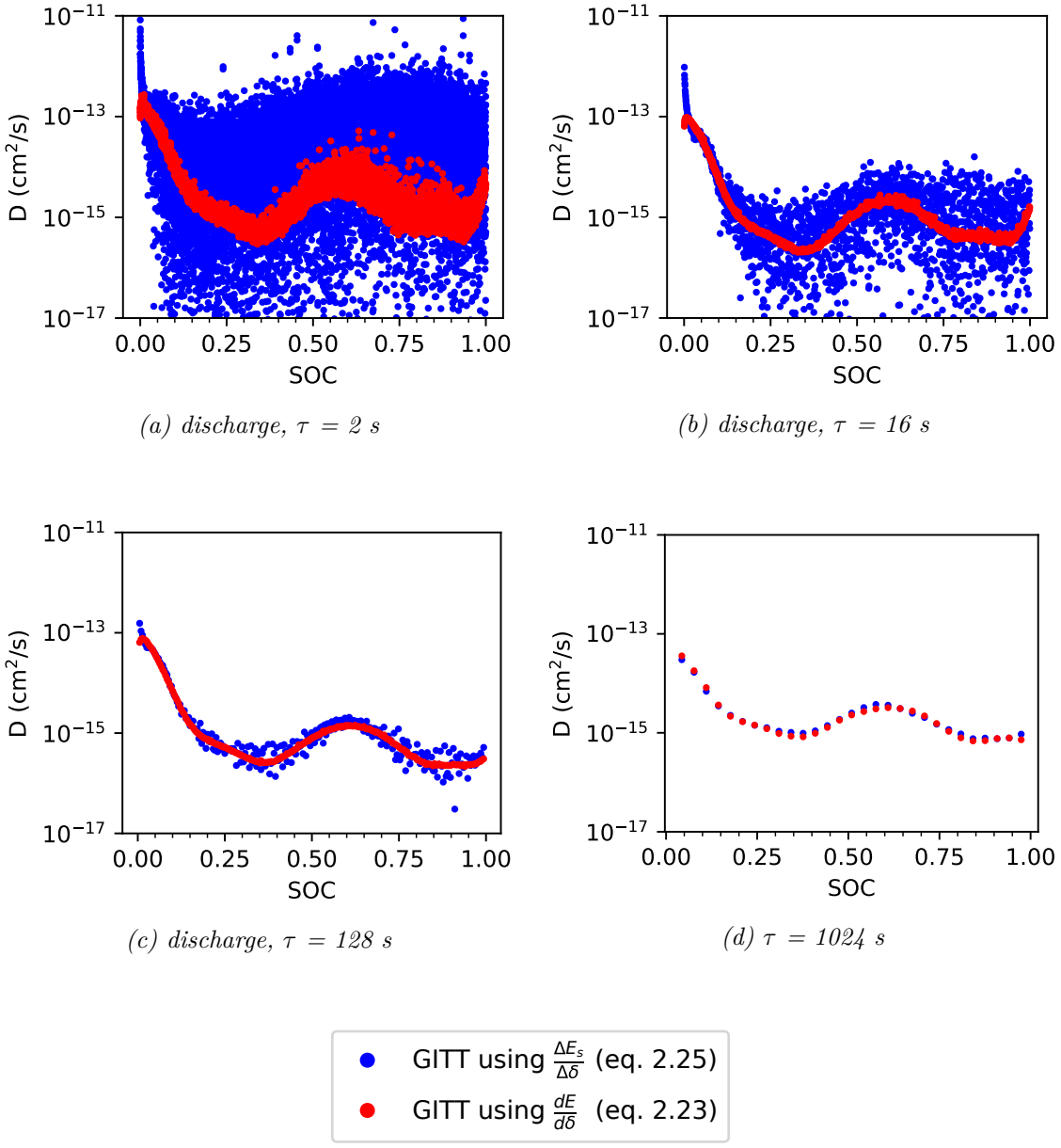

(a) discharge, $\tau = 2$ s

(b) discharge, $\tau = 16$ s

(c) discharge, $\tau = 128$ s

(d) $\tau = 1024$ s

Figure 4.11: Comparison of diffusion coefficients calculated from curve fit GITT ($\frac{dE}{d\delta}$) and regular GITT (ΔE_s). These plots are from a cell with an 80 nm thin film and a current rate of C/10.

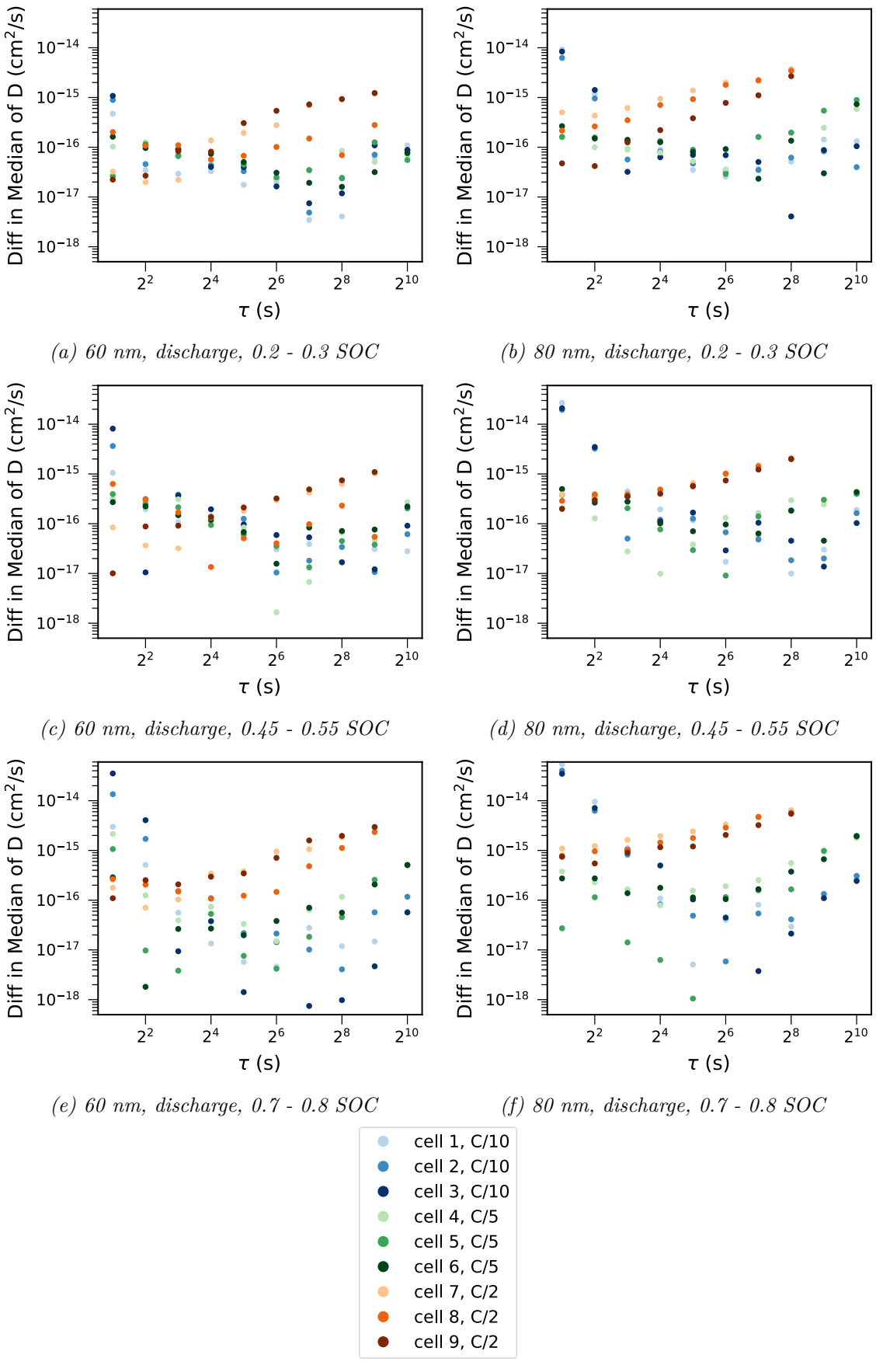

(a) 60 nm, discharge, 0.2 - 0.3 SOC

(b) 80 nm, discharge, 0.2 - 0.3 SOC

(c) 60 nm, discharge, 0.45 - 0.55 SOC

(d) 80 nm, discharge, 0.45 - 0.55 SOC

(e) 60 nm, discharge, 0.7 - 0.8 SOC

(f) 80 nm, discharge, 0.7 - 0.8 SOC

Figure 4.12: Difference between the median D values calculated from regular GITT (eq. (2.25)) and GITT using a curve fit for the determination of $\frac{dE}{d\delta}$ (eq. (2.23))

4.4.1 Using the Parameterization

Another way to calculate diffusion coefficients through eq. (2.23) is to use the parameterization of the equilibrium potential as a function of SOC formulated by Sethuraman et. al. [44] (see Section 3.4.6). Figure 4.13 illustrates how this parameterization differs from the polynomial fitted to the end of relaxation voltage curves.

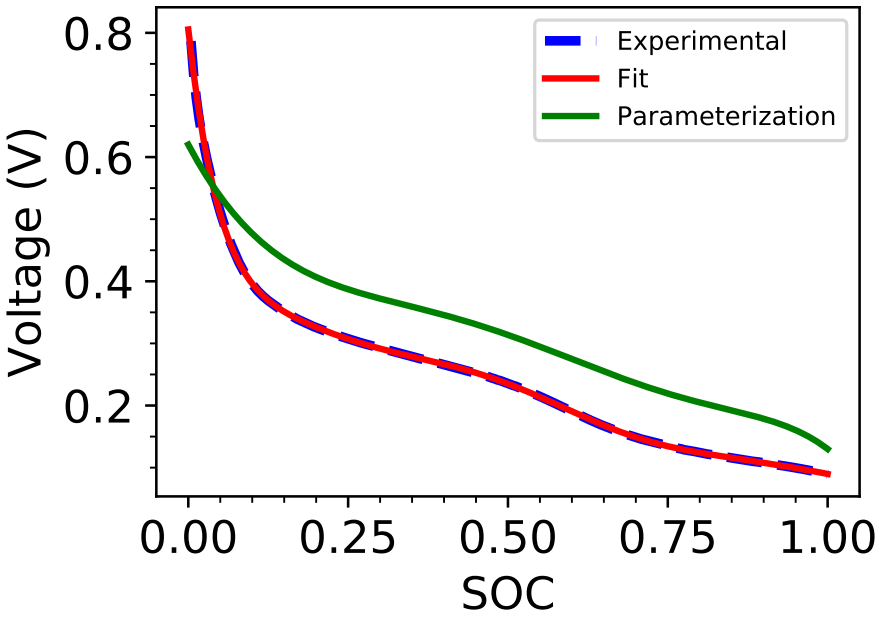

Figure 4.13: The parameterization given by Sethuraman et al. [44] compared with a ninth degree polynomial function fitted to the end of relaxation period voltages versus normalized capacity curve.

The value for $\frac{dE}{d\delta}$ is then found by estimating the derivative of the parameterization at the average SOC in each current pulse. All other variables used were the same as in Section 4.4. Plots corresponding to the ones in Figure 4.11 were made using the parameterization, and are given in Figure 4.14. Again the medians for each pulse length in chosen SOC windows were calculated, and the difference between the medians found from the regular GITT and the GITT using the parameterization was calculated. These results can be found in Figure 4.15.

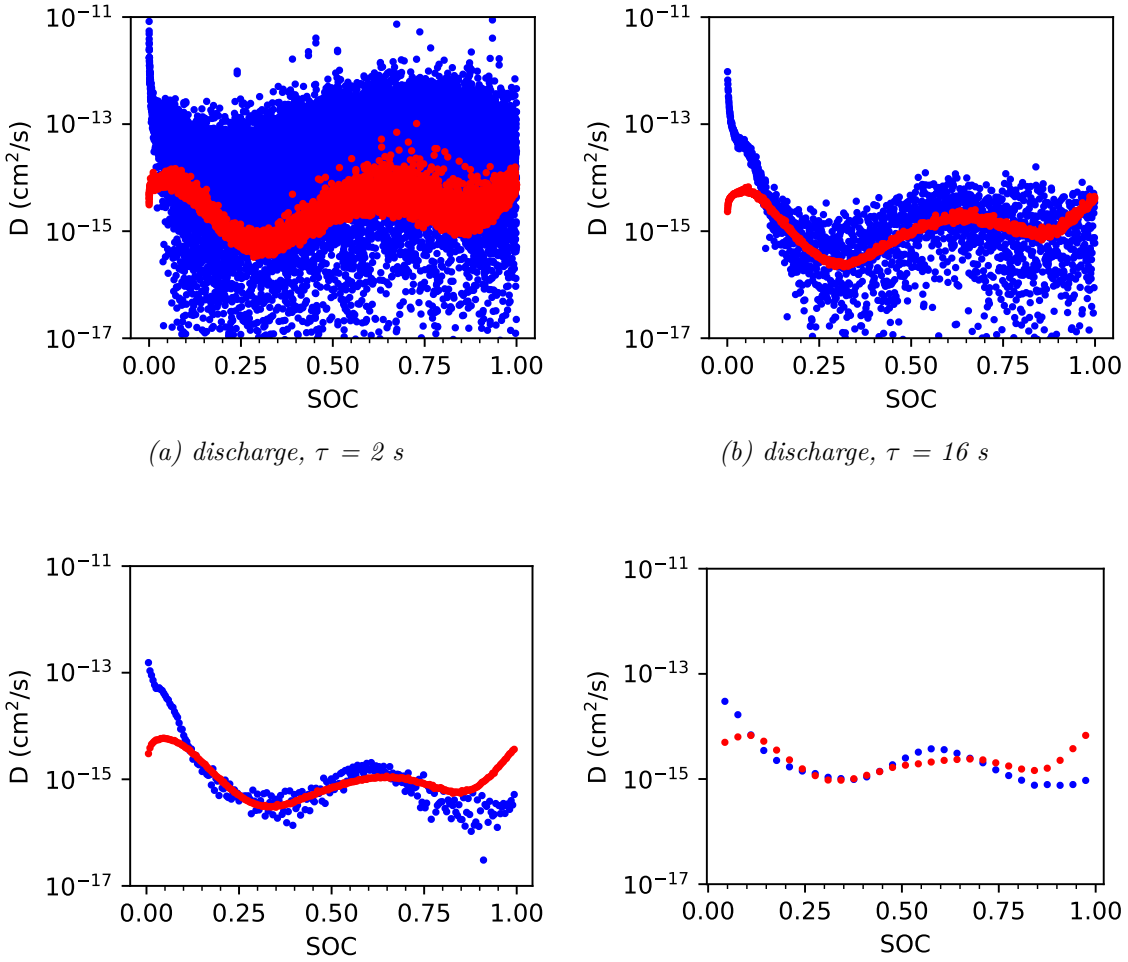

(a) discharge, τ = 2 s

(b) discharge, τ = 16 s

(c) discharge, τ = 128 s

(d) τ = 1024 s

Figure 4.14: Comparison of diffusion coefficients calculated from parameterization GITT (red dots) and regular GITT (blue dots). These plots are from a cell with an 80 nm thin film and a current rate of C/10.

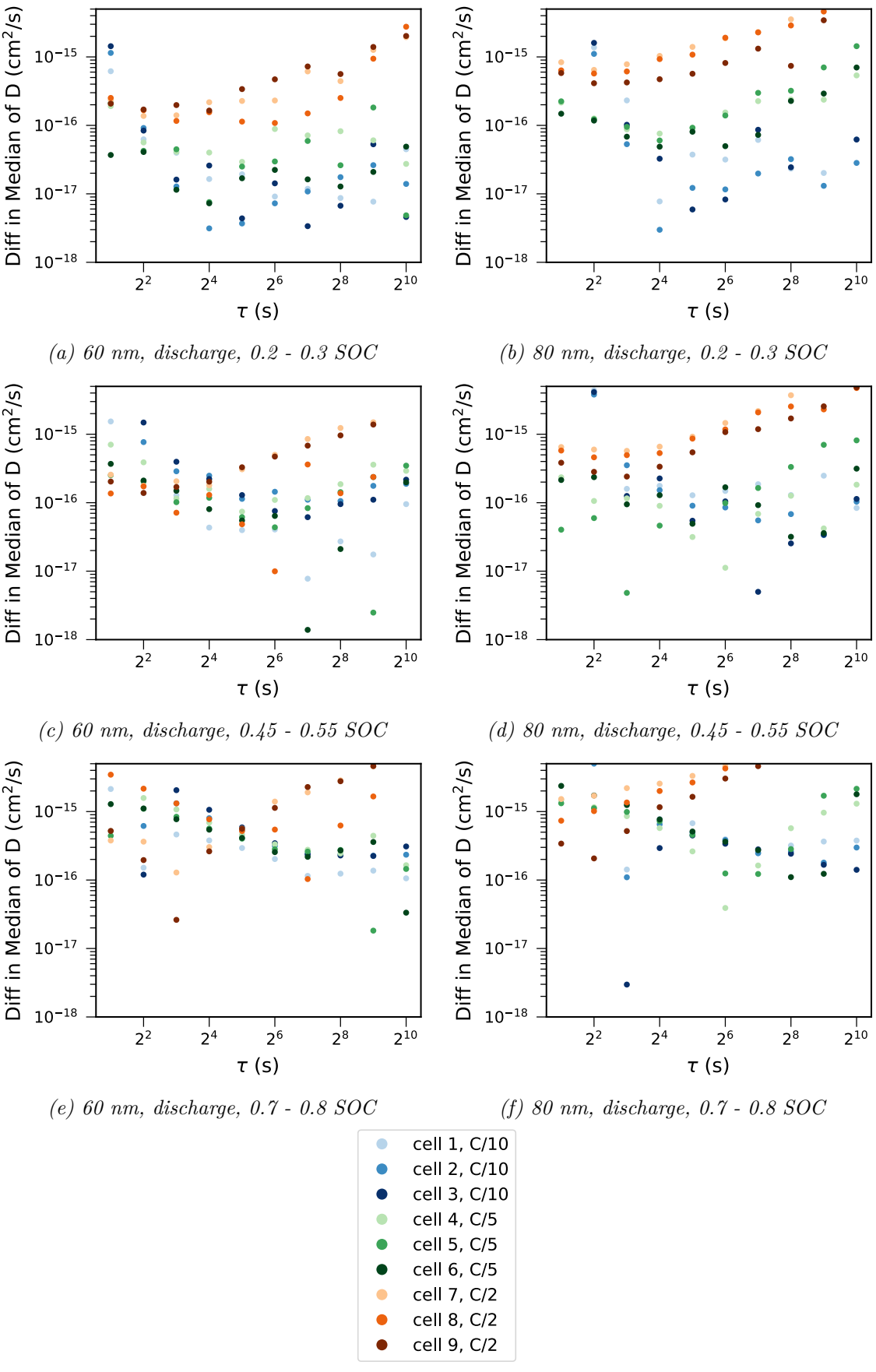

(a) 60 nm, discharge, 0.2 - 0.3 SOC

(b) 80 nm, discharge, 0.2 - 0.3 SOC

(c) 60 nm, discharge, 0.45 - 0.55 SOC

(d) 80 nm, discharge, 0.45 - 0.55 SOC

(e) 60 nm, discharge, 0.7 - 0.8 SOC

(f) 80 nm, discharge, 0.7 - 0.8 SOC

Figure 4.15: Difference between the median D values calculated from regular GITT and GITT using the parameterized curve of the equilibrium voltage versus SOC.

4.5 Linearity of E(δ)

Another method to check the validity of assuming $\frac{dE}{d\delta}$ equal to $\frac{\Delta E}{\Delta \delta}$ is to look at how linear the E vs δ curve is in a δ window equal to the δ change in the cell during one GITT pulse. The relationship between δ and SOC is explained in Section 3.4.6. The $E(\delta)$ and $E(SOC)$ curves have the same curvature, but differ by a constant. The curvature of $E(\delta)$ in one δ window is the same as the curvature of $E(SOC)$ in the corresponding SOC window. As can be seen in the plot of $\frac{d^2E}{dSOC^2}$ in Figure 4.16, the curvature changes the most at values close to 0 SOC. The $\frac{d^2E}{dSOC^2}$ curve shown is from the end of relaxation time voltages in a cycle with pulse time 128 s and relaxation time 384 in the cell TFSi_80_2. It is therefore enough to look at the linearity in the first SOC window, as this will be the limiting factor. This was done for the cell TFSi_80_2, and the result for the last six cycles (cycle 8 to cycle 13) is shown in Figure 4.17. The E versus SOC curve used to check the linearity was the same E versus SOC curve that was differentiated in Figure 4.16, i.e. cycle 10 from cell TFSi_80_2.

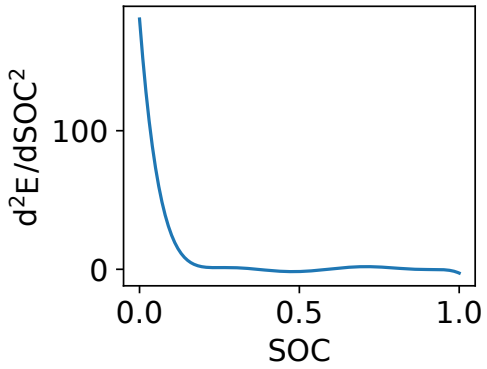

Figure 4.16: Plot of $\frac{d^2E}{dSOC^2}$ for a cell with h = 80 nm and current rate C/10, for cycle 10 (pulse time 128 s, pause time 384 s).

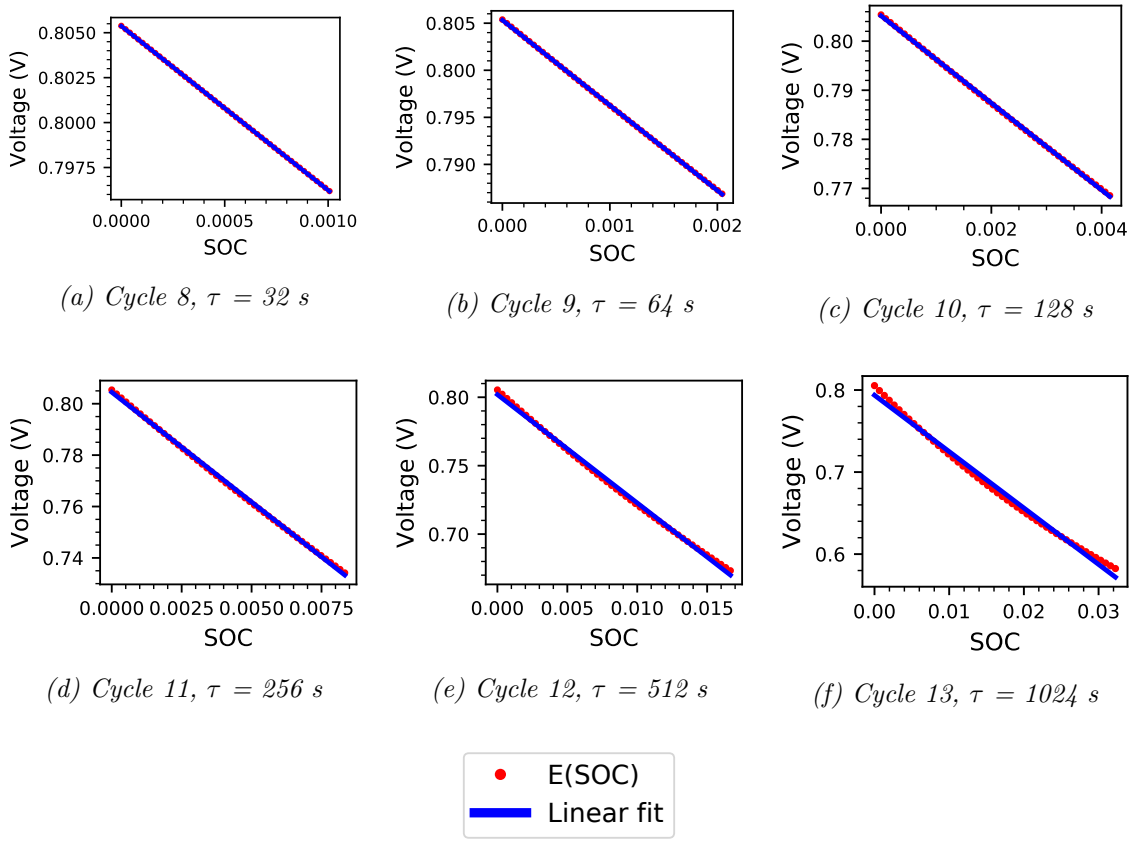

(a) Cycle 8, τ = 32 s

(b) Cycle 9, τ = 64 s

(c) Cycle 10, τ = 128 s

(d) Cycle 11, τ = 256 s

(e) Cycle 12, τ = 512 s

(f) Cycle 13, τ = 1024 s

Figure 4.17: Linearity of E as function of SOC for voltage windows corresponding to one GITT pulse for varying pulse lengths. The red dots are the experimental data points and the blue line is a linear fit. All the plots are from the cell TFSi_80_2, with a current rate of C/10.

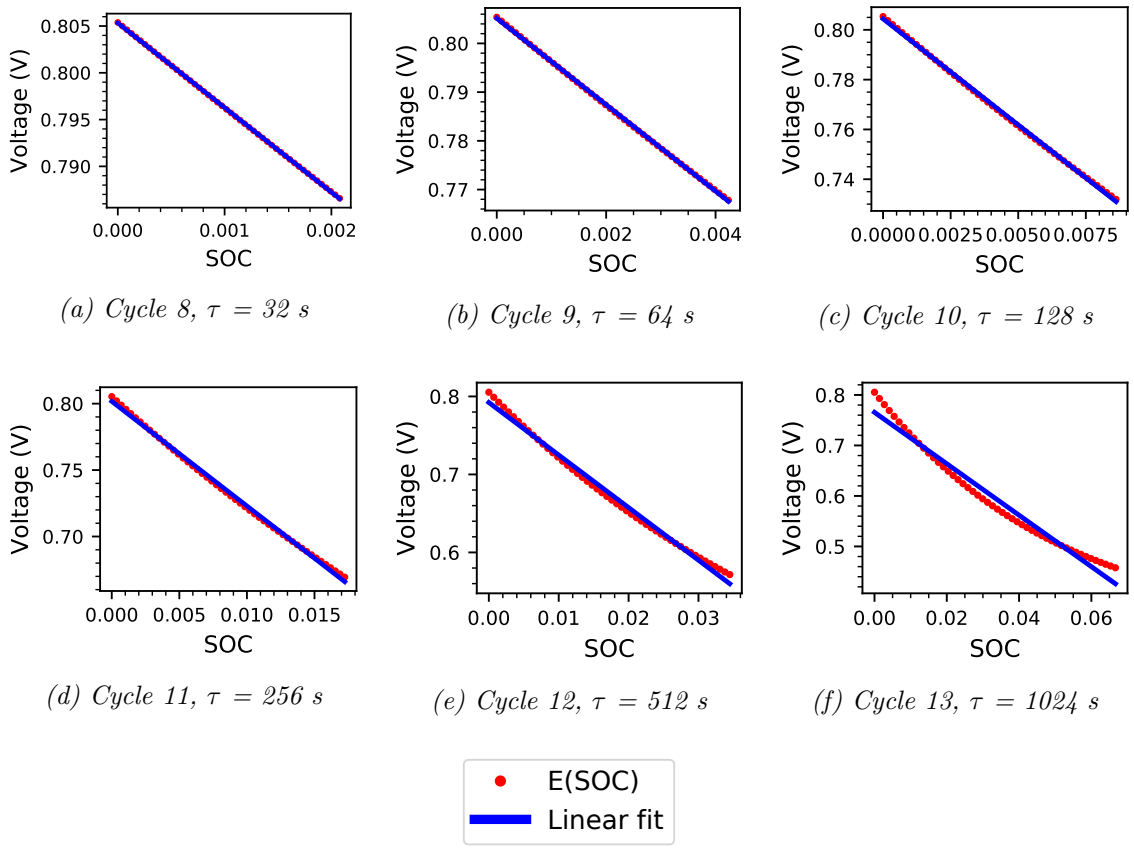

(a) Cycle 8, τ = 32 s

(b) Cycle 9, τ = 64 s

(c) Cycle 10, τ = 128 s

(d) Cycle 11, τ = 256 s

(e) Cycle 12, τ = 512 s

(f) Cycle 13, τ = 1024 s

Figure 4.18: Linearity of E as function of SOC for voltage windows corresponding to one GITT pulse for varying pulse lengths. The red dots are the experimental data points and the blue line is a linear fit. All the plots are from the cell TFSi_80_8, with a current rate of C/5.

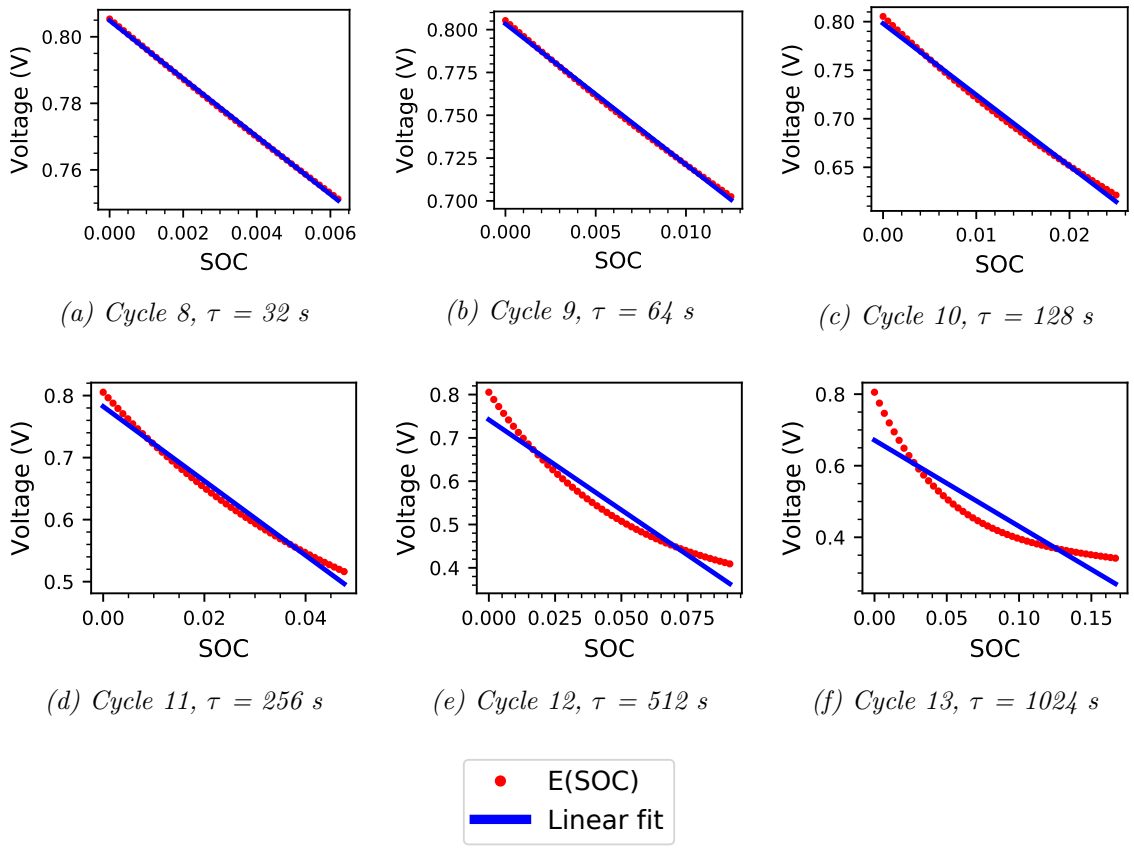

(a) Cycle 8, τ = 32 s *(b) Cycle 9, τ = 64 s* *(c) Cycle 10, τ = 128 s*

(d) Cycle 11, τ = 256 s *(e) Cycle 12, τ = 512 s* *(f) Cycle 13, τ = 1024 s*

Figure 4.19: Linearity of E as function of SOC for voltage windows corresponding to one GITT pulse for varying pulse lengths. The red dots are the experimental data points and the blue line is a linear fit. All the plots are from the cell TFSi_80_8, with a current rate of C/2.

4.6 Experiment With Long Relaxation Time

As explained in Section 3.3.1, a second experiment was performed to test the influence of a long relaxation period on GITT results. A pulse length of 16 s and a relaxation period of 5 h were used in this experiment. This was done on two of the cells, one with a 60 nm thin film (TFSi_60_2, C/10) and one with an 80 nm thin film (TFSi_80_2, C/10). Three GITT pulses were performed at a SOC of 0.25, 0.5 and 0.75, a 5 h relaxation period before and after. The data from these experiments were used to calculate diffusion coefficients according to equation (2.25). These calculated diffusion coefficients were then plotted together with the diffusion coefficients calculated previously, for the GITT cycle having the same pulse length of 16 s. The results of this are shown in Figure 4.20.

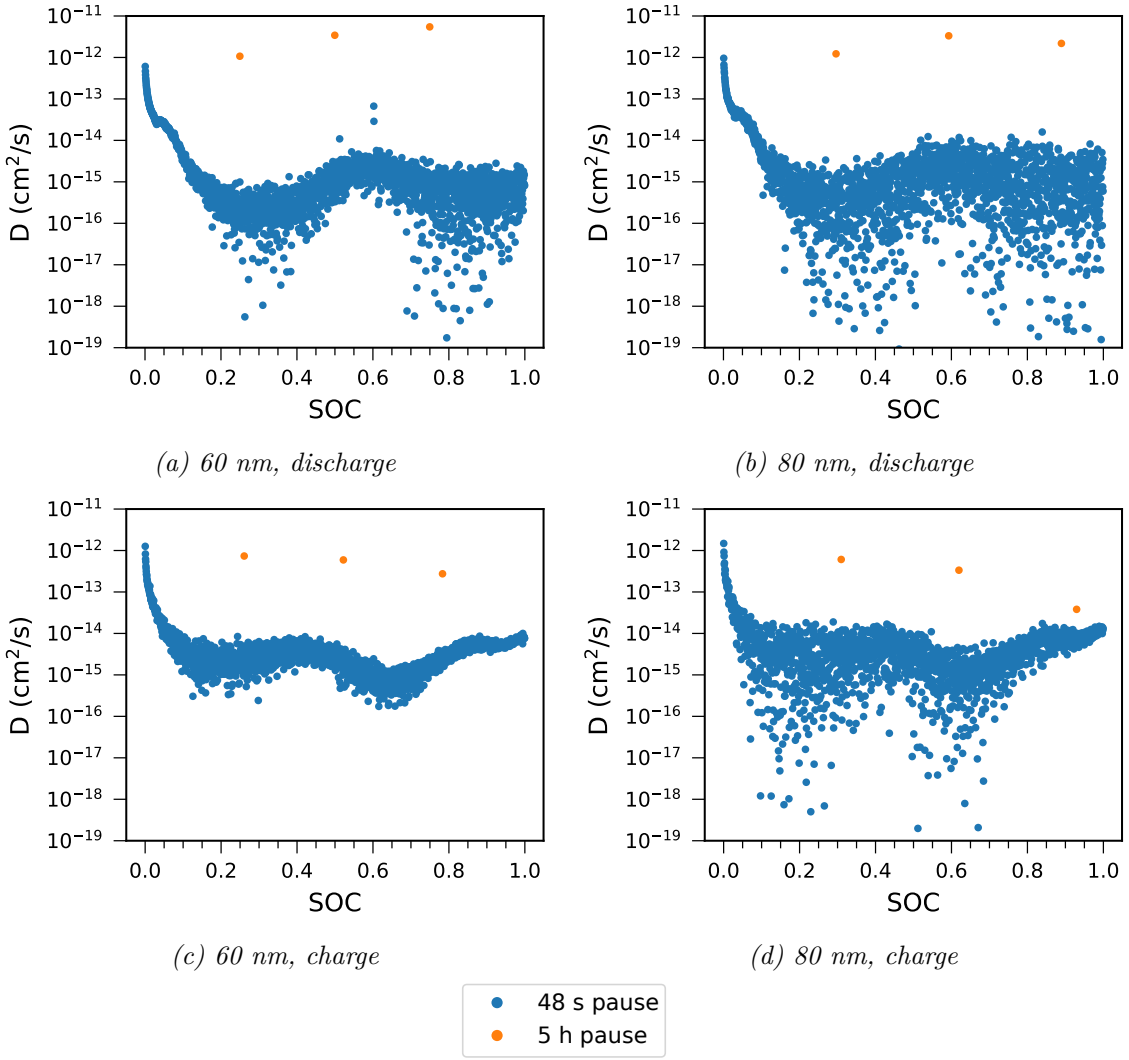

(a) 60 nm, discharge

(b) 80 nm, discharge

(c) 60 nm, charge

(d) 80 nm, charge

Figure 4.20: Logarithmic plot of calculated diffusion coefficients for a pulse length of 16 s.

4.7 Slope of Relaxation Curves

In GITT experiments it is desirable to let the cell relax until it gets close to equilibrium between each current pulse. During the relaxation period after each GITT pulse the voltage will increase (during discharge) or decrease (during charge), as

explained in Section 2.5. This voltage increase/decrease happens rather quickly in the beginning and flattens out as more time passes. It is possible to get an idea of how close to equilibrium the cells get by looking at how flat the voltage curve gets near the end of the relaxation period. Relaxation curves for single relaxation periods of length 24, 192 and 3072 s are shown in Figure 4.21 for the cell TFSi_80_2 (thickness 80 nm, C/10).

The experiment made with long relaxation periods was made to see how the relaxation voltage curves behave when given a long time to relax. The relaxation time in this experiment was 5 h or 18000 s. Relaxation curves for these long relaxation times during both charge and discharge for the same cell as above (TFSi_80_2) are shown in Figure 4.22.

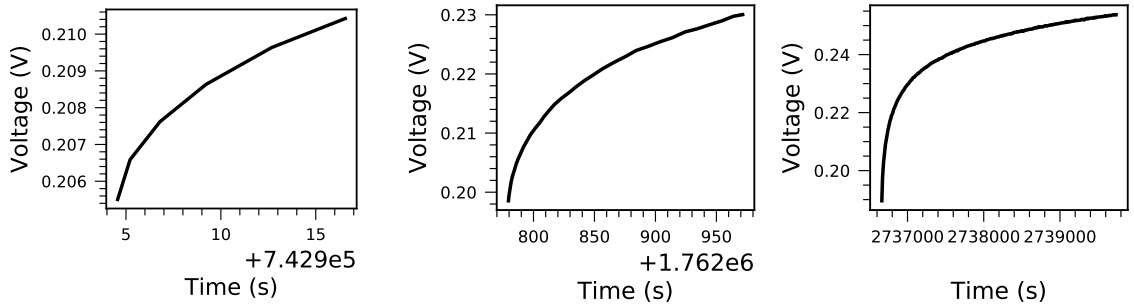

(a) 12 s relaxation *(b) 192 s relaxation* *(c) 3072 s relaxation*

Figure 4.21: Voltage development during relaxation periods of different lengths. The x axis shows the time since the start of testing. All the plots are from a cell with 80 nm thin film and C/10 current rate, during discharge.

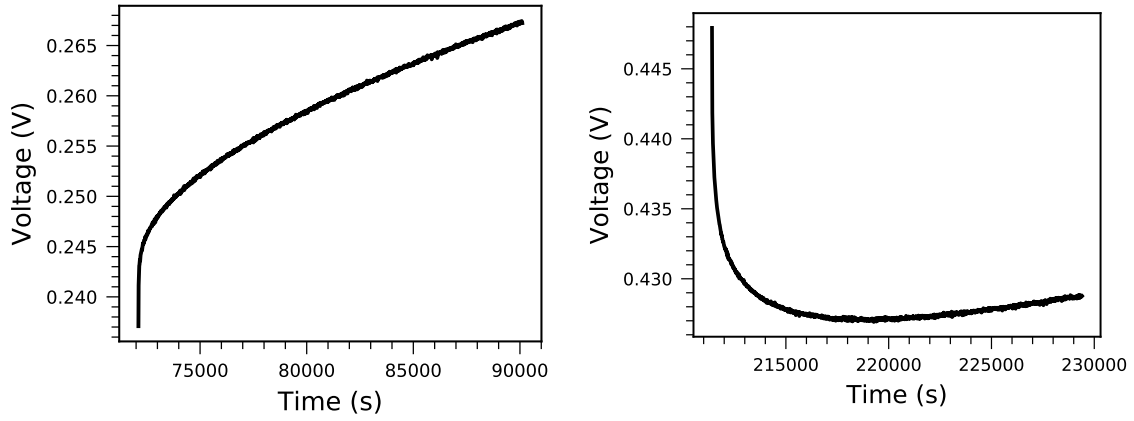

(a) discharge *(b) charge*

Figure 4.22: Voltage development during relaxation periods of new experiment with a long relaxation time of 18000 s. The x axis shows the time since the start of testing. The plots are from the cell with 80 nm thin film and a current rate of C/10.

4.8 Pulse Length Limits

In doing the simplification from eq. (2.19) to eq. (2.10) an important assumption was made: the pulse time is much shorter than the diffusion length squared divided by

the diffusion coefficients. This has to do with an assumption that the concentration gradient is close to the surface [13]. The value for this $\frac{L^2}{D}$ limit was calculated for different diffusion coefficients in a range corresponding to the values calculated so far in this work. The calculated values for a diffusion length 60 nm are given in table 4.1 and the values for 80 nm are given in table 4.2.

Table 4.1: Calculated pulse length limits for varying diffusion coefficients for a diffusion length of 60 nm.

D (cm^2/s)	L^2/D	10 % of L^2/D	1 % of L^2/D
$1 * 10^{-10}$	0.36	0.036	0.0036
$1 * 10^{-11}$	3.6	0.36	0.036
$1 * 10^{-12}$	36	3.6	0.36
$1 * 10^{-13}$	360	36	3.6
$1 * 10^{-14}$	3600	360	36
$1 * 10^{-15}$	36000	3600	360
$1 * 10^{-16}$	360000	36000	3600

Table 4.2: Calculated pulse length limits for varying diffusion coefficients for a diffusion length of 80 nm.

D (cm^2/s)	L^2/D	10 % of L^2/D	1 % of L^2/D
$1 * 10^{-10}$	0.64	0.064	0.0064
$1 * 10^{-11}$	6.4	0.64	0.064
$1 * 10^{-12}$	64	6.4	0.64
$1 * 10^{-13}$	640	64	6.4
$1 * 10^{-14}$	6400	640	64
$1 * 10^{-15}$	64000	6400	640
$1 * 10^{-16}$	640000	64000	6400

4.9 Derivative of E(SOC)

Areas where an electrode goes through a phase change can be seen as voltage plateaus in a plot of the voltage as a function of SOC. One such voltage versus SOC plot can be seen in Figure 4.23. The Figure shows a ninth degree polynomial fitted to the end of relaxation period voltages during discharge of cycle 10 ($\tau = 128$ s) for the cell TFSi_80_2. These voltage plateaus are not always easy to identify from such a plot, so it is easier to look for peaks in the derivative of the curve. This method for finding two plateau regions in the E vs SOC curve was also utilized by Ding et al. [16]. The derivative of the curve in Figure 4.23 is shown in Figure 4.24. The derivative was found by using the SymPy library for symbolic mathematics. A symbolic expression was made from the fitted ninth degree polynomial and this was differentiated using the `diff(func, var)` method in SymPy. The peaks in the dV/dSOC curve show where the slope of the E vs SOC curve is closest to zero and where the turning points in the V vs SOC curve are.

The extreme values of the derivative can be found by finding where the second derivative is equal to zero. Again, the SymPy library was used to differentiate

the derivative function and solve the equation $d^2V/dSOC^2 = 0$. The maximum values were found to be at 0.37 SOC and 0.86 SOC. Evaluating the original E(SOC) function at these points gave 0.27 V and 0.12 V, respectively.

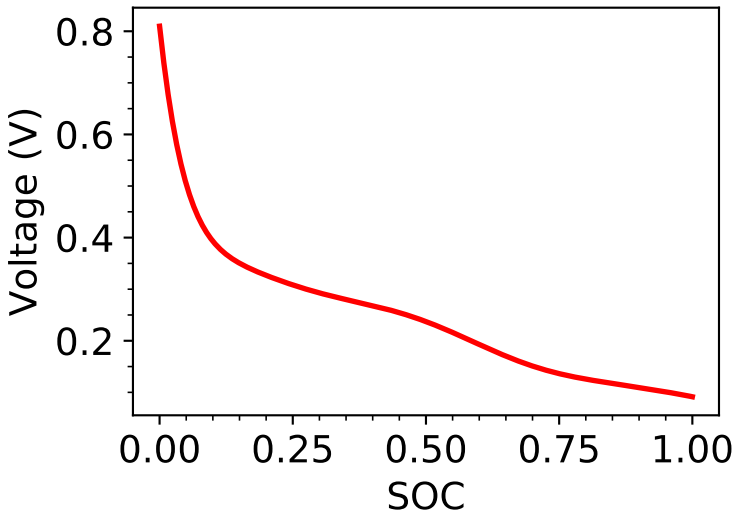

Figure 4.23: Plot of E as function of SOC during discharge of cycle 10 (τ = 128 s) for the cell TFSi_80_2 (current rate C/10).

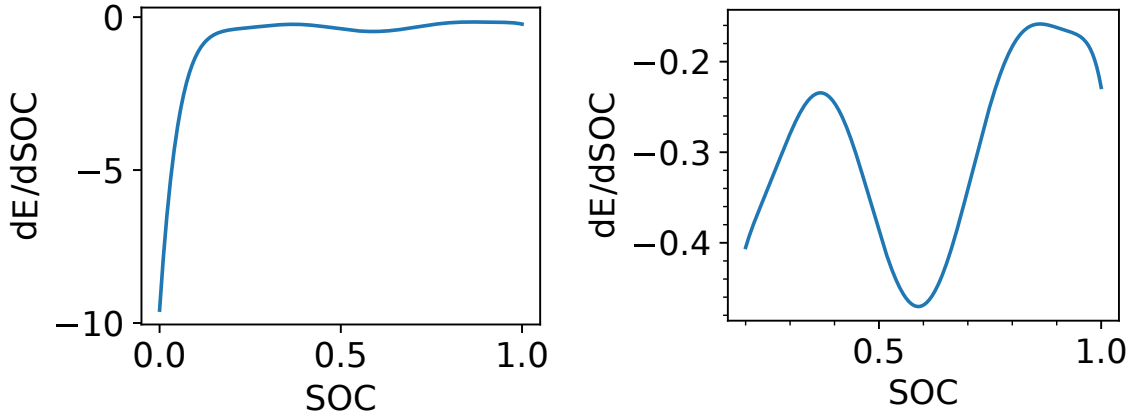

(a) 0 - 1 SOC

(b) 0.2 - 1 SOC

Figure 4.24: The derivative of the E versus SOC curve from figure 4.23. The figure on the left shows the whole curve, while the figure on the right shows the area from 0.2 - 1 SOC to better show how the curve behaves in this area.

Chapter 5

Discussion

5.1 Median of Diffusion Coefficients

Looking at Figure 4.4 and 4.5 it can be seen that the median of the diffusion coefficients decreased as the pulse time increased until they reached a turning point and then the medians started to increase as the pulse time increased. This turning point happened at different times for the different current rates. The cells with the highest current rate, C/2, reached their turning point first, followed by the cells with current rate C/5 and lastly C/10.

If the pulse length criteria $\tau << L^2/D$ was the only criteria important to the accuracy of GITT calculations, the median of the diffusion coefficients would be expected to stabilize at low pulse lengths where this criteria is fulfilled. Taking Figure 4.4 c) as an example, the calculated diffusion coefficients were for the most part in the area of 10^{-16} cm^2/s - 10^{-14} cm^2/s. Assuming that 1% of L^2/D counts as much less than L^2/D, Table 4.1 suggests a pulse length limit of 36 - 3600 s. In Figure 4.4 c) the diffusion coefficients gathered around a pulse length of 8 - 16 s, but instead of staying stable below this value they diverged again. A similar pattern was seen for the other plots in Figure 4.4; the diffusion coefficients for different currents met at some point when the pulse length decreased, but at the lowest pulse lengths they diverged again. This suggests that other effects in addition to the pulse length play a role in determining the accuracy of GITT calculations.

Another point is that the current rate is not included in the pulse length criteria, and should therefore not have a large influence on the result if that was the only criteria influencing the outcome. In Figure 4.4 it is clear that the current rate used influenced the calculated diffusion coefficients. This supports the idea that the pulse length criteria cannot be the only relevant criteria when deciding GITT parameters.

When deriving eq. 2.24, Weppner and Huggins [12] made two simplifications based on assumptions of a constant slope if the current rate is low enough and pulse time is short enough, as explained in Section 2.5. These simplifications could also be influential to the accuracy of GITT calculations when using the simplified equation (2.25). The simplified equation (2.25) is easier to than utilize than eq. (2.21)). For eq. (2.25) all that is needed is the voltage at specific points in the GITT curve, while eq. (2.21) requires estimation of the slope of both E versus $\sqrt{t}$ and E versus

δ. Being able to make these simplifications is thus desirable, and it is worth looking at the pulse length and current rate limitations this sets. In the next section these simplifications are discussed further.

5.2 Simplifications for GITT Equation

5.2.1 E($\sqrt{t}$) is Linear Within the Pulse Length

For short pulse times it is expected that the $\frac{dE}{d\sqrt{t}}$ curve within one current pulse is approximately constant, i.e., that the $E(\sqrt{t})$ curve is linear [12]. Looking at the plots of E($\sqrt{t}$) in Figure 4.8 and in Appendix G there was a linear area after some threshold time of around 4 - 10 s. This linear area lasted until around 40 - 80 s. After that, the line started curving significantly. Verma et al. [14] also observed a linear trend line in the E vs $\sqrt{t}$ curve after some threshold time. They suggested that this linear trend line could be due to the existence of a concentration overpotential, while the initial nonlinear voltage rise is associated with ohmic and charge transfer overpotential. To compute the $\frac{dE}{d\sqrt{t}}$ values needed in equation (2.21), Verma et al. [14] used the slope of this linear area.

Due to the small nonlinear section at the start of each GITT pulse, the curve was not entirely linear for any of the pulse lengths tested. This implies that $\frac{dE}{d\sqrt{t}}$ is never equal to the $\frac{\Delta E_t}{\Delta\sqrt{t}}$ value calculated from the voltage difference over the whole current pulse. The slope of the linear portion was steeper than a line drawn between the first and last points in the voltage curve, giving $\frac{dE}{d\sqrt{t}}$ a higher value than the $\frac{\Delta E_t}{\Delta\sqrt{t}}$. Since $\frac{dE}{d\sqrt{t}}$ is in the denominator in equation (2.21), a lower value for the voltage change will result in a higher diffusion coefficient. This means that using $\frac{\Delta E_t}{\Delta\sqrt{t}}$ instead of the of $\frac{dE}{d\sqrt{t}}$ will result in a calculated diffusion coefficient that is too high. This could be part of the explanation for why the diffusion coefficients in Figure 4.4 increased with increasing pulse length. Looking at a specific example, the curves in Figure 4.8 and in Appendix G started to get past the linear area at around the 64 or 128 s pulse length. In Figure 4.9 the difference for the C/10 current rate started to increase around the 64 s pulse length, so this fits well.

For short pulse length most of the curve was close to linear, so the error in using the simplified formula should not be very large. As the pulse times increase, using the linear approximation produces an increasing amount of error. Figure 4.9 shows the difference between the diffusion coefficients calculated using the simplified GITT equation (eq. (2.25)) and the ones calculated using the slope (eq. (2.22)). As seen in this figure, the difference increased approximately exponentially (since the plots are on a logarithmic scale) after the first few cycles. In the first couple of cycles this difference was quite erratic, and in some cases large. The large difference could be due to the fact that the shortest pulse lengths last shorter than the nonlinear part in the beginning of the pulse. As the pulse lengths increased, the difference between the two methods became smaller as an increasing portion of the curve was linear. Then as the curve passed the point when it stopped being linear, the difference increased again.

The process of finding the linear area by visual inspection and then making a linear

fit to this area was a time consuming process, and was therefore only done for three GITT pulses during discharge and three during charge in each cycle, at a state of charge of approximately 0.25, 0.5 and 0.75. The differences plotted in Figure 4.9 are thus calculated from one single GITT step and might not be the best representation of the calculated GITT value at this state of charge. This is especially the case for the shortest pulse lengths, where the calculated diffusion coefficients varied a lot, as seen in Figure 3.8. The use of only one GITT pulse instead of the mean or median of a larger data set could explain some of the erratic behavior seen in the short pulse lengths in Figure 4.8. This should not be a large problem for longer pulse lengths as they had very little noise in the calculated diffusion coefficients, as seen in Figure 4.1. The best linear fit was also, as previously mentioned, found by visual inspection, so there is a possibility that the linear fit was not entirely optimized.

It could be expected that the error in using $\frac{\Delta E_t}{\Delta\sqrt{t}}$ instead of $\frac{dE}{d\sqrt{t}}$ should depend mainly on the length of the GITT pulse. This did not appear to be the case when looking at Figure 4.9. In the figure, the different current rates diverged in a similar manner as in figure 4.4, thus indicating that the error in equating $\frac{\Delta E_t}{\Delta\sqrt{t}}$ with $\frac{dE}{d\sqrt{t}}$ is influenced also by the current rate. When the current rate is larger, the voltage change over one current pulse is also larger. The linear portion then started at an earlier time than at shorter pulse lengths, and also ended at an earlier time. It is possible that the concentration overpotential becomes the most important factor at an earlier time with a higher current rate.

5.2.2 E(δ) is Linear Within one δ Window

The second simplification made when deriving the GITT equation is based on the assumption that a short pulse time together with a low current rate leads to a small enough change in equilibrium voltage during each current step, that the slope can be considered constant. This is another way of saying that the E vs δ curve should be approximately linear over the δ window gone through in one pulse. As explained in Section 3.4.6, the curvature of the E vs δ curve over one δ window should be equal to the curvature of the E vs SOC curve over the corresponding SOC window. The plot of E vs SOC was utilized to check linearity, due to ease of implementation. This was done for one cell with each current rate with SOC windows corresponding to the SOC change during one pulse at the different pulse length tested. Looking through all the SOC windows for each pulse length would be a time consuming activity, especially for shorter pulse lengths where there are many pulses in one cycle. A $d^2E/dSOC^2$ plot was therefore made to check where the curvature is largest. This was found to be at SOC values close to zero. The linearity of the E vs SOC curve was thus only checked in the first SOC window of each pulse length, as this would be the least linear part of the curve. If the first SOC window is approximately linear, the other SOC windows for the same pulse length should be so as well.

The E vs SOC curve together with a linear fit for the last 6 GITT cycles (pulse length 32 s to 1024 s) for the cell TFSi_80_2 are shown in Figure 4.17. The plots show that for the lowest current rate (C/10), the E vs SOC curve was approximately linear up til a pulse length of 256 s. Since these plots are the worst case scenarios, they suggest that making the simplification from $\frac{dE}{d\delta}$ to $\frac{\Delta E_t}{\Delta\sqrt{t}}$ should be reasonable up til a pulse length of at least 256 s at a current rate of C/10. At higher current

rates the curve stopped being linear at shorter pulse lengths. Figure 4.18 and 4.19 show the E vs SOC curve together with a linear fit for cells with a current rate of C/5 and C/2 respectively. For a current rate of C/5, the curve stopped being linear around a pulse length of 128 - 256 s. And for C/2 it happened around 64 - 128 s.

The diffusion coefficients calculated from eq. (2.23) and eq. (2.25) for cell TFSi_80_2 are compared in Figure 4.11. These seem to fit fairly well, but there were differences between calculated diffusion coefficients from the two methods. Figure 4.12 shows the difference in median D values from using eq. (2.23) versus using eq. (2.25). The difference decreased slightly in the beginning and increased again towards the highest pulse lengths. Especially for the highest current rates, the difference increased with increasing pulse length, but the trend line was not as clear for the other current rates. The diffusion coefficients calculated using the parameterization by Sethuraman et al. [44] were generally close to the values calculated using the simplified GITT equation, as seen in Figure 4.14. They did however differ significantly at some areas, especially at high and low states of charge.

The value of x_{max} used in eq. (3.2) was 3.75, which corresponds to a fully lithiated silicon electrode. The electrodes in this experiment did not reach full lithiation before reaching the cut off voltage. The value of x_{max} corresponding to a SOC of one is therefore slightly lower than 3.75. Substituting the actual value of x_{max} gives a slightly higher diffusion coefficient and would shift the diffusion coefficients from eq. (2.23) in Figure 4.12 upwards. This could explain why some of the values calculated from eq. (2.23), such as the one where $\tau = 2$, seem a bit low compared to the ones calculated from eq. (2.25). The correct value for x_{max} to use for each cycle could be found by comparing the maximum capacity reach in each cycle with the capacity of a fully lithiated electrode, 3579 mAh/g. This correction was not done in the calculations in this work, but is a potential area of improvement.

Another possible source of error is the fit of the ninth degree polynomial used. The polynomial is a good fit of the E vs SOC curve, as seen in Figure 4.10, but it is not perfect. At some points in the curve the polynomial had a slightly different slope than the E vs SOC curve. This introduces a small error in the result, with the direction depending on which slope is highest at that particular point. The polynomial seems like a good fit though, so this error was deemed insignificant.

The slopes of the E vs SOC curves in Figures 4.17 - 4.19 look like they would be fairly similar to the linear curve when evaluated at the middle of the curve, even when the curve is no longer linear in the whole SOC window. This could mean that the diffusion coefficients found from eq. (2.23) are more similar to the ones from eq. (2.25) than it appears they should be based on the linearity seen in Figures 4.17 - 4.19. The curves not being linear means that it is not valid to assume a constant slope throughout the whole SOC window, even though the simplification gives a similar result. When using the formula without simplifications, one value for the slope is used for the whole pulse. In long pulse times, when the E vs SOC is not linear in the current pulse, the slope will not be the same during the whole current pulse, in which case this is not a valid approximation. The slope was considered constant until $\tau = 256$ s for C/10, $\tau = 128$ - 256 s for C/5 and $\tau = 64$ - 128 s for C/2.

5.3 Phase Transformations

As mentioned in Section 5.3, a Si anode goes through some phase transformation processes during charge/discharge. The Si anode studies by Ogata et al. [47] was based on crystalline Si, while the Si thin films used in this work were amorphous. Crystalline Si is, however, converted into amorphous Si during the first cycle, so the two materials should be comparable after the first cycle. In the voltage range used in the experiment in this work (0.05 V to 1 V) Ogata et al. describe two processes; a gradual lithiation of a-Si to form $Li_{\sim 2.0}Si$ at $\sim$ 300 - 250 mV vs Li/Li+ and a formation of $Li_{\sim 3.5}Si$ at 100 mV vs Li/Li+ [47]. They also describe a crystallisation from a-LixSi to c-$Li_{\sim 3.75}Si$ at around 50 mV vs Li/Li+, but this was not expected to happen in the experiments in this work since the cells stop discharging at this point. This was confirmed to be the case by the absence of the characteristic delithiation plateau associated with c-$Li_{\sim 3.75}Si$ at 430 mV vs Li/Li+.

The GITT method does not take phase-transformations into consideration. It relies on Ficks's law of diffusion, and does not consider the effect of any interphase boundary movement. This means that only an apparent diffusion coefficient can be found in the two-phase region [59]. Zhu and Wang [59] looked at GITT used on a $LiFePO_4$ electrode that goes through a phase transformation. They found the apparent diffusion coefficients obtained from GITT to be 2-3 orders of magnitude lower in the two phase region than in the single phase region and attributed this to the phase transformation. Furthermore, Zhu and Wang [59] developed a new GITT for phase transforming electrodes. The diffusion coefficients obtained in the two phase region with this new method were similar to the diffusion coefficients obtained in the single phase region with the normal GITT method. Since Zhu and Wang [59] study a different electrode material than the one in this work, the results are not entirely comparable. It does however suggest that the presence of a phase change will lead to a smaller apparent diffusion coefficient in the phase change regions when using the regular GITT method.

The smaller apparent diffusion coefficient in phase change regions likely explain the W shape of the D vs SOC curves in Figures 4.2 and 4.3. A similar W shape for the diffusion coefficients has also been observed in other studies [16, 35]. The two bottom points in the W shaped curve during discharge seem to fall around 0.3 - 0.35 SOC and around 0.9 SOC (see Figure 4.2). This fits quite well with the estimated SOC areas for phase changes in Section 4.9; 0.37 SOC and 0.86 SOC. These SOC values correspond to voltages of 0.27 V and 0.12 V vs Li/Li+ respectively. The voltage plateau around 0.27 V matches well with the first discharge process described by Ogata et al. [47] at 0.300 - 0.250 V vs Li/Li+. The second voltage plateau at around 0.12 V similarly correspond decently with the discharge process at 0.100 V vs Li/Li+. These results indicate that the local minimum values seen in Figure 4.2 were related to phase transitions.

Implementation of the phase transformation GITT developed by Zhu and Wang [59] was not attempted in this work. The new GITT method is substantially more complicated to implement than the regular GITT method and requires solving a set of two partial differential equations (PDEs) and one ordinary differential equation (ODE). Additionally, the method probably needs some adjusting to fit a Si electrode instead of a $LiFePO_4$ electrode.

5.4 Length of Relaxation Period

GITT theory dictates that the cells should be near equilibrium at the start of each current pulse. During the relaxation period, the cell voltage will increase (during discharge) asymptotically towards the equilibrium potential. Figures 4.21 and 4.22 show the voltage evolution with varying relaxation times. They show that for short relaxation times the curve was still fairly steep when the relaxation ends. As the relaxation time increases the slope of the curve became smaller; however, it never got entirely horizontal, even after the longest relaxation times tested (5h). The curve in Figure 4.22 shows a decreasing voltage at the start, but as time passed the voltage flattened out and started increasing. A similar voltage development during relaxation was seen by Sethuraman et al. [44]. They let a cell relax for 48 h and still observed a changing potential. A very long relaxation period is thus needed for the cell to reach equilibrium. There are also additional complications from the presence of side reactions, which lead to self-discharge (self delithiation) of the electrode [44]. Due to the extremely long relaxation times needed to reach close to equilibrium it is generally not feasible to let the cell relax completely between each GITT pulse. A compromise has to be made between what is deemed sufficient relaxation for the cell and the time available for the GITT experiment.

Though it is unlikely that the cell can be allowed time to reach very close to equilibrium, the relaxation period should be significantly longer than the pulse period. This has to do with two assumptions made when deriving GITT. The first assumption is that the lithium does not have time to diffuse very far into the material during the current pulse, so that the concentration gradient is close to the surface. This is related to the $\tau \ll L^2/D$ criteria described previously [13]. The second assumption is that the cell has a homogeneous composition throughout the electrode (i.e. it is in equilibrium) at the beginning of each current pulse. For both of these assumptions to hold true, the relaxation period needs to be significantly longer than the pulse period. This is not always seen in the literature, e.g. in [19] where the pulse period and the relaxation period has the same length (10 min).

A too short relaxation period could be partially responsible for the inconsistent results in GITT cycles with short pulse lengths. The relaxation period in the first couple of cycles was only a few seconds long, which was too short for the electrode to get close to equilibrium, despite the short current pulse only constituting a small perturbation from equilibrium. This is illustrated in Figure 4.21 a), where the relaxation curve is still steep at the end of the relaxation period. The cell was thus not close to a homogeneous concentration of Li when the next GITT cycle started. This could cause some uncertainty in the GITT results and could also be the reason for the increase in diffusion coefficients seen at shorter pulse lengths.

5.5 Experiment Setup

When planning the main experiment in this thesis, a relaxation period three times the pulse period was chosen. As explained in the previous Section, the shorter relaxation periods used were found to be too short for the cell to relax properly. This relaxation time was chosen as a compromise between letting the cell relax as much as possible between pulses, and the time available for the experiment. If the same

relaxation period was to be used for all the different pulse lengths it would need to be longer than the longest pulse period of 1024 s. Applying such a long relaxation period to the cycles with short pulse lengths, and therefore many pulses, would result in an experiment that lasts much longer than the time available. Choosing a fixed relaxation period that fits with the shorter pulse lengths would result in the relaxation period being shorter than the pulses for longer pulse lengths, resulting in insufficient relaxation. A choice was thus made to scale the relaxation time with the pulse time. This at least satisfies the requirement that the relaxation time is longer than the pulse time, even though the resulting relaxation times were not found to be entirely satisfactory for the shortest pulse times.

A possible solution to the choice between a longer relaxation period and a short enough experiment is what was done in the second experiment. In this experiment only three GITT pulses were performed at set states of charge, with a long relaxation time before and after. This allows the use of a longer relaxation time while still keeping the experiment time sufficiently short. The downside to this approach is that it only gives the diffusion coefficient at a few chosen points during charge and discharge. How the diffusion coefficients vary with SOC could therefore not be seen with such a setup. This method would also result in much less data to analyse, and it would not be possible to graphs of E vs δ as in Figure 4.10.

The pulse lengths chosen were meant to give a wide window of pulse lengths to study. The diffusion coefficient of lithium in silicon has previously been reported between 10^{-14} to 10^{-10} cm^2/s [16, 60–62]. These values were taken as a basis for which pulse lengths should be tested. The L^2/D limit for different diffusion coefficients are given in tables 4.1 and 4.2. The limits span over many orders of magnitude, and it is not practicable to test the whole range in one experiment. Thus a range of pulse lengths around the middle of this spread was chosen. The pulse lengths were doubled each iteration to span the necessary range, while maintaining a suitable resolution at shorter pulse lengths. An additional benefit of the doubling was to allow equal spacing between data points on a logarithmic scale.

5.6 Experiment With Longer Relaxation Period

When it became clear that even the longest relaxation period of 3072 s was insufficient to get a flat relaxation curve (see fig. 4.21 c)), a new experiment with longer relaxation time was performed. The diffusion coefficients from this new experiment differ from the ones done with the same pulse length in the main experiment by several orders of magnitude, as seen in Figure 4.20. This implies that the length of the relaxation period has a large impact on GITT results. The longer relaxation time lets the cell get closer to equilibrium between each GITT step, as dictated by GITT theory, and it is therefore likely that these new experiment returned more accurate results. These results were also closer to the diffusion coefficients of $\sim 10^{-12}$ previously reported by Ding et al. [16].

5.7 Volume Change in Silicon

One of the major challenges to commercialization of Si anodes is the large volume change during lithiation/delithiation, that can be over 300% (see Section 2.3.4). This large volume change could also cause a problem with the use of the GITT equation to determine diffusion coefficients. As mentioned in Section 2.5 one of the assumptions made in the derivation of the GITT equation was that any changes in molar volume of the electrode as the electrode composition changes during lithiation/delithiation could be neglected. This is a good assumption for electrodes that experience a small volume change upon lithiation/delithiation. This is, however, not the case for Si anodes, which means that the GITT method is not necessarily ideal for use with Si anodes.

In the normal GITT formula generally used to calculate diffusion coefficients (eq. (2.24)), both the volume and the electrode surface area are included. When the electrode is a thin film, the volume and the surface cancel each other out and the thickness of the thin film, h, is left, as seen in eq. (2.25). When calculating the diffusion coefficients in this thesis, h was assumed to be constant and equal to the initial thin film thickness throughout the whole lithiation and delithiation. During lithiation, the electrode volume increases, resulting in a larger actual value for h. As seen in eq. (2.25), using a larger value for h will result in a higher diffusion coefficient. When the thin film thickness increases with increasing amount of Li in the anode, continued use of the smaller initial thickness could lead to an underestimation of the diffusion coefficient at higher degrees of lithiation. It could therefore be interesting to investigate the possibility of doing GITT calculations with h changing as the electrode becomes more lithiated, but that was not done in this work.

Another effect related to the volume change is that it typically introduces internal stress in the material, which may fracture the electrode. Cracks in the material as a result of volume change can also influence the apparent diffusion coefficient as the cracks can create an easy pathway for fast lithium diffusion [35]. The films in this work were, however, deemed sufficiently thin to be dimensionally stabilized in the course of the 10 cycles used for this GITT analysis. This has been confirmed in previous long term cycling experiments using equivalent films [63].

5.8 Choices Made when Plotting the Data

5.8.1 Smoothing

When smoothing the D versus SOC plots in Figures 4.2 and 4.3, a Gaussian filter with sigma 300 was used, with 20 000 data points between 0 and 1 SOC. The same amount of smoothing was used on all the curves to ease comparison. It was, however, difficult to decide on an amount of smoothing that was ideal for all the pulse lengths. A compromise had to bee made between smoothing away all the minor fluctuations and keeping the shape of the curve as best as possible. It was challenging to keep as much of the nuance as possible, especially at the beginning of the cycle where the curve is steep.

5.8.2 Removal of outliers

When creating the diffusion coefficient as function of SOC plot in Figures 4.2, 4.3 and in Appendix D a median filter was applied to the data to remove any outliers before the data was smoothed further with a Gaussian filter. Simply removing the outliers in this manner is not always appropriate. In this case the outliers all seemed to come from problems with the data set, e.g. in the form of missing data points (see Section 3.4.4). In the cycles with shorter pulse lengths, where each current pulse may have only 2 - 4 data points, missing one data point at the end or the beginning of a pulse or relaxation period made a significant difference in the calculated ΔE values, which further had a large influence on the calculated diffusion coefficient. In cycles with a longer pulse and relaxation period, the voltage change was larger, so one missing data point did not make a big difference. This explains why these outliers were primarily present in the first few cycles. The ΔE values calculated from these pulses with missing data points were incorrect since some of the information was missing and thus the diffusion coefficients calculated were false values. Since the outliers were related to a problem with the data acquisition and gave false diffusion coefficients, removing them was deemed the best option. If the outliers were kept in the data set when doing smoothing they would influence the resulting curve.

Another method for removing the outliers was also tested. That method was to remove all data points where the pulse step or the previous/following relaxation step was significantly shorter than it should have been. It was not immediately clear how much shorter the outlier steps should be in order to remove only the outliers that were skewing the data the most, but not remove an unnecessary amount of data. Because of this, this method was discarded and replaced with the application of a median filter, as described above.

5.9 Noise for Short Pulse Lengths

The cycles with short pulse lengths had a high amount of noise in the calculated diffusion coefficients, as seen in Figure 3.8. The voltage change during one GITT pulse and relaxation period was only a few mV for the shortest pulse lengths and lowest current rate. This is illustrated in Figure 5.1, where a voltage change around 1 mV was seen during both the pulse and pause. The measurement precision of Arbin is < 1 mV. When the change in voltage for each pulse or relaxation period is only a few mV, an uncertainty of < 1 mV is a significant amount. A slightly too high or too low start or end voltage can influence the GITT calculations notably when the margins are already so small. As the pulse lengths increase the voltage change during one pulse/relaxation is larger, so the uncertainty makes less impact. This is illustrated in Figure 5.2, where the end of relaxation time voltages for a pulse length of 2 s and 128 s are shown. There was more variation in the voltages for the shortest pulse length.

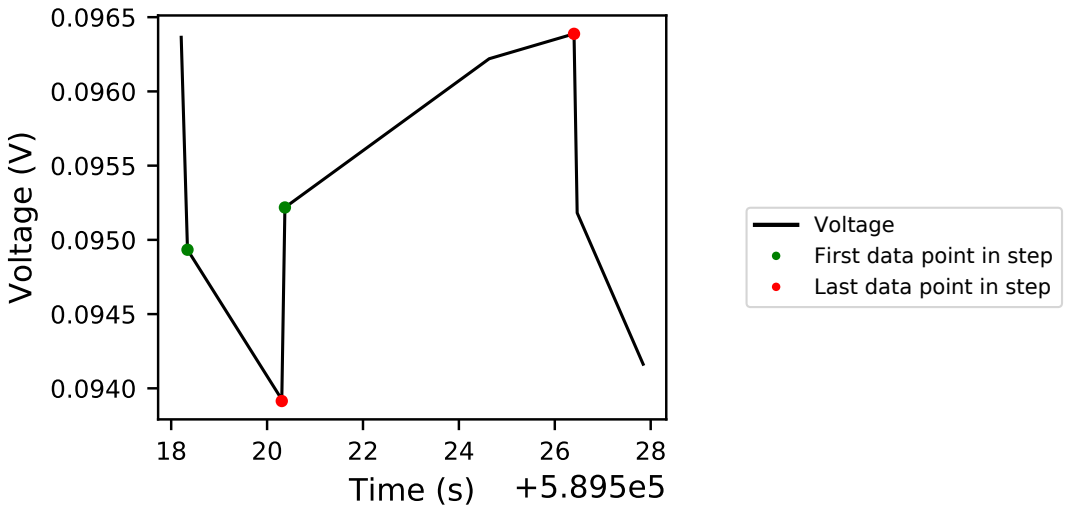

Figure 5.1: Illustration of voltage change during one 2 s pulse and one 6 s relaxation period with a current rate of C/10.

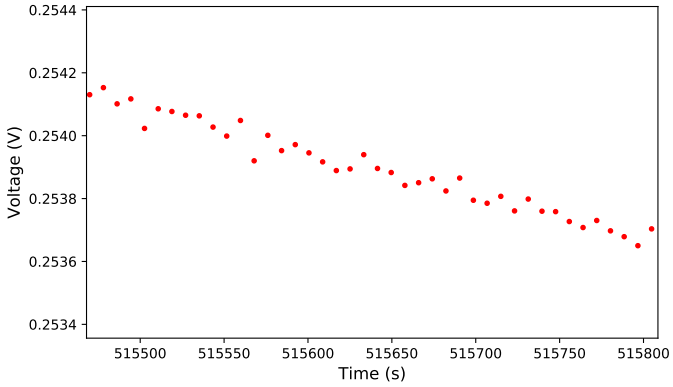

(a) Pulse time 2 s, relaxation time 6 s.

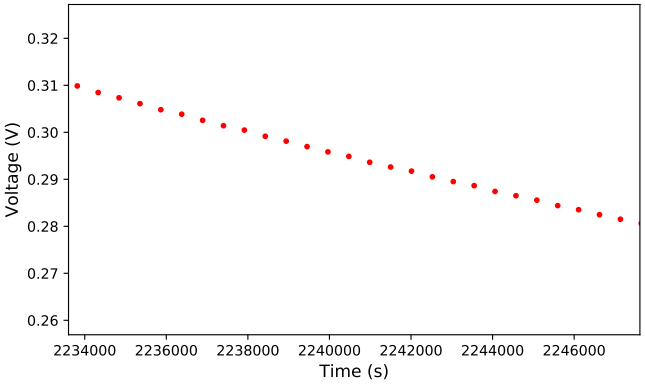

(b) Pulse time 128 s, relaxation time 384 s.

Figure 5.2: Illustration of variation in end of relaxation voltages for a pulse length of 2 s and a pulse length of 128 s, with a current rate of C/10.

The plots in Figure 4.11 imply that much of the noise comes from the calculation of ΔE_s. In these plots the diffusion coefficients calculated using $\frac{dE}{d\delta}$ had much less noise

than the ones calculated using ΔE_s. Thus small variations in the end of relaxation time voltages, possibly due to the measurement precision of Arbin, are likely the main cause of the noise. Assuming that this noise is largely uncorrelated, however, the large number of data points produced when using shorter pulse lengths makes these datasets suitable for smoothing to improve the signal to noise ratio.

5.10 IR Drop

Looking at plots of one GITT pulse or relaxation period it seems that the largely instantaneous IR drop happened before the first data point was saved. This can be seen in Figure 5.1. It was therefore not necessary to add a step in the code to remove the IR drop. As long as the acquisition voltage resolution is high enough that the first data point measured is just after the whole IR drop has happened (meaning that the acquisition voltage change trigger should be smaller than the IR drop is expected to be). If this is the case, as it was in the experiments in this thesis, no effort needs to be taken to remove the IR drop before doing GITT calculations.

Chapter 6

Conclusion

The main goal of this thesis was to test the influence of experimental parameters on the results obtained from GITT analysis. This was done to investigate potential weaknesses with the technique under different circumstances, and to give an idea of things to think about when choosing GITT parameters. The experiments conducted showed that both pulse time, relaxation time and current rate affect the diffusion coefficients determined by the GITT method. The calculated diffusion coefficients were found to vary by several orders of magnitude depending on the selected parameters.

Two simplifications made in the derivation of the GITT equation (eq. (2.25) were checked. The first simplification was the $\frac{dE}{d\sqrt{t}}$ to $\frac{\Delta E_t}{\Delta\sqrt{t}}$, which is valid when $E(\sqrt{t})$ is approximately linear within one current pulse. The $E(\sqrt{t})$ curve was found to have a linear area that starts after some threshold value. The start and end of this linear area depends on the current rate used. For the cells tested in this thesis, the linear approximation is decent until a pulse length around 64 - 128 s for C/10, 32 - 64 s for C/5 and 16 - 32 s for C/2. The pulse length should also be at least 4 s, in order to avoid that the nonlinear area in the beginning of the pulse significantly affects the result.

The second simplification was the $\frac{dE}{d\delta}$ to $\frac{\Delta E_s}{\Delta\delta}$, which is valid when the $E(\delta)$ curve is approximately linear over the range of δ values covered during one pulse. The validity of this simplification is also dependent on both the pulse length and current rate, as they together determine the range of δ values covered during one pulse. In the experiments in this work, the linear approximation was found to be valid for pulse lengths up to at least 256 s for C/10, 128 s for C/5 and 64 s for C/2. The linearity was tested in the most curved part of $E(\delta)$, so these numbers represent the worst case scenarios.

The largest variation in calculated diffusion coefficients came from the experiment with long relaxation time. The calculated diffusion coefficients with a 16 s pulse were in the range 10^{-16} - 10^{-14} when using a 48 s pause length, while the same pulse length with a 5h pause before and after resulted in diffusion coefficients in the range 10^{-13} - 10^{-11}. Reaching very close to equilibrium takes a very long time, and it was found that even after 5 hour pause, the cell potential was still in the process of relaxing. This shows that the cells should be allowed as much relaxation time

between pulses as is practical for the experiment conducted. The pause should at least be several times as long as the pulse. The longer relaxation time was only tested at three points along the SOC curve and only on two cells. Additional testing of the impact from the relaxation time would be beneficial.

The calculated diffusion coefficients vs SOC curve was found to have a W shape. This is in accordance with observations in previous studies, e.g. Ding et al. [16]. This W shape is likely related to phase transformation processes in silicon anodes. Developing a phase transformation GITT for Si anodes, based on the method by Zhu and Wang [59], could be an interesting further step.

The overall conclusion of this work is that both pulse length, pause length and current rate influences GITT results. Due to the variations in GITT results, this method is probably best suited to give an order of magnitude estimation and not an exact result for the diffusion coefficients. In these experiments, a longer pause was found to have the larges impact on the result, and a long relaxation period should therefore be prioritized. The current rate and pulse length was found to be connected, as expected from the $\frac{dE}{d\delta}$ criterion. At a lower current rate, a longer pulse length can be used. The pulse times chosen should ideally be short, but not so short that it introduces too much noise and that the majority of the pulse is in the nonlinear area of $E(\sqrt{t})$. For the cells tested in this thesis, a pulse length between 8 - 64 s seems the best at a current rate of C/10. Of the two simplifications investigated ($\frac{dE}{d\delta}$ to $\frac{\Delta E_s}{\Delta\delta}$ and $\frac{dE}{d\sqrt{t}}$ to $\frac{\Delta E_t}{\Delta\sqrt{t}}$), $\frac{dE}{d\sqrt{t}}$ to $\frac{\Delta E_t}{\Delta\sqrt{t}}$ was the limiting factor for valid pulse lengths.

Chapter 7

Further Work

The main focus of this thesis was to investigate the influence of experimental parameters on GITT results, with the parameters tested being the pulse time, relaxation time and current rate. In addition to this the effects from phase transformations and volume change is silicon anodes were discussed. Some suggestions for further work that should be done to examine this more closely include:

- Comparing the GITT results to other methods of calculating diffusion coefficient (i.e. EIS or PITT) or modelling, to validate the accuracy of the results.
- Conduct further experiments to test the influence of the relaxation time.
- Developing a phase transformation GITT method for silicon anodes, based on the GITT for Phase-Transformation Electrodes developed by Zhu and Wang [59].
- The effect of volume change in Si on the GITT results should be further researched. Specifically, the possibility of doing GITT calculations with a varying thin film thickness, h, should be tested.
- The $\frac{dE}{d\delta}$ to $\frac{\Delta E_s}{\Delta \delta}$ simplification should be tested using a maximum value for δ corresponding to the actual amount of lithiation achieved in the experiment, instead of the fully lithiated state of $\delta = 3.75$.

Bibliography

[1] IPCC (Core Writing Team; Pachauri, R.K. and Meyer, L.A. (eds.)). Climate change 2014: Synthesis report. contribution of working groups i, ii and iii to the fifth assessment report of the intergovernmental panel on climate change. IPCC, Geneva, Switzerland, 2014. [Accessed: 11.03.2020], URL: `https://archive.ipcc.ch/report/ar5/syr/`.

[2] Ingvild U. Jakobsen and Steffen Kallbekken. Parisavtalen, 2015. Store norske leksikon, [last updated 19.02.2020, accessed 13.03.2020]. URL: `https://snl.no/Parisavtalen`.

[3] Ghassand Zubi, Rodolfo Dufo-López, Monica Carvalho, and Guzay Pasaoglu. The lithium-ion battery: State of the art and future perspectives. *Renewable and Sustainable Energy Reviews*, 89:292–308, 2018. doi: 10.1016/j.rser.2018.03.002.

[4] International Energy Agency. Renewables, 2020. Website, [last updated 11.02.2020 , accessed 06.05.2020]. URL: `https://www.iea.org/fuels-and-technologies/renewables`.

[5] Mauro Pasta, Colin D. Wessells, Robert A. Huggins, and Yu Cui. A high-rate and long cycle life aqueous electrolyte battery for grid-scale energy storage. *Nature Communications*, 3:1149, 2012. doi: 10.1038/ncomms2139.

[6] International Energy Agency. Co_2 emissions from fuel combustion. IEA Publications, 2018. Accessed: 21.02.2020.

[7] Naoki Nitta, Feixiang Wu, Jung T. Lee, and Gleb Yushin. Li-ion battery materials: present and future. *Materials Today*, 18:252–264, 2015. doi: 10.1016/j.mattod.2014.10.040.

[8] Thomas Bowen, Ilya Chernyakhovskiy, and Paul Denholm. Grid-scale battery storage, 2019. National Renewable Energy Laboratory, [accessed 06.05.2020]. URL: `https://www.nrel.gov/docs/fy19osti/74426.pdf`.

[9] Dave Andre, Sung-Jin Kim, Peter Lamp, Simon F. Lux, Filippo Maglia, Odysseas Paschos, and Barbara Stiaszny. Future generations of cathode materials: an automotive industry perspective. *Journal of Materials Chemistry A*, 3:6709–6732, 2015.

[10] D. Anseán, M. Dubarry, A. Devie, B.Y. Liaw, V.M. García, J. C. Viera, and M. González. Fast charging technique for high power $LiFePO_4$ batteries: A

mechanistic analysis of aging. *Journal of Power Sources*, 321:201–209, 2016. doi: 10.1016/j.jpowsour.2016.04.140.

[11] Abdilbari S. Mussa, Matilda Klett, Mårten Behm, Göran Lindbergh, and Rakel W. Lindström. Fast-charging to a partial state of charge in lithium-ion batteries: A comparative ageing study. *Journal of Energy Storage*, 13:325–333, 2017. doi: 10.1016/j.est.2017.07.004.

[12] W. Weppner and R. A. Huggins. Determination of the kinetic parameters of mixed-conducting electrodes and application to the system Li_3Sb. *J. Electrochem. Soc: SOLID-STATE SCIENCE AND TECHNOLOGY*, 124:1569–1578, 1977.

[13] Dennis W. Dees, Shigehiro Kawauchi, Daniel P. Abraham, and Jai Prakash. Analysis of the galvanostatic intermittent titration technique (gitt) as applied to a lithium-ion porous electrode. *Journal of Power Sources*, 189:263–268, 2009.

[14] Ankit Verma, Kandler Smith, Shiram Santhanagopalan, Daniel Abraham, Koffi P. Yao, and Partha P. Mukherhjee. Galvanostatic intermittent titration and performance based analysis of $LiNi_{0.5}Co_{0.2}Mn_{0.3}O_2$ cathode. *Journal of The Electrochemical Society*, 164:A3380–A3392, 2017.

[15] Jan Kaspar, Magdalena Graczyk-Zajac, and Ralf Riedel. Determination of the chemical diffusion coefficient of li-ions in carbon-rich silicon oxycarbide anodes by electro-analytical methods. *Electrochimica Acta*, 115:665–670, 2014.

[16] N. Ding, J. Xu, Y. X. Yao, G. Wegner, X. Fang, C.H. Chen, and I. Lieberwirth. Determination of the diffusion coefficient of lithium ions in nano-si. *Solid State Ionics*, 180:222–225, 2009.

[17] M.D. Levi, K. Gamolsky, D. Aurbach, U. Heider, and R. Oesten. Determination of the li ion chemical diffusion coefficient for the topotactic solid-state reactions occurring via a two-phase or single-phase solid solution pathway. *Journal of Electroanalytical Chemistry*, 477:32–40, 1999.

[18] Ke Pana, Feng Zoub, Marcello Canovaa, Yu Zhub, and Jung-Hyun Kima. Systematic electrochemical characterizations of si and SiO anodes for highcapacity li-ion batteries. *Journal of Power Sources*, 413:20–28, 2019.

[19] Autolab. Galvanostatic intermittent titration technique, 2014.

[20] Shunyi Yang, Xianyou Wang, Xiukang Yang, Yansong Bai, Ziling Liu, Hongbo Shu, and Qiliang Wei. Determination of the chemical diffusion coefficient of lithium ions in spherical $Li[Ni_{0.5}Mn_{0.3}Co_{0.2}]O_2$. *Electrochimica Acta*, 66:88–93, 2012.

[21] E. Markevich, M. D. Levi, and D. Aurbach. Comparison between potentiostatic and galvanostatic intermittent titration techniques for determination of chemical diffusion coefficients in ion-insertion electrodes. *Journal of Electroanalytical Chemistry*, 580:231–237, 2005.

[22] R. M. Dell and D. A. J. Rand. *Understanding Batteries*. The Royal Society of Chemistry, Cambridge, UK, 2001.

[23] Jung-Ki Park. *Principles and Applications of Lithium Secondary Batteries*. Wiley-VCH, 2012.

[24] David Linden. Chapter 1 basic consepts. In David Linden and Thomas B. Reddy, editors, *Handbook of Batteries*. McGraw-Hill, 3rd edition, 2002.

[25] Ivar Gunvaldsen, Steinar Mathiesen, and Knut A. Rosvold. batteri, 2019. Store Norske Leksikon. [Last updated 24.07.2019, accessed 24.01.2020], URL: `https://snl.no/batteri`.

[26] Yoshio Nishi. The development of lithium ion secondary batteries. *The Chemical Record*, 1:406–413, 2001. doi: 10.1016/j.mattod.2014.10.040.

[27] J. M. Tarascon and M. Armand. Issues and challenges facing rechargeable lithium batteries. *Nature*, 414:359–367, 2001.

[28] Asbjørn Ulvestad. *Performance and Characteristics of Silicon Nitride as a Convertible Alloy Anode Material for Li-ion Batteries*. PhD thesis, University of Oslo, 2018.

[29] John Broadhead and Han C. Kuo. Chapter 1 electrochemical principles and reactions. In David Linden and Thomas B. Reddy, editors, *Handbook of Batteries*. McGraw-Hill, 3rd edition, 2002.

[30] Grant M. Erlich. Chapter 35 lithium-ion batteries. In David Linden and Thomas B. Reddy, editors, *Handbook of Batteries*. McGraw-Hill, 3rd edition, 2002.

[31] George Crabtree, Elizabeth Kócs, and Lynn Trahey. The energy-storage frontier: Lithium-ion batteries and beyond. *MRS Bulletin*, 40:1067–1078, 2015. doi: 10.557/mrs.2015.259.

[32] The Editors of Encyclopaedia Britannica. Electroplating. Encyclopædia Britannica, 2018. [Last updated 26.03.2018, accessed 05.02.2020], URL: `https://www.britannica.com/technology/electroplating`.

[33] Matthew Li, Jun Lu, Zhongwei Chen, and Khalil Amine. 30 years of lithium-ion batteries. *Advanced Materials*, 30:1800561, 2018. doi: 10.1002/adma.201800561.

[34] P. G. Bruce and J. T. S. Irvine. Insertion compounds. In K. H. J. Buschow, Robert W. Cahn, Merton C. Flemings, Bernhard Ilschner, Edward J. Kramer, Subhash Mahajan, and Patrick Veyssière, editors, *Encyclopedia of Materials: Science and Technology*, pages 4115–4121. Elsevier, 2nd edition, 2001. ISBN 978-0-08-043152-9.

[35] François Ozanam and Michel Rosso. Silicon as anode material for li-ion batteries. *Materials Science and Engineering B*, 213:2–11, 2016. doi: 10.1016/j.mseb.2016.04.016.

[36] Seung-Ho Yu, Xinran Feng, Na Zhang, Jeesoo Seok, and Héctor D. Abruña. Understanding conversion-type electrodes for lithium rechargeable batteries. *Accounts of chemical research*, 51:273–281, 2018. doi: 10.1021/acs.accounts.7b00487.

[37] Yan Lu, Le Yu, and Xiong W. Lou. Nanostructured conversion-type anode materials for advanced lithium-ion batteries. *Chem*, 4:972–996, 2018. doi: 10.1016/j.chempr.2018.01.003.

[38] William D. Jr. Callister. *Materials Science and Engineering: an introduction*. John Wiley & Sons, Inc, 7th edition, 2007.

[39] Richard Schmuch, Ralf Wagner, Gerhard Hörpel, Tobias Placke, and Martin Winter. Performance and cost of materials for lithium-based rechargeable automotive batteries. *Nature Energy*, 3:267–278, 2018.

[40] Matthew B. Pinson and Martin Z. Bazant. Theory of sei formation in rechargeable batteries: Capacity fade, accelerated aging and lifetime prediction. *Journal of The Electrochemical Society*, 160:A243, 2013. doi: 10.1149/2.044302jes.

[41] Pallavi Verma, Pascal Maire, and Petr Novák. A review of the features and analyses of the solid electrolyte interphase in li-ion batteries. *Electrochimica Acta*, 55:6332–6341, 2010. doi: 10.1016/j.electacta.2010.05.072.

[42] Hui Wu, Gerentt Chan, Jang W. Choi, Ill Ryu, Yan Yao, Matthew T. McDowell, Seok W. Lee, Ariel Jackson, Yuan Yang, Liangbing Hu, and Yi Cui. Stable cycling of double-walled silicon nanotube battery anodes through solid-electrolyte interphase control. *Nature Nanotechnology*, 7:310 – 315, 2012. doi: 10.1038/NNANO.2012.35.

[43] Maziar Ashuri, Qianran He, and Leon L. Shaw. Silicon as a potential anode material for li-ion batteries: where size, geometry and structure matter. *Nanoscale*, 8:74, 2016. doi: 10.1039/c5nr05116a.

[44] Vijay A. Sethuraman, Venkat Srinivasan, and John Newmana. Analysis of electrochemical lithiation and delithiation kinetics in silicon. *Journal of The Electrochemical Society*, 160:A394–A403, 2013.

[45] Matthew T. McDowell, Seok Woo Lee, William D. Nix, and Yi Cui. 25th anniversary article: Understanding the lithiation of silicon and other alloying anodes for lithium-ion batteries. *Advanced Materials*, 25:4966 – 4985, 2013. doi: 10.1002/adma.201301795.

[46] Wu Hui and Yi Cui. Designing nanostructures si anodes for high energy lithium ion batteries. *Nano Today*, 7:414 – 429, 2012. doi: 10.1016/j.nantod.2012.08.004.

[47] K. Ogata, E. Salager, Kerr C. J., A. E. Fraser, C. Ducati, A. J. Morris, S. Hofmann, and C. P. Grey. Revealing lithium-silicide phase transformations in nano-structured silicon-based lithium ion batteries via is situ nmr spectroscopy. *Nature Communications*, 5:3217, 2014. doi: 10.1038/ncomms3217.

[48] E. J. Mittemeijer. *Fundamentals of Materials Science*. Springer-Verlag, Berlin, Heidelberg, 2011?

[49] Syed A. Ashter. *Thermoforming of Single and Multilayer Laminates*. Elsevier, Inc, 2014.

[50] P. O'Brien. Chemical vapor deposition. In K. H. J. Buschow, Robert W. Cahn, Merton C. Flemings, Bernhard Ilschner, Edward J. Kramer, Subhash

Mahajan, and Patrick Veyssière, editors, *Encyclopedia of Materials: Science and Technology*, pages 1173–1176. Elsevier, 2nd edition, 2001. ISBN 978-0-08-043152-9.

[51] J. R. Creighton and P. Ho. Introduction to chemical vapor deposition (cvd). ASM International, 2001. [Accessed: 29.04.2020] URL: `https://www.asminternational.org/documents/10192/1849770/ACFAA6E.pdf`.

[52] L. Martinu, O. Zabeida, and J. E. Klemberg-Sapieha. Plasma-enhanced chemical vapor deposition of functional coatings. In Peter M. Martin, editor, *Handbook of Deposition Technologies for Films and Coatings*, pages 392–465. Elsevier Inc., 3rd edition, 2001. ISBN 978-0-8155-2031-3.

[53] Seong J. An, Jianlin Li, Zhijia Du, Claus Daniel, and David L. Wood, III. Fast formation cycling for lithium ion batteries. *Journal of Power Sources*, 342: 846–852, 2017.

[54] Guido Van Rossum and Fred L. Drake. *Python 3 Reference Manual*. CreateSpace, Scotts Valley, CA, 2009. ISBN 1441412697.

[55] Jan Petter Mæhlen. Cellpy. URL `https://github.com/jepegit/cellpy`.

[56] Wilhelm Burger and Mark J. Burge. *Digital Image Processing*. Springer, London, 2nd edition, 2016.

[57] Aaron Meurer, Christopher P Smith, Mateusz Paprocki, Ondřej Čertík, Sergey B Kirpichev, Matthew Rocklin, AMiT Kumar, Sergiu Ivanov, Jason K Moore, Sartaj Singh, et al. Sympy: symbolic computing in python. *PeerJ Computer Science*, 3:e103, 2017.

[58] P. De Bievre, S. Valkiers, R. Gonfiantini, P. D. P. Taylor, H. Bettin, F. Spieweck, A. Peuto, S. Pettorruso, M. Mosca, K. Fujii, M. Tanaka, Y. Nezu, A. J. Leistner, and W. J. Giardini. The molar volume of silicon [avogadro constant]. *IEEE Transactions on Instrumentation and Measurement*, 46(2):592–595, 1997.

[59] Yujie Zhu and Chunsheng Wang. Galvanostatic intermittent titration technique for phase-transformation electrodes. *The Journal of Physical Chemistry C*, 114: 2830–2841, 2010. doi: 10.1021/jp9113333.

[60] Riccardo Ruffo, Seung Sae Hong, Candace K. Chan, Robert A. Huggins, and Yi Cui. Impedance analysis of silicon nanowire lithium ion battery anodes. *The Journal of Physical Chemistry C*, 113:11390–11398, 2009. doi: 10.1021/jp901594.

[61] J. Xie, N. Imanishi, T. Zhang, A. Hirano, Y. Takeda, and Yamamoto O. Li-ion diffusion in amorphous si films preparedby rf magnetron sputtering: A comparison of using liquid and polymer electrolytes. *Materials Chemistry and Physics*, 120:421–425, 2010. doi: 10.1016/j.matchemphys.2009.11.031.

[62] Kazutaka Yoshimura, Junji Suzuki, Kyoichi Sekine, and Tsutomu Takamura. Measurement of the diffusion rate of li in silicon by the use of bipolar cells. *Journal of Power Sources*, 174:653–657, 2007. doi: 10.1016/j.jpowsour.2007.06.115.

[63] A. Ulvestad, H. F. Andersen, I. J. T. Jensen, T. T. Mongstad, J. P. Mæhlen, Ø. Prytz, and M. Kirkengen. Substoichiometric silicon nitride – an anode material for li-ion batteries promising high stability and high capacity. *Scientific Reports*, 8 (1):8634, 2018. doi: 10.1038/s41598-018-26769-8.

Appendix A

Cell Names

Table A.1: List of all cell names and corresponding current rate and Si thin film thickness.

Cell name	Current rate (c-rate)	Thin film thickness (nm)
TFSi_60_1	C/10	60
TFSi_60_2	C/10	60
TFSi_60_3	C/10	60
TFSi_60_4	C/5	60
TFSi_60_5	C/5	60
TFSi_60_6	C/5	60
TFSi_60_7	C/2	60
TFSi_60_8	C/2	60
TFSi_60_9	C/2	60
TFSi_80_1	C/10	80
TFSi_80_2	C/10	80
TFSi_80_3	C/10	80
TFSi_80_4	C/5	80
TFSi_80_5	C/5	80
TFSi_80_6	C/5	80
TFSi_80_7	C/2	80
TFSi_80_8	C/2	80
TFSi_80_9	C/2	80

Appendix B

Code

```
1
2 import numpy as np
3
4 def calc_D(cycle_number, steptable, h, tau=None, remove_outliers=
    False):
5     # Creating a step table for only one cycle and extracting
    possible GITT steps
6     st = steptable.loc[steptable.cycle == cycle_number]
7     st = st[st.type.isin(["charge", "discharge", "ocvrlx_up", "
    ocvrlx_down",
8                           "rest"])]
9
10    if st.empty:
11        print("the given cycle is not found")
12        return
13
14    # Finding the length of each step
15    if tau is None:
16        tau = st["step_time_last"] - st["step_time_first"]
17
18    st["tau"] = tau
19
20    # Checking which steps are GITT pulse steps
21    t0 = st["type"]
22    t1 = st["type"].shift(periods=-1)   # All values are shifted
    once upwards
23    t2 = st["type"].shift(periods=-2)   # All values are shifted
    twice upwards
24    # Want every other step to be the same and the one in between
    should be ocv/rest step
25    valid_D = (t0==t2) & (t1.str.contains("ocv") | t1.str.contains(
    "rest"))
26
27    # Calculating diffusion coefficients by GITT formula
28    st["DEt"] = st["voltage_last"] - st["voltage_first"] # should
    remove the IR drop here (maybe calculate it based on the
    measured IR time the current?)
29    st["DEs"] = st["voltage_last"].shift(periods=1) - st["
    voltage_last"].shift(periods=-1)
30    st["D"] = 4/(np.pi*tau) * (h)**2 * (st["DEs"].loc[valid_D] / st
    ["DEt"].loc[valid_D])**2
```

```
31
32      if remove_outliers:
33          # Finding what the pulse and rest times should be
34          pulse_tau = round(np.mean(st['tau'].
35                                    loc[st['type'] == "discharge"]))
36          rest_tau = round(np.mean(st['tau'].loc[(st['type'] == "rest
    ")
37                                           | ( st['type'].str.contains("
    ocv"))]))
38
39          # Removing steps with a too short pulse length
40          tau_lim_pulse = 2/3*pulse_tau
41          st['D'].loc[(st['tau'] < tau_lim_pulse) \
42                      & (st['type'] == "discharge")] = float('nan')
43
44          # Removing steps with too short rest period
45          tau_lim_rest = 2/3*rest_tau
46          inds = st.index[(st['tau'] < tau_lim_rest) & ((st['type']
    == "ocvrlx_up") | \
47                                  (st['type'] =="rest"))]
48
49          for ind in inds.to_numpy():
50              if st.shift(-1).loc[ind, 'type'] == st.shift(1).loc[ind
    , 'type']:
51                  if ind - 1 in st.index:
52                      st.loc[ind - 1, 'D'] = float('nan')
53                  if ind + 1 in st.index:
54                      st.loc[ind + 1, 'D'] = float('nan')
55
56      return st
```

Listing B.1: Code for calculating diffusion coefficients based on equation (2.24)

```
from scipy.ndimage import gaussian_filter1d, median_filter
from scipy.interpolate import interp1d
import numpy as np

def smooth_y(steptable, selector, int_num=None, size=100, sigma=100, variable="D", smooth_mode="gaussian"):
    """Takes in a step table with calculated D values and calculates new smoothed y values using gaussian or median smoothing and interpolation"""

    # Getting out the x and y values to plot from the steptable
    steptable_no_nan = steptable[[selector + '_avr', 'DEt', 'DEs', 'D']].loc[steptable.type==selector].dropna()

    if int_num is not None:
        x = steptable_no_nan[selector + '_avr']
        x_norm = x/x.max()
        y = steptable_no_nan[variable]

        x_int = np.linspace(x_norm.min(), x_norm.max(), int_num)
        f = interp1d(x_norm, y)
        y_int = f(x_int)
    else:
        x = steptable_no_nan[selector + '_avr']
        x_int = x/x.max()
        y_int = steptable_no_nan[variable]

    if smooth_mode == "gaussian":
        return x_int, gaussian_filter1d(y_int, sigma, mode='nearest')
    elif smooth_mode == "median":
        return x_int, median_filter(y_int, size, mode='nearest')
    elif smooth_mode == "med_gauss":
        y_median = median_filter(y_int, size, mode='nearest')
        y_gaussian = gaussian_filter1d(y_median, sigma, mode='nearest')
        return x_int, y_gaussian
```

Listing B.2: Code for increasing the number of data points in a data set by interpolation followed by smoothing of the data with a median filter or a Gaussian filter or both.

Appendix C

Product Specifications for Arbin

Product Specifications

Hardware Specifications		
Number of Channels		96 channels
Bipolar Linear Circuitry		Allows cross-zero linearity and no switching time between charge/discharge
Voltage	**Voltage range (min/max)**	-5 to 5V
	Measurement Resolution	24 Bit <10uV
	Measurement Precision	<100 ppm
	Control Accuracy	< +/- 0.02%
	Input Impedance	10 G Ohm
Current	**Standard Current Ranges**	200mA/10mA/1mA/100uA
	Measurement Resolution	18 Bit 0.0003% (as low as 6nA)
	Measurement Precision	<100 ppm
	Control Accuracy	0.02% FSR (as low as 0.4uA)
	Minimum V at Maximum Current	-5V @ 200mA
	Current rise time	~200uS
Time	**Minimum Step Time**	5ms
	Data Logging Rate	2,000 points per second, per system
	Measurement Resolution	100us
Maximum continuous power per channel		1 W
Connection for Batteries		Coin cell holders Option: various battery holders for coin cells, cylindrical cells, or flat cells
Connection to Computer		TCP/IP (Ethernet)
Ventilation Method		Air cooled with *variable speed* fans
Computer Specifications		PC with 22” flat-screen monitor is included, preloaded with our MITS 7 testing software

Appendix D

Plots of D as Function of SOC, Comparing Pulse Lengths

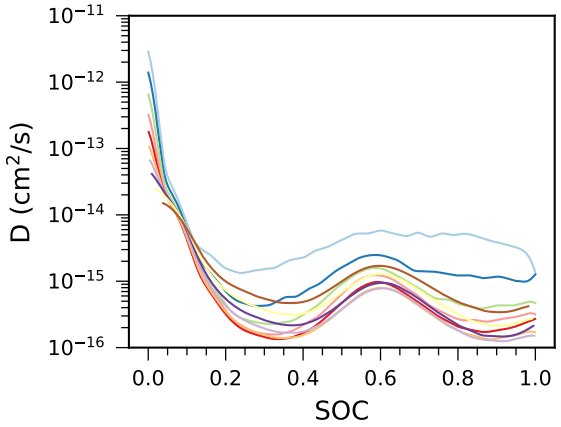

(a) 60 nm, C/10, 1, discharge

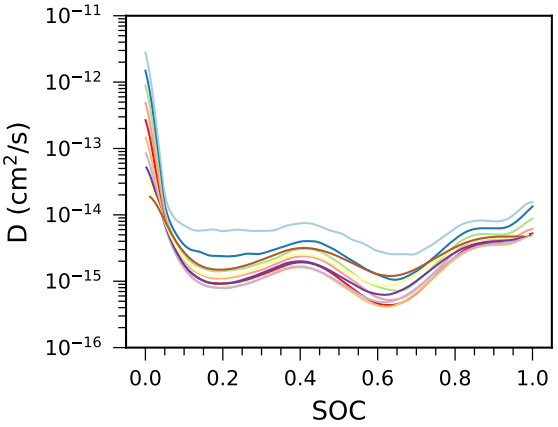

(b) 60 nm, C/10, 1, charge

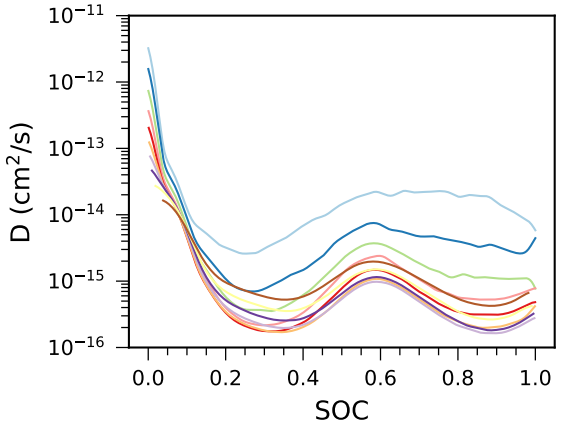

(c) 60 nm, C/10, 2, discharge

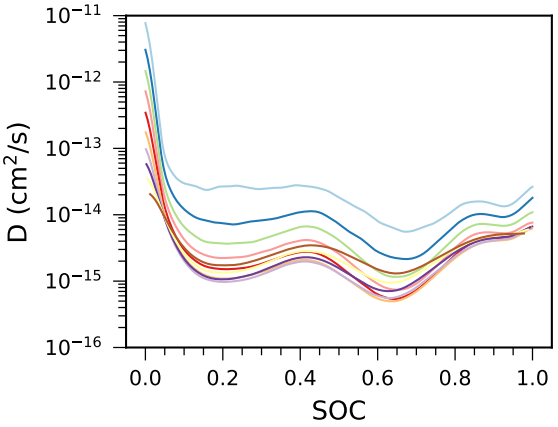

(d) 60 nm, C/10, 2, charge

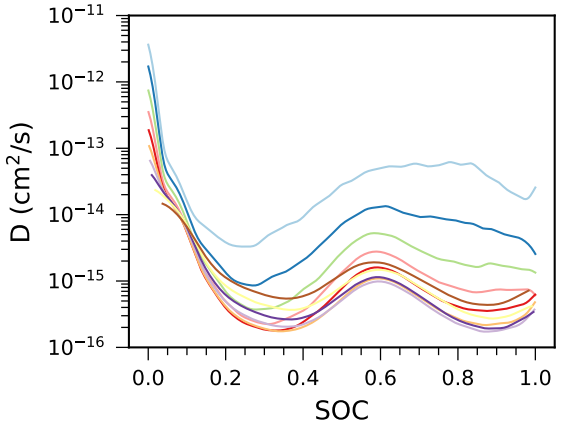

(e) 60 nm, C/10, 3, discharge

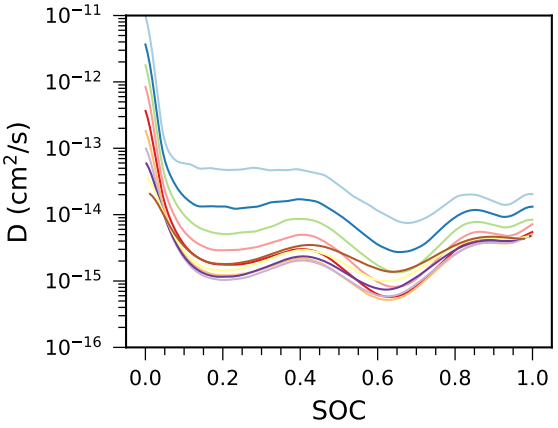

(f) 60 nm, C/10, 3, charge

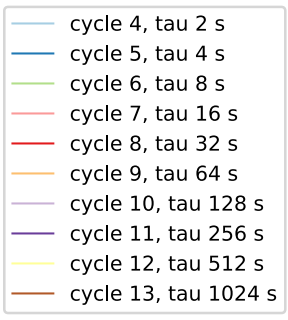

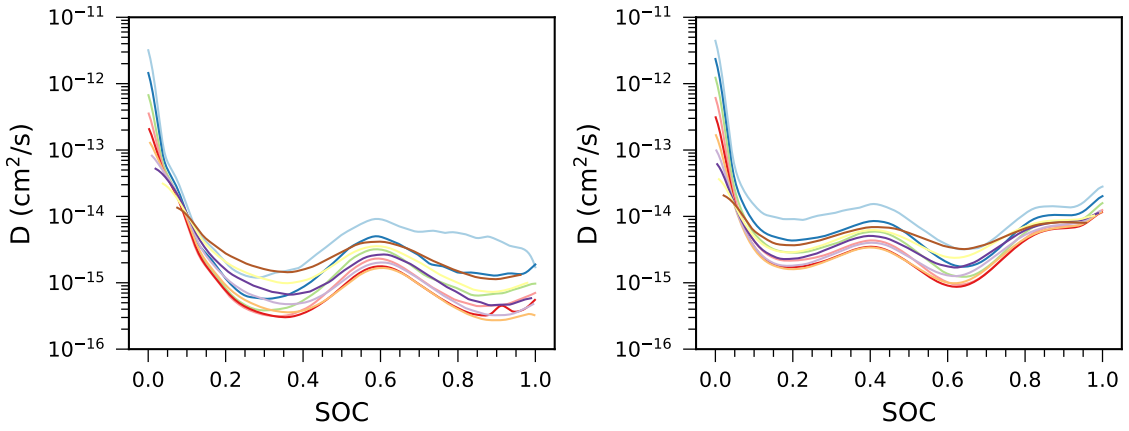

(a) 60 nm, C/5, 1, discharge

(b) 60 nm, C/5, 1, charge

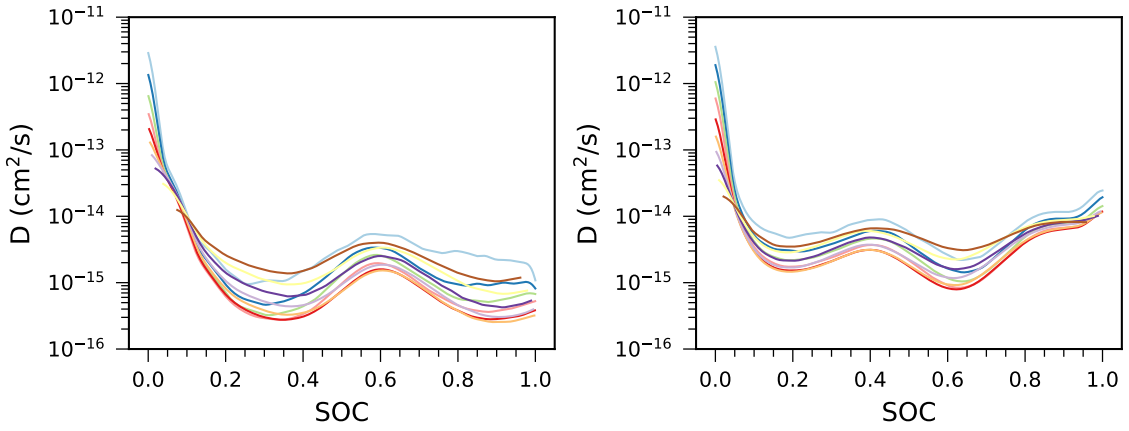

(c) 60 nm, C/5, 2, discharge

(d) 60 nm, C/5, 2, charge

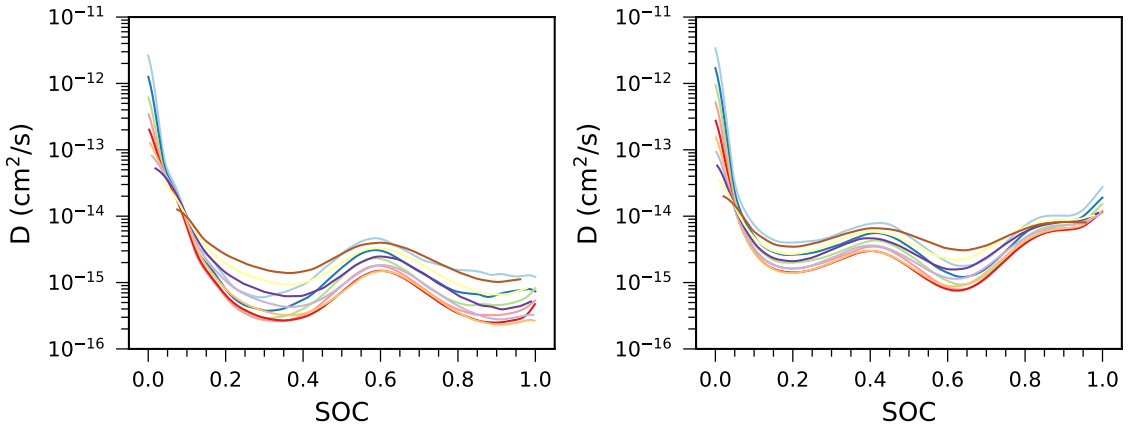

(e) 60 nm, C/5, 3, discharge

(f) 60 nm, C/5, 3, charge

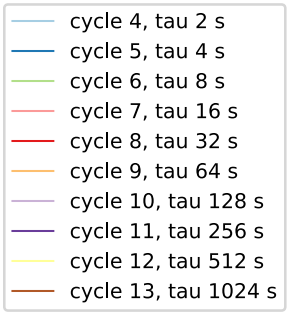

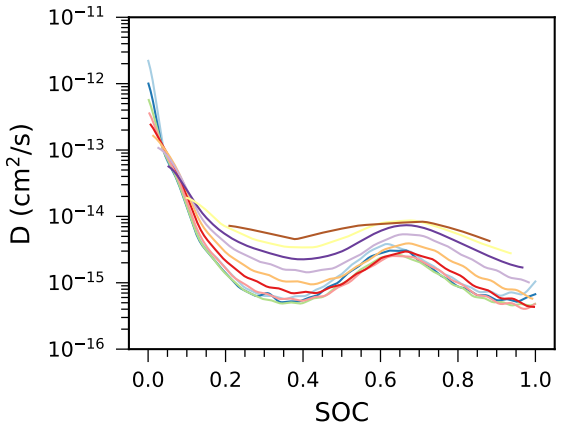

(a) 60 nm, C/2, 1, discharge

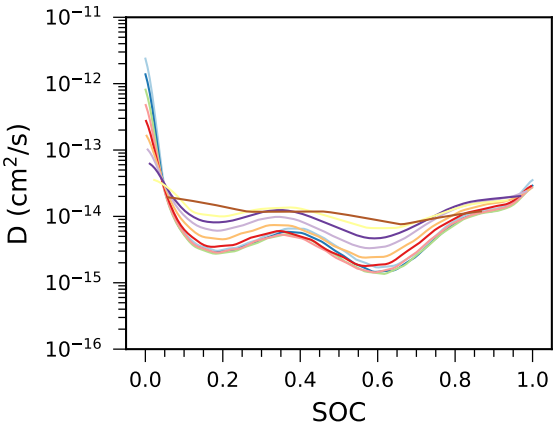

(b) 60 nm, C/2, 1, charge

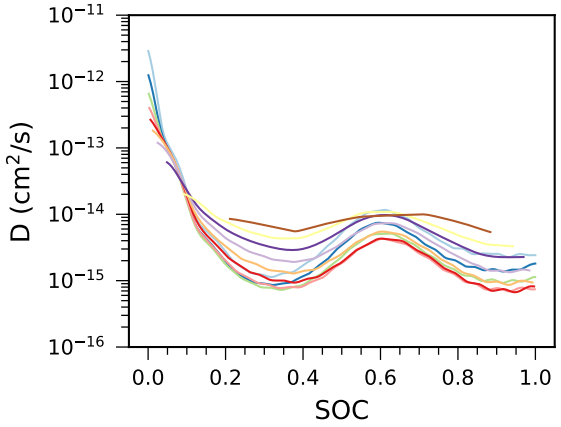

(c) 60 nm, C/2, 2, discharge

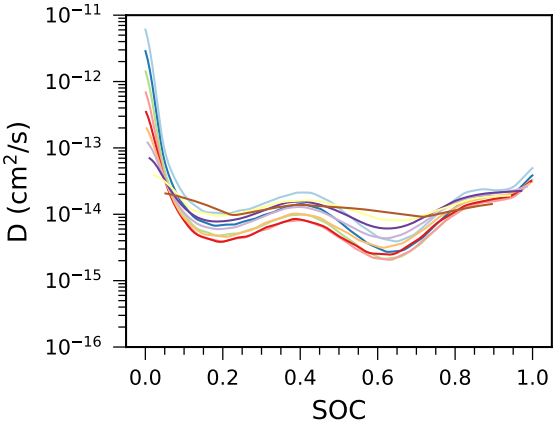

(d) 60 nm, C/2, 2, charge

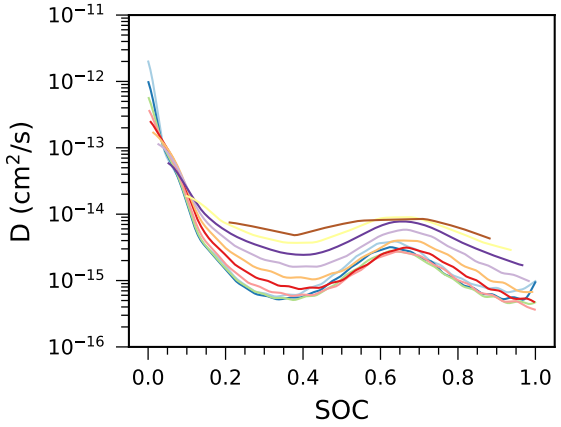

(e) 60 nm, C/2, 3, discharge

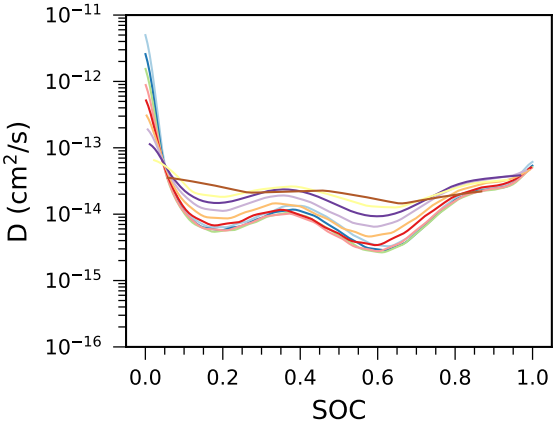

(f) 60 nm, C/2, 3, charge

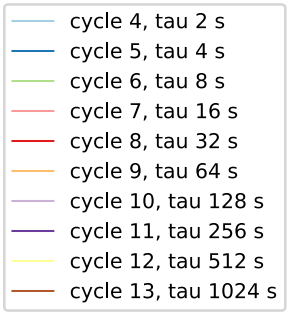

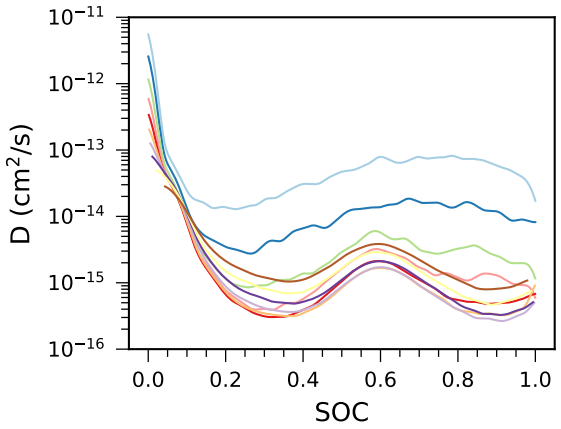

(a) 80 nm, C/10, 1, discharge

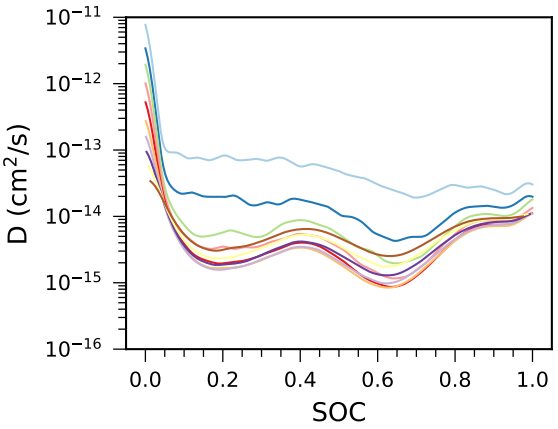

(b) 80 nm, C/10, 1, charge

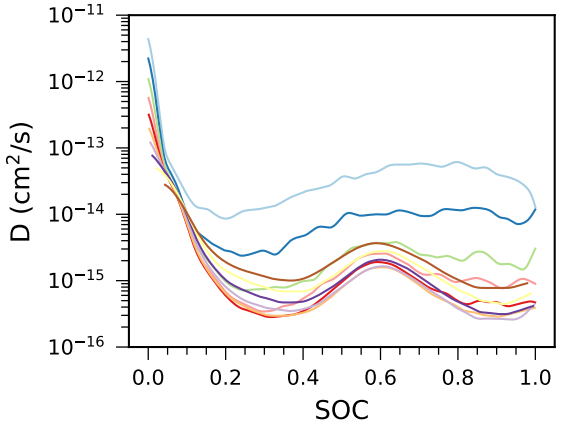

(c) 80 nm, C/10, 2, discharge

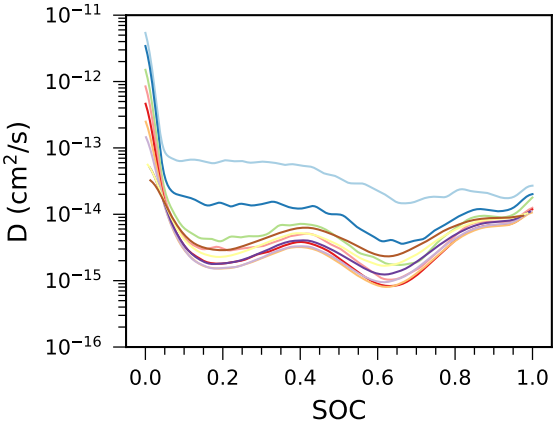

(d) 80 nm, C/10, 2, charge

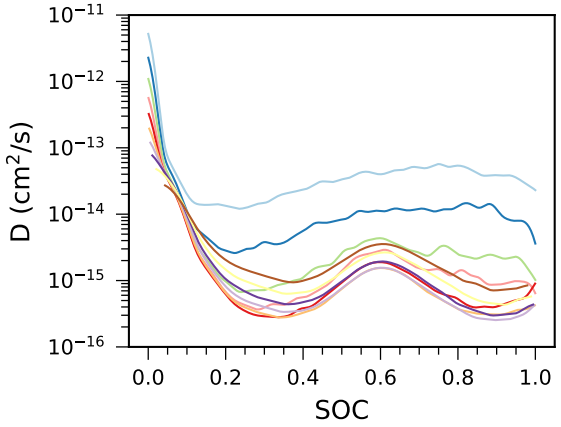

(e) 80 nm, C/10, 3, discharge

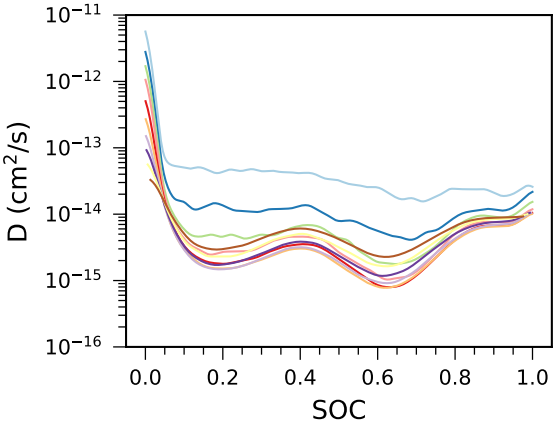

(f) 80 nm, C/5, 3, charge

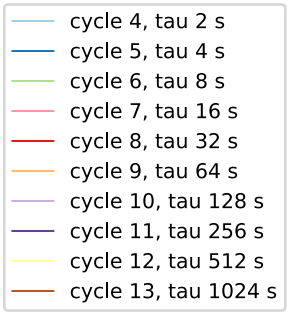

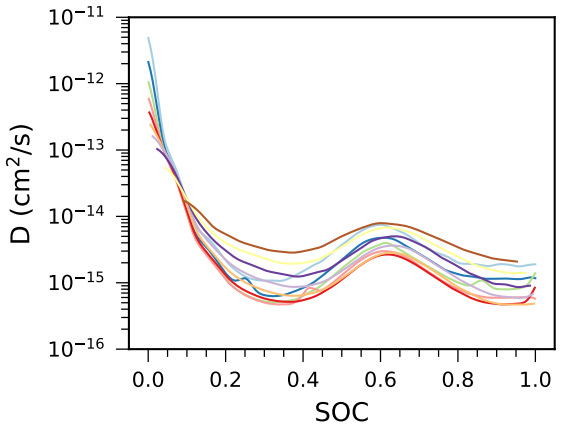

(a) 80 nm, C/5, 1, discharge

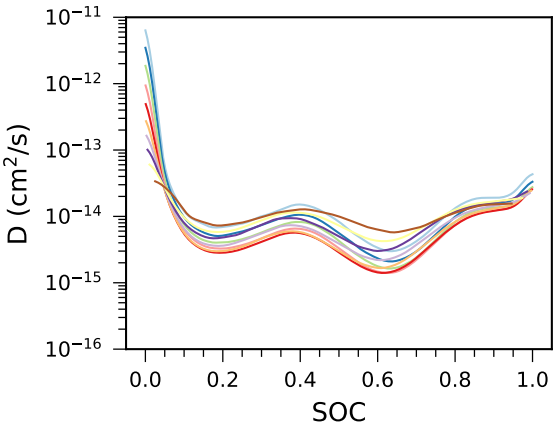

(b) 80 nm, C/5, 1, charge

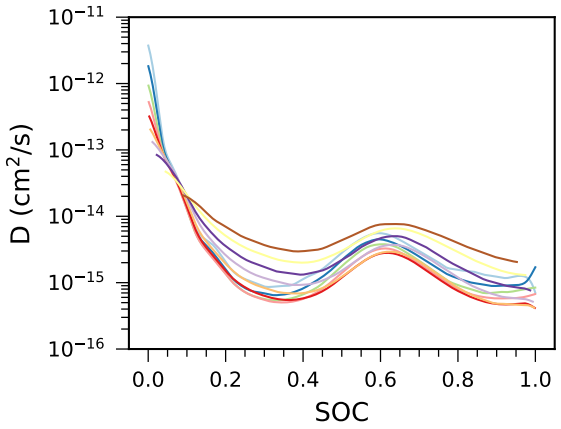

(c) 80 nm, C/5, 2, discharge

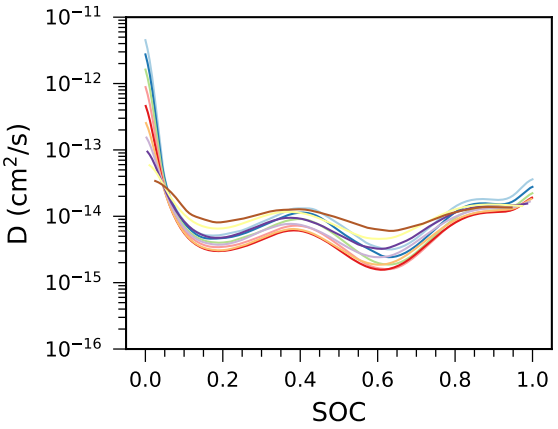

(d) 80 nm, C/5, 2, charge

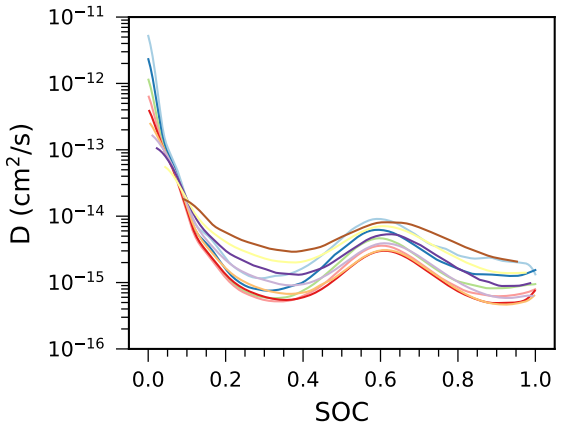

(e) 80 nm, C/5, 3, discharge

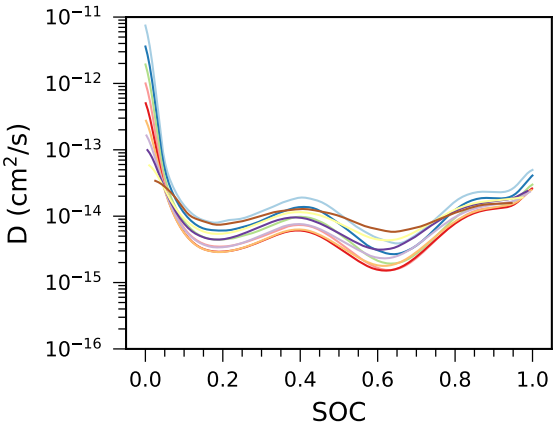

(f) 80 nm, C/5, 3, charge

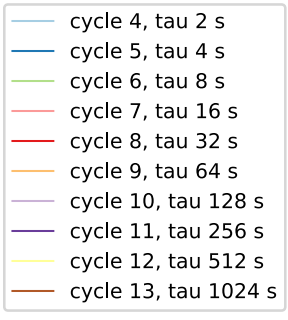

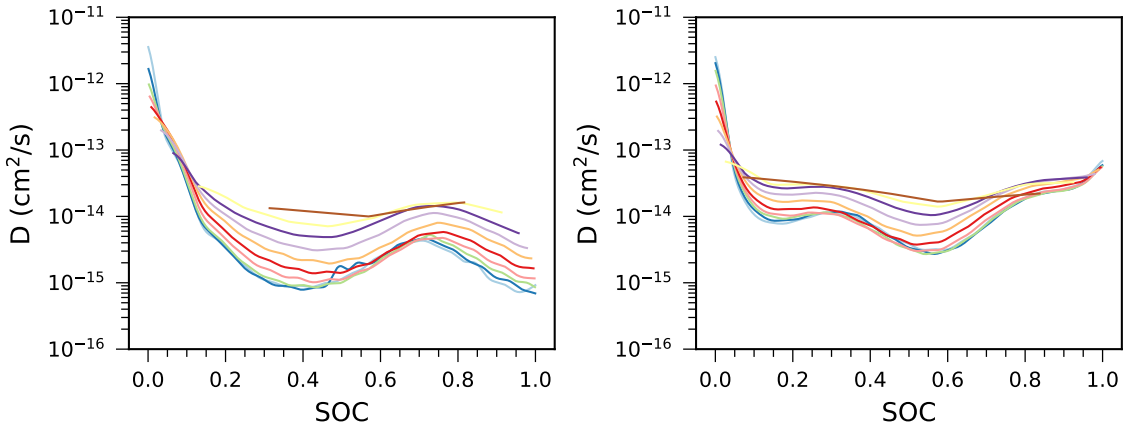

(a) 80 nm, C/2, 1, discharge

(b) 80 nm, C/2, 1, charge

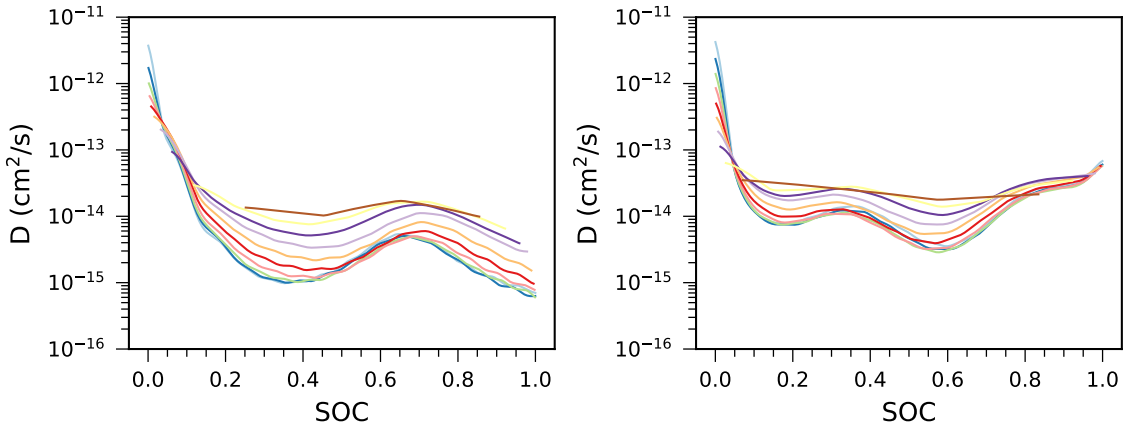

(c) 80 nm, C/2, 2, discharge

(d) 80 nm, C/2, 2, charge

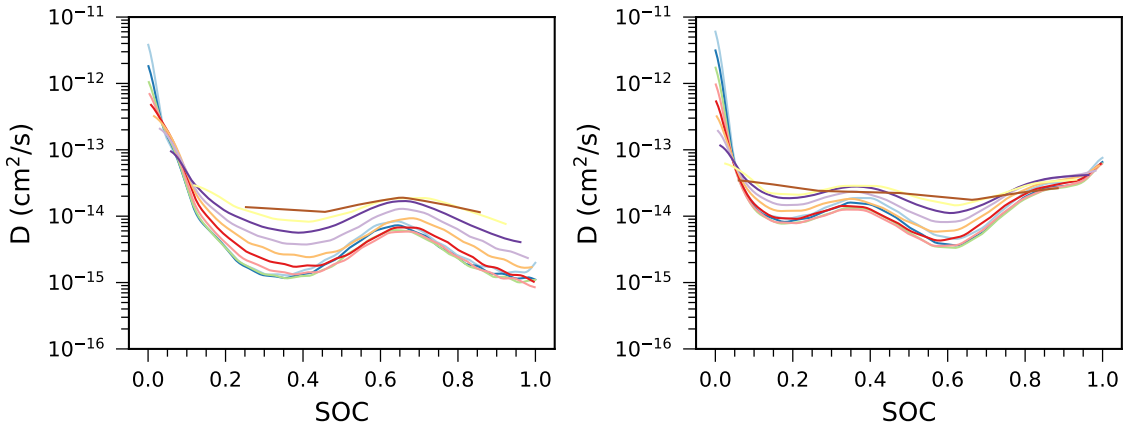

(e) 80 nm, C/2, 3, discharge

(f) 80 nm, C/2, 3, charge

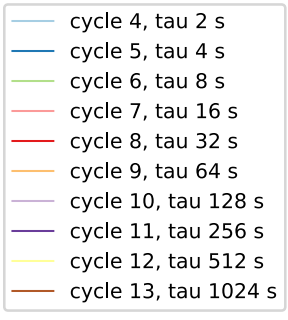

Appendix E

Plots of D as Function of SOC, Comparing Currents

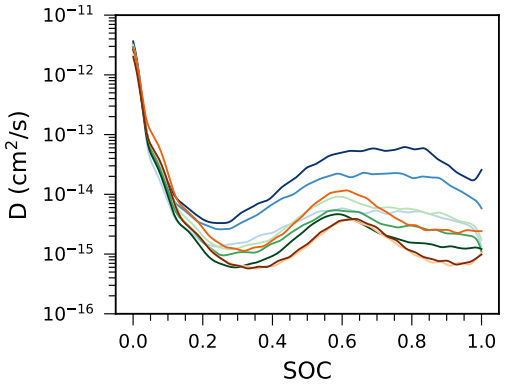

(a) 60 nm, τ = 2 s, discharge

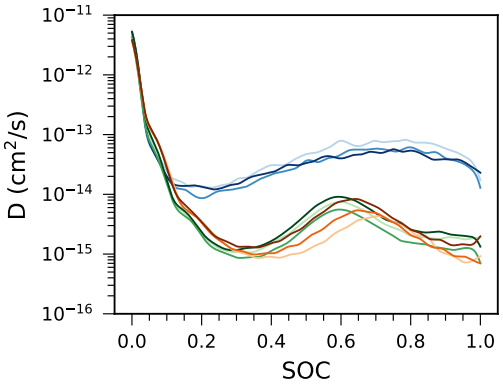

(b) 80 nm, τ = 2 s, discharge

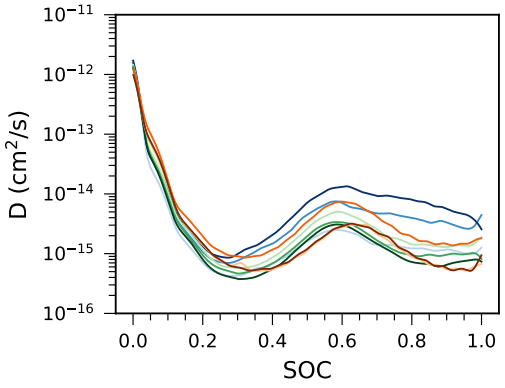

(c) 60 nm, τ = 4 s, discharge

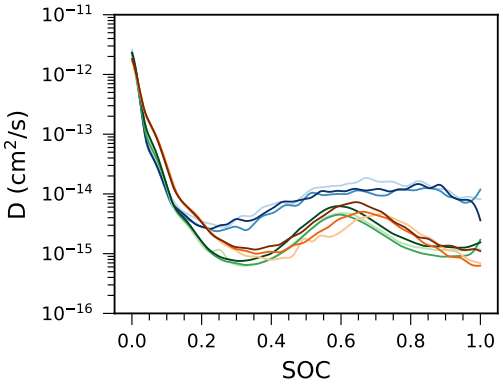

(d) 80 nm, τ = 4 s, discharge

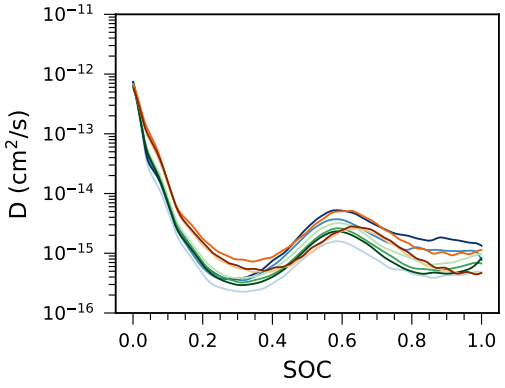

(e) 60 nm, τ = 8 s, discharge

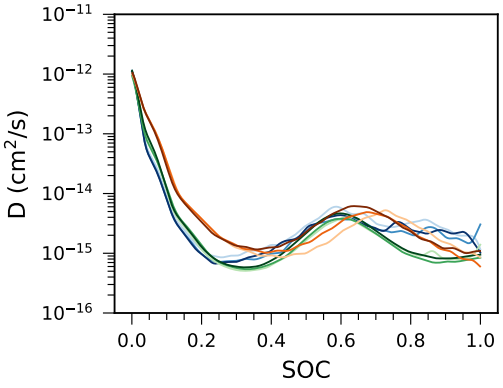

(f) 80 nm, τ = 8 s, discharge

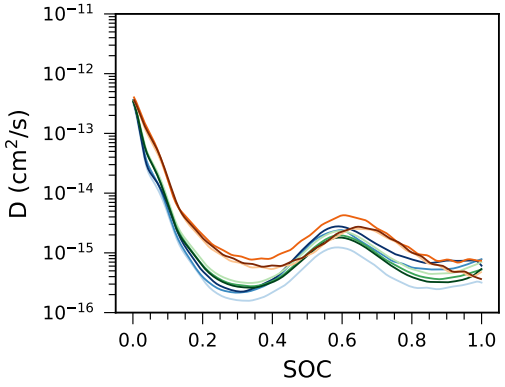

(g) 60 nm, τ = 16 s, discharge

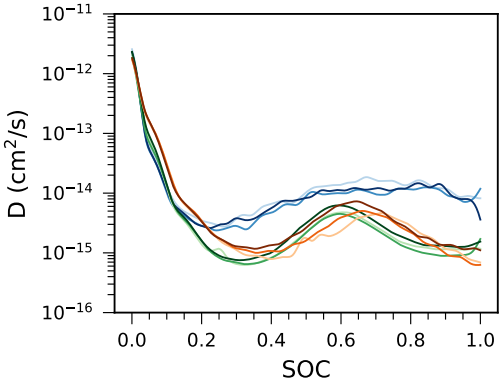

(h) 80 nm, τ = 16 s, discharge

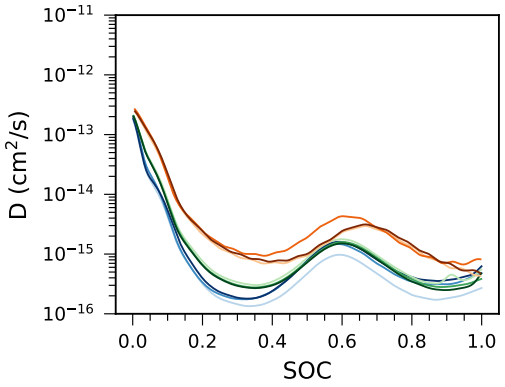

(i) 60 nm, τ = 32 s, discharge

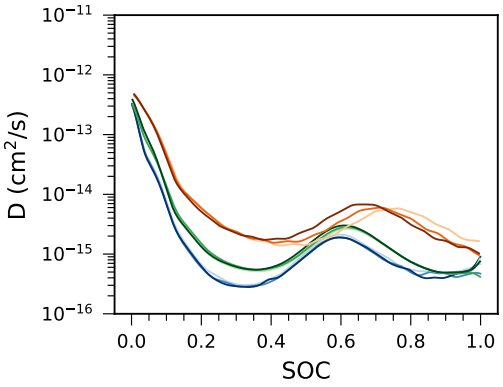

(j) 80 nm, τ = 32 s, discharge

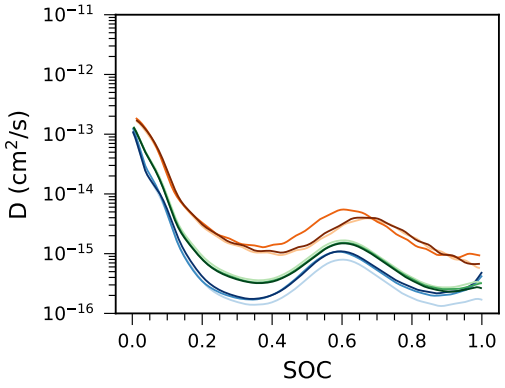

(k) 60 nm, τ = 64 s, discharge

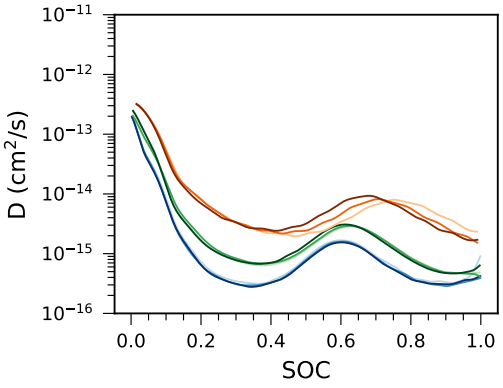

(l) 80 nm, τ = 64 s, discharge

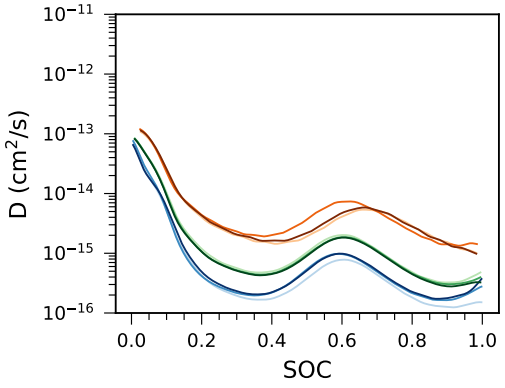

(m) 60 nm, τ = 128 s, discharge

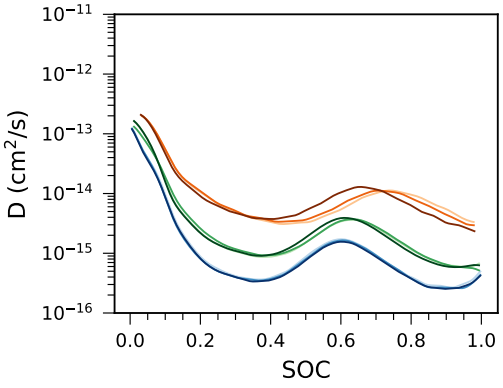

(n) 80 nm, τ = 128 s, discharge

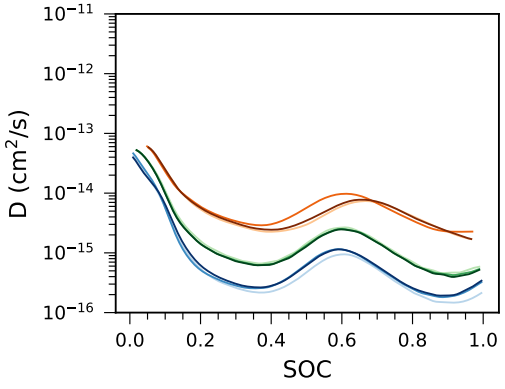

(o) 60 nm, τ = 256 s, discharge

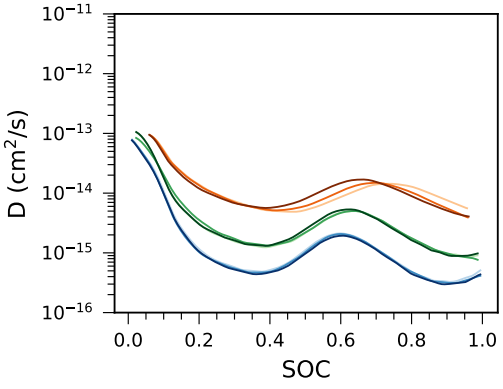

(p) 80 nm, τ = 256 s, discharge

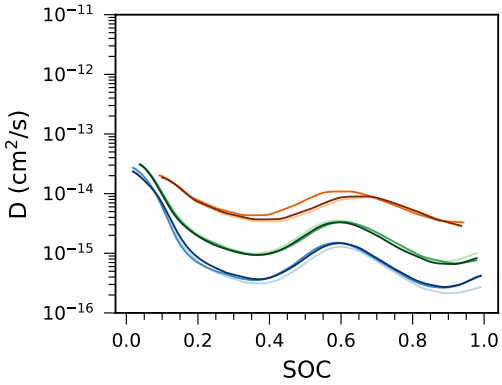

(q) 60 nm, τ = 512 s, discharge

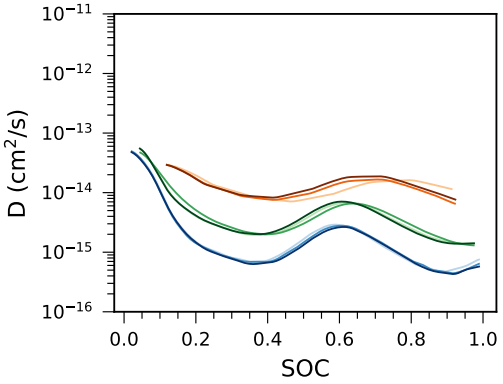

(r) 80 nm, τ = 512 s, discharge

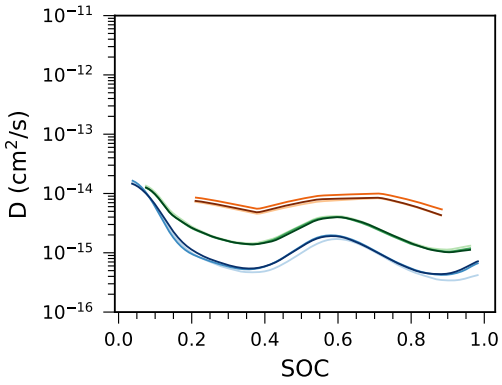

(s) 60 nm, τ = 1024 s, discharge

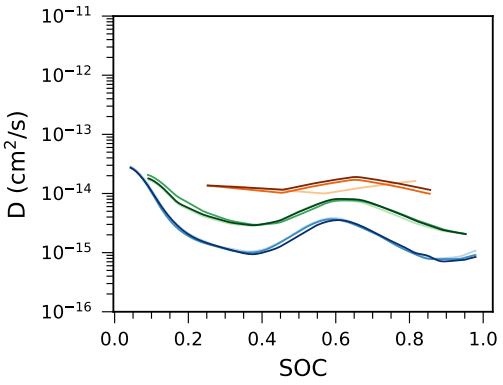

(t) 80 nm, τ = 1024 s, discharge

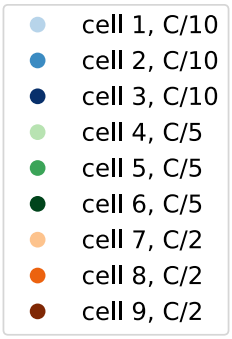

Figure E.1: Computed diffusion coefficients as function of SOC for discharge, comparing currents.

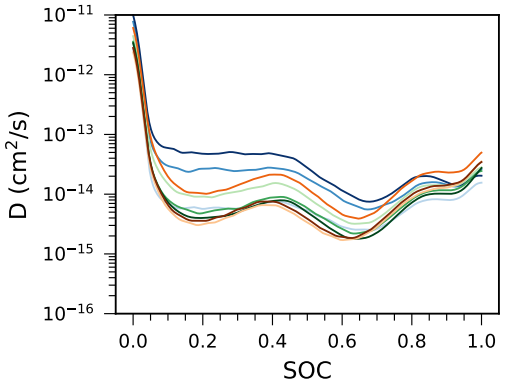

(a) 60 nm, τ = 2 s, charge

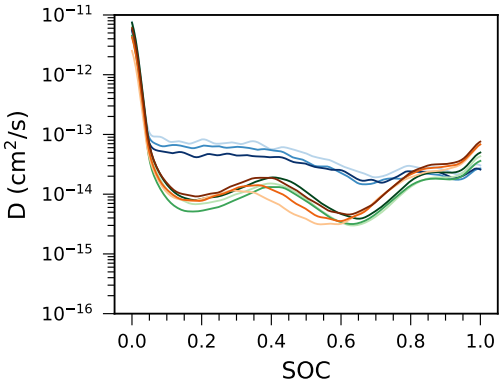

(b) 80 nm, τ = 2 s, charge

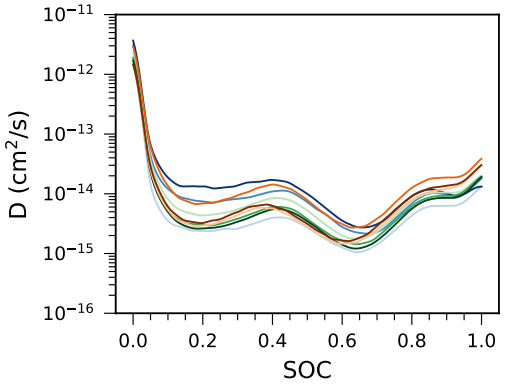

(c) 60 nm, τ = 4 s, charge

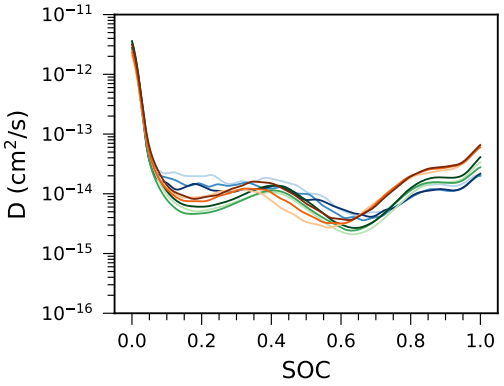

(d) 80 nm, τ = 4 s, charge

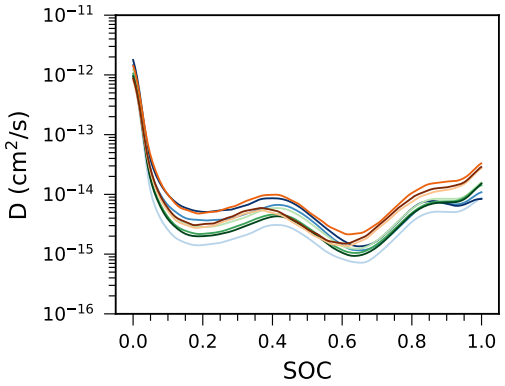

(e) 60 nm, τ = 8 s, charge

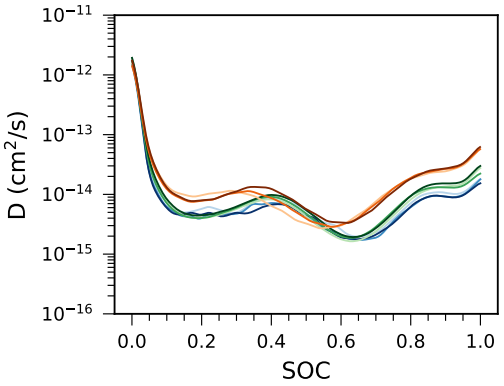

(f) 80 nm, τ = 8 s, charge

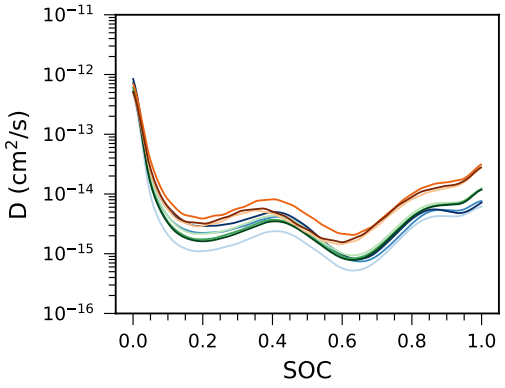

(g) 60 nm, τ = 16 s, charge

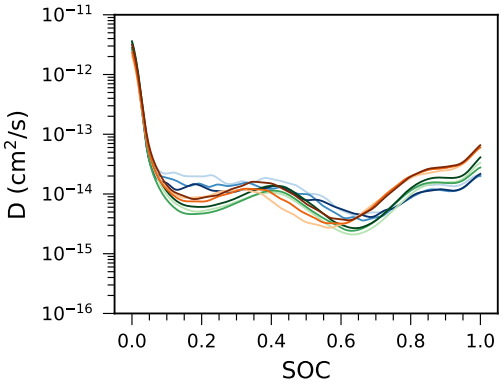

(h) 80 nm, τ = 16 s, charge

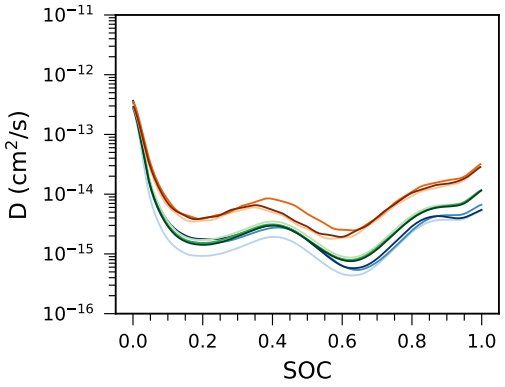

(i) 60 nm, τ = 32 s, charge

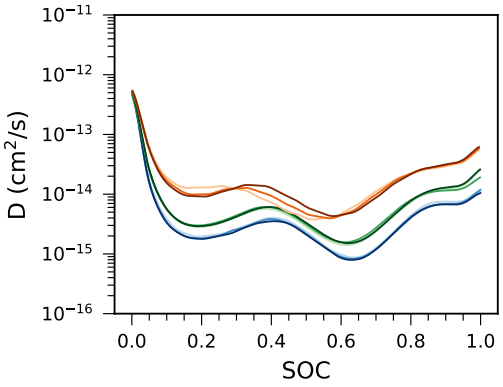

(j) 80 nm, τ = 32 s, charge

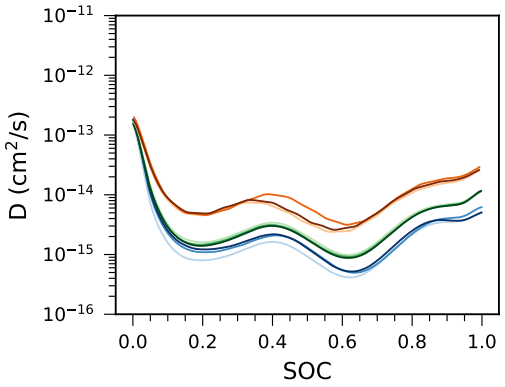

(k) 60 nm, τ = 64 s, charge

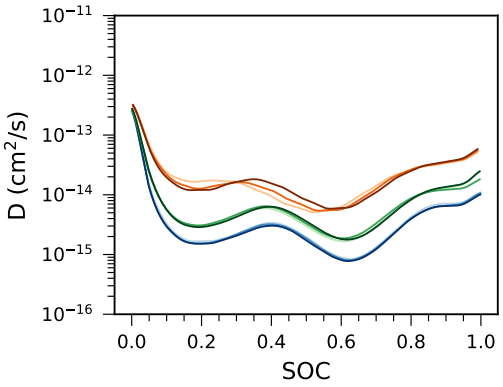

(l) 80 nm, τ = 64 s, charge

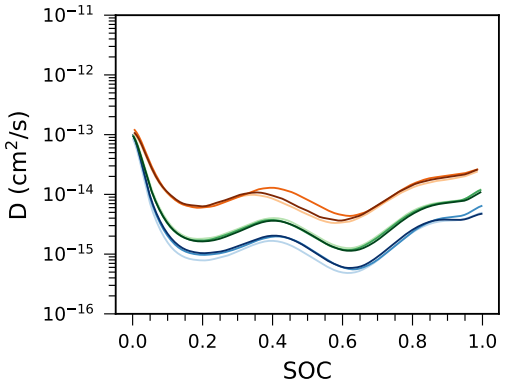

(m) 60 nm, τ = 128 s, charge

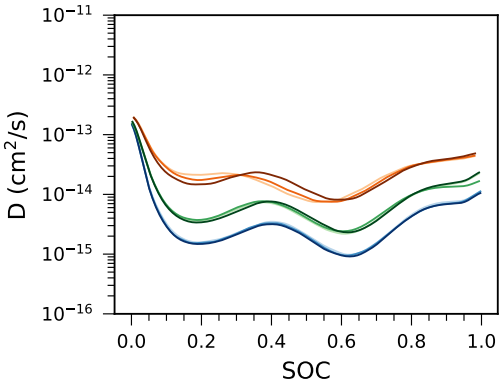

(n) 80 nm, τ = 128 s, charge

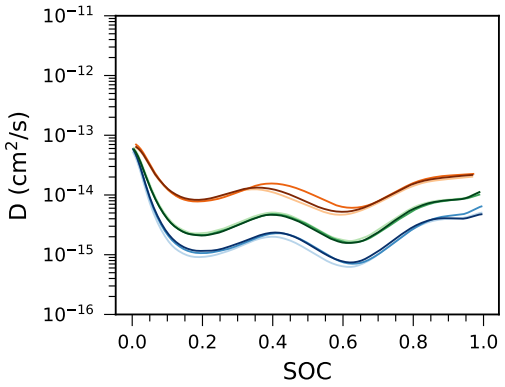

(o) 60 nm, τ = 256 s, charge

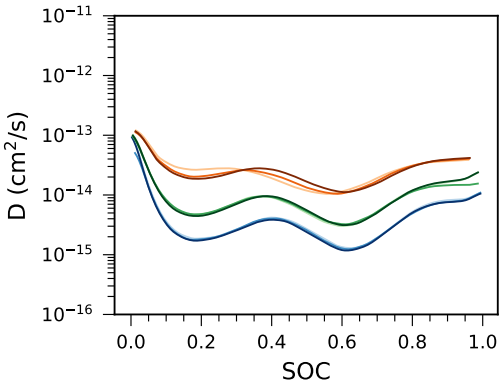

(p) 80 nm, τ = 256 s, charge

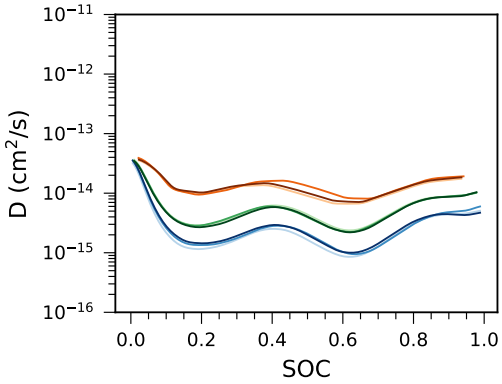

(q) 60 nm, τ = 512 s, charge

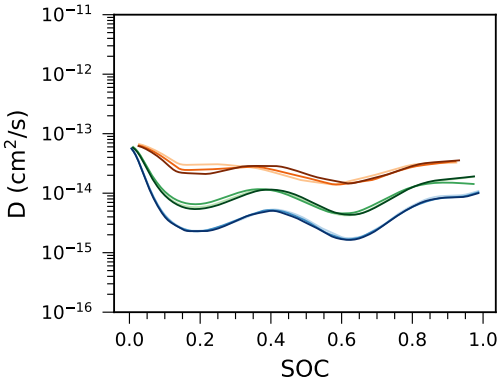

(r) 80 nm, τ = 512 s, charge

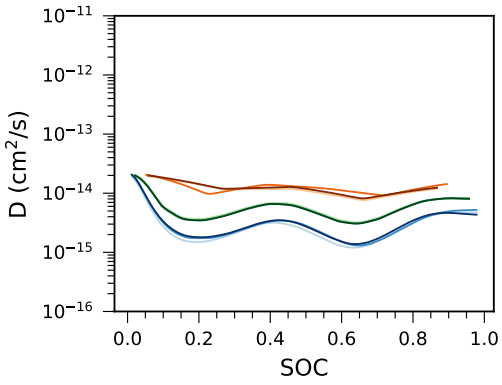

(s) 60 nm, τ = 1024 s, charge

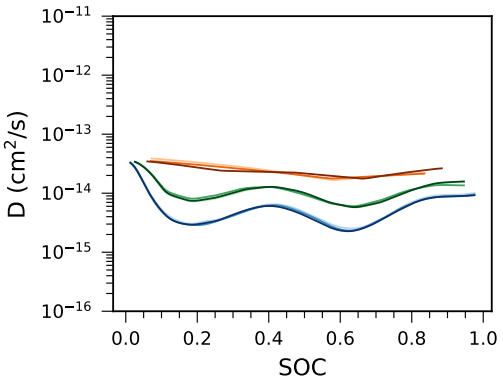

(t) 80 nm, τ = 1024 s, charge

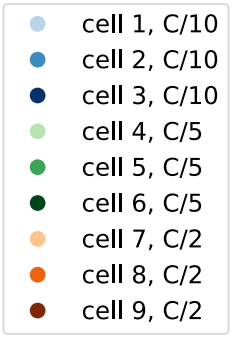

Figure E.2: Computed diffusion coefficients as function of SOC during charge, comparing currents.

Appendix F

Plots of Median of D at Varying SOC Windows

This appendix contains plots of the median of D at varying SOC windows. The legend for all the plots is given in Figure F.1.

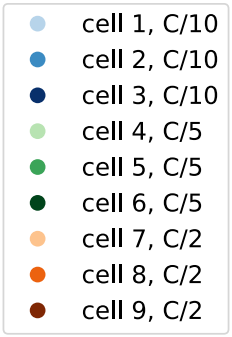

Figure F.1: Legends for Median of D plots.

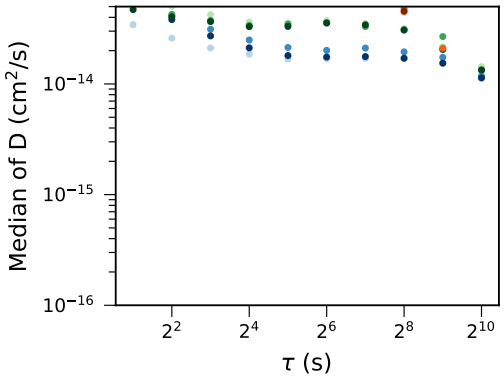

(a) 60 nm, discharge, 0 - 0.1 SOC

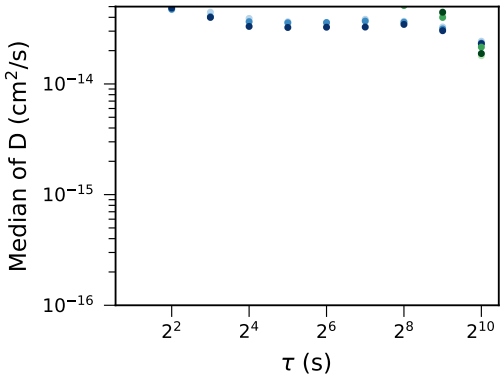

(b) 80 nm, discharge, 0 - 0.1 SOC

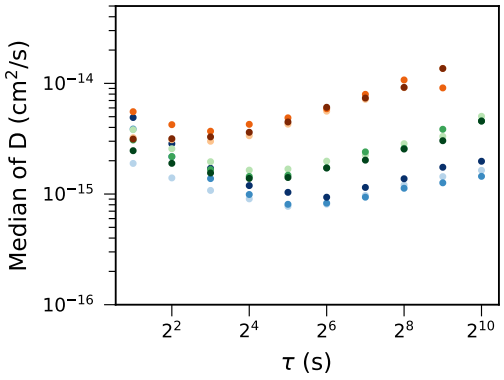

(c) 60 nm, discharge, 0.1 - 0.2 SOC

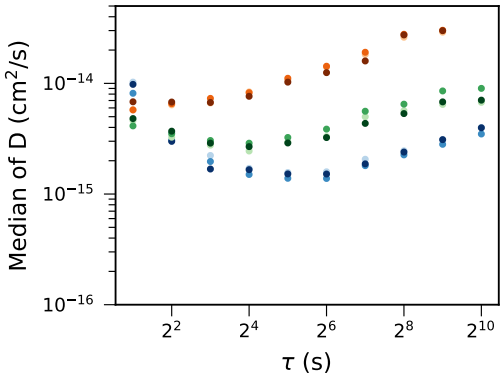

(d) 80 nm, discharge, 0.1 - 0.2 SOC

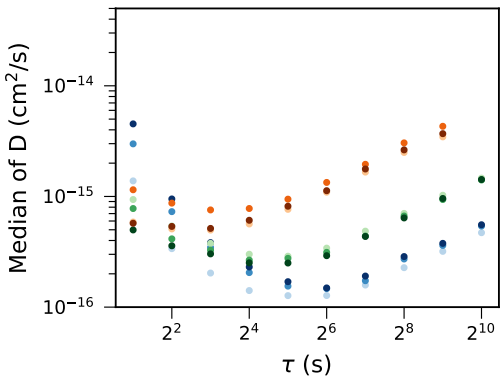

(e) 60 nm, discharge, 0.3 - 0.4 SOC

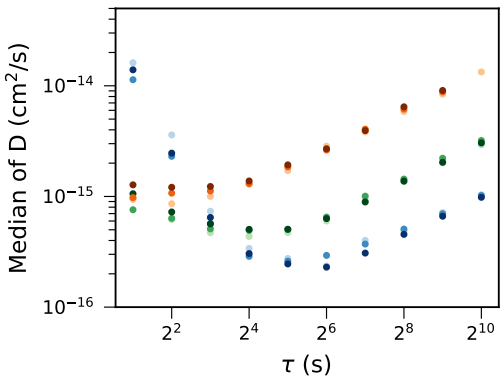

(f) 80 nm, discharge, 0.3 - 0.4 SOC

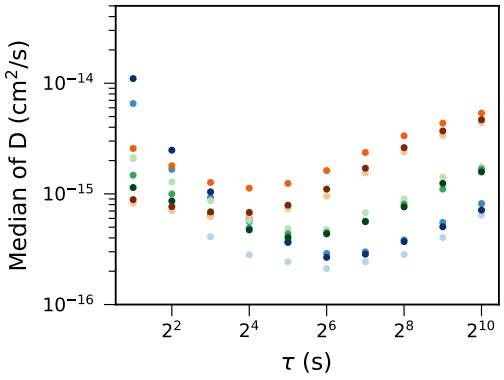

(g) 60 nm, discharge, 0.4 - 0.5 SOC

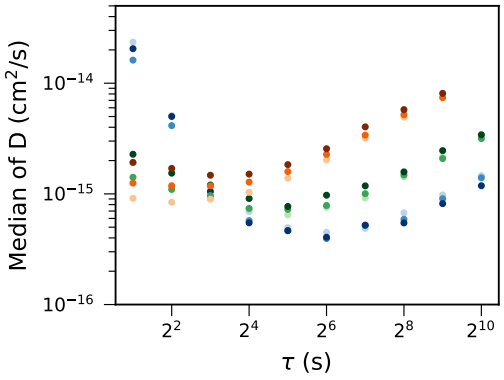

(h) 80 nm, discharge, 0.4 - 0.5 SOC

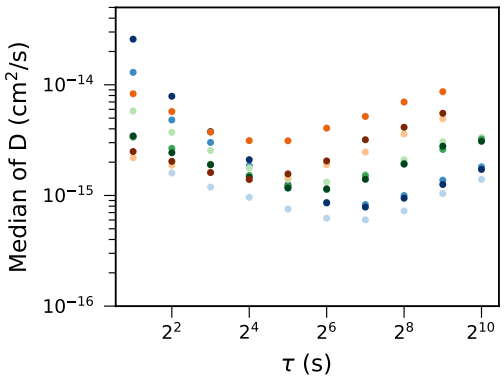

(i) 60 nm, discharge, 0.5 - 0.6 SOC

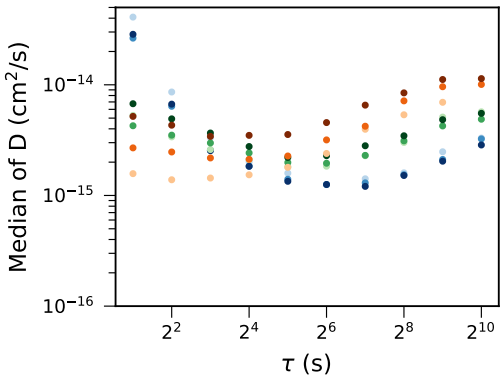

(j) 80 nm, discharge, 0.5 - 0.6 SOC

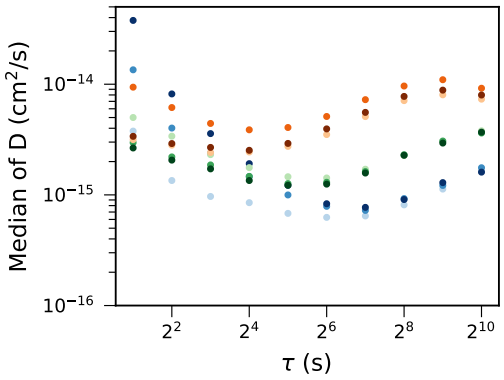

(k) 60 nm, discharge, 0.6 - 0.7 SOC

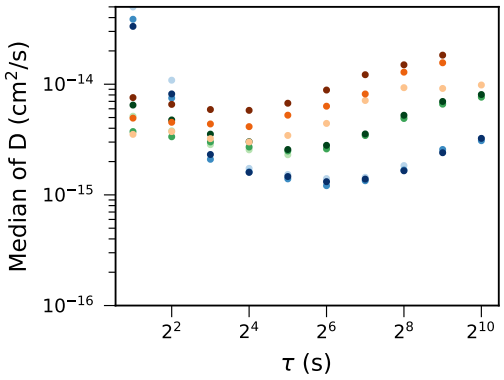

(l) 80 nm, discharge, 0.6 - 0.7 SOC

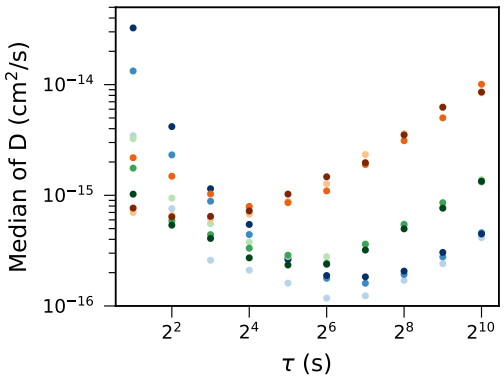

(m) 60 nm, discharge, 0.8 - 0.9 SOC

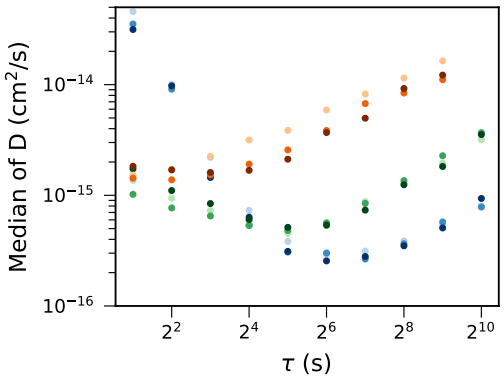

(n) 80 nm, discharge, 0.8 - 0.9 SOC

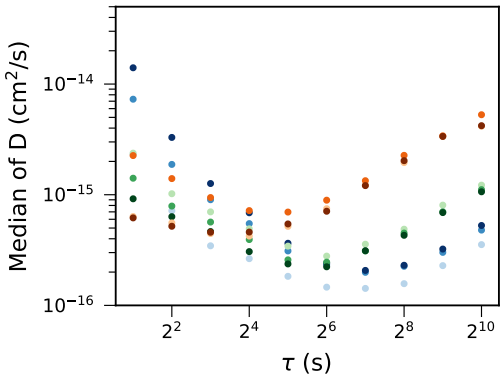

(o) 60 nm, discharge, 0.9 - 1.0 SOC

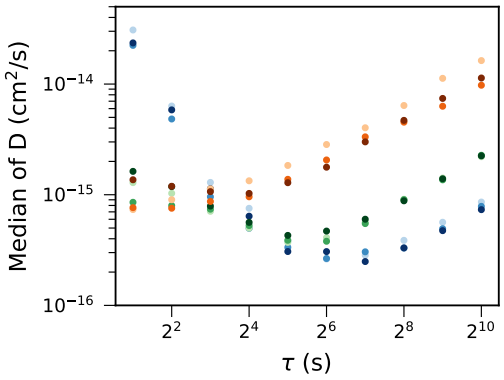

(p) 80 nm, discharge, 0.9 - 1.0 SOC

Figure F.2: Median of D for different SOC windows, discharge.

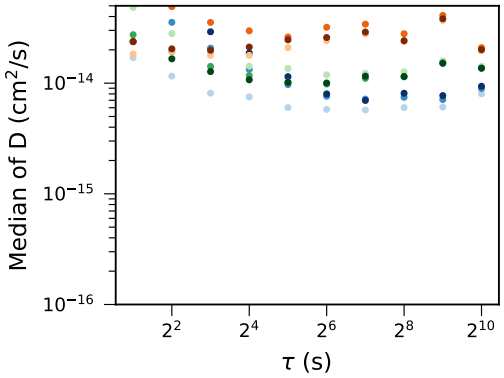

(a) 60 nm, charge, 0 - 0.1 SOC

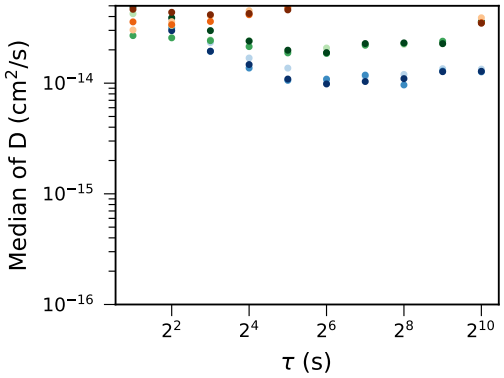

(b) 80 nm, charge, 0 - 0.1 SOC

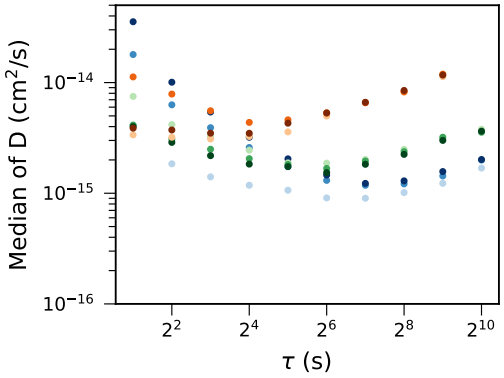

(c) 60 nm, charge, 0.1 - 0.2 SOC

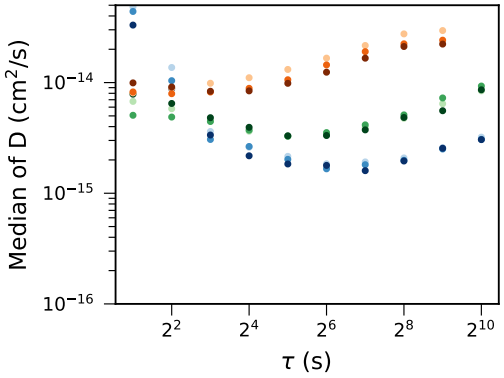

(d) 80 nm, charge, 0.1 - 0.2 SOC

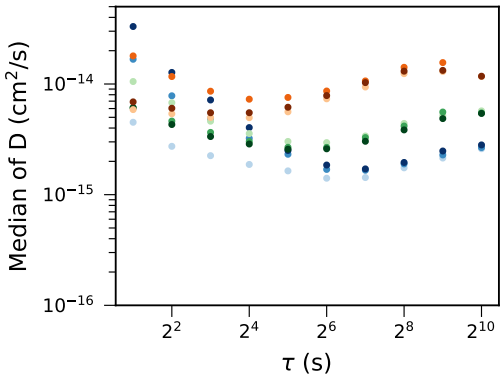

(e) 60 nm, charge, 0.3 - 0.4 SOC

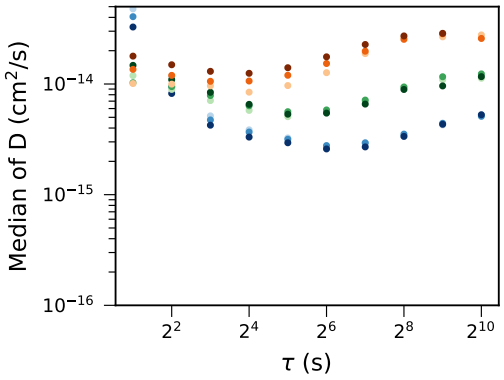

(f) 80 nm, charge, 0.3 - 0.4 SOC

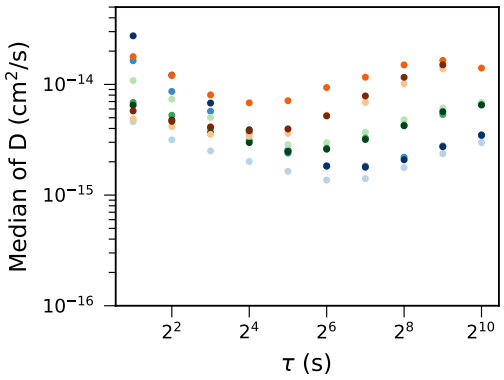

(g) 60 nm, charge, 0.4 - 0.5 SOC

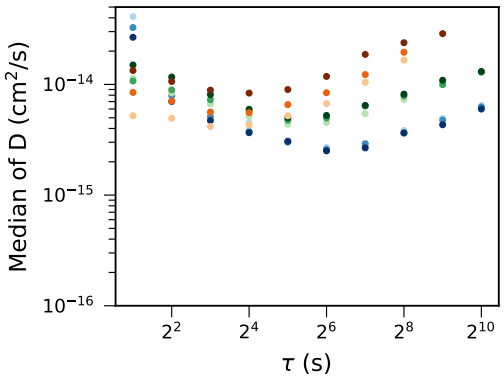

(h) 80 nm, charge, 0.4 - 0.5 SOC

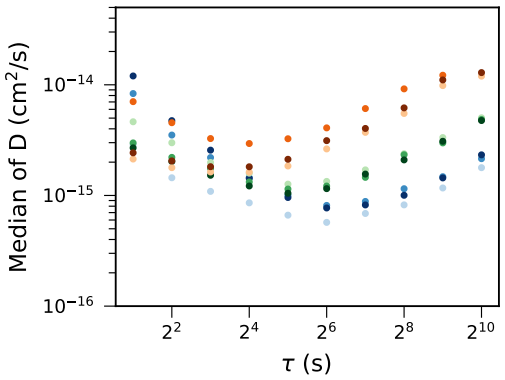

(i) 60 nm, charge, 0.5 - 0.6 SOC

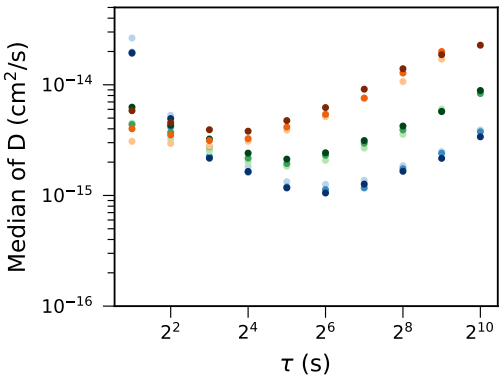

(j) 80 nm, charge, 0.5 - 0.6 SOC

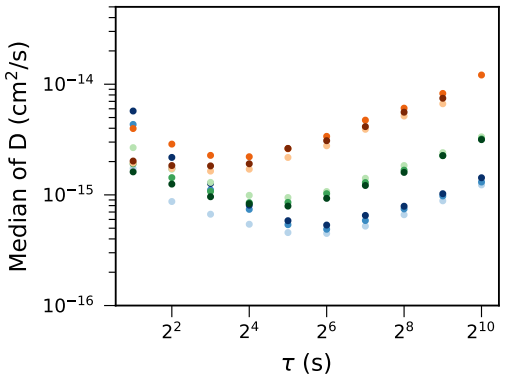

(k) 60 nm, charge, 0.6 - 0.7 SOC

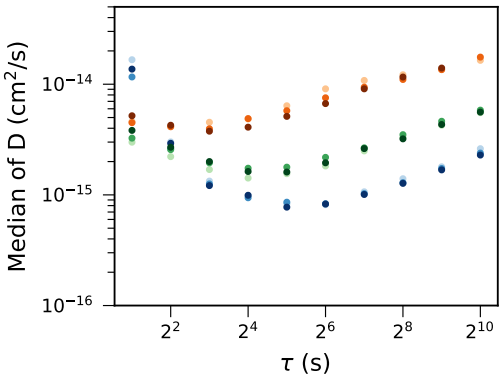

(l) 80 nm, charge, 0.6 - 0.7 SOC

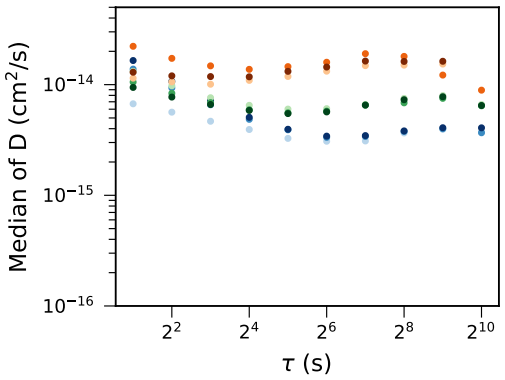

(m) 60 nm, charge, 0.8 - 0.9 SOC

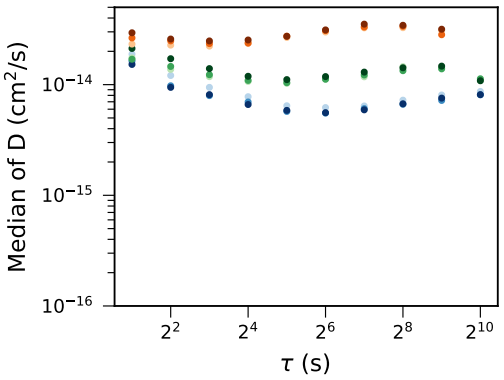

(n) 80 nm, charge, 0.8 - 0.9 SOC

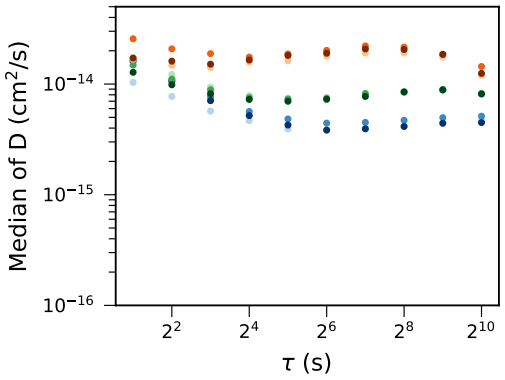

(o) 60 nm, charge, 0.9 - 1.0 SOC

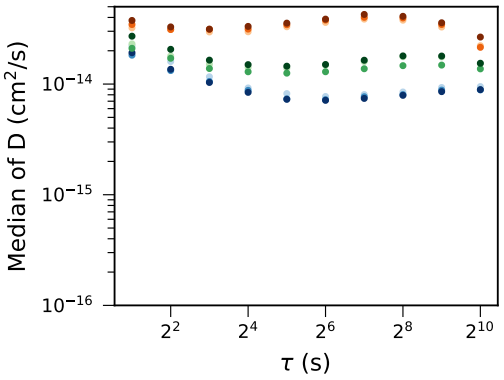

(p) 80 nm, charge, 0.9 - 1.0 SOC

Figure F.3: Median of D for different SOC windows, charge.

Appendix G

Linear Fits of E($\sqrt{t}$)

This appendix shows plots of $\frac{\Delta E}{\Delta\sqrt{t}}$ compared with the $E(\sqrt{t})$ curve. Figure G.1 show the legends for these plots.

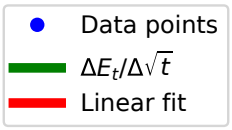

Figure G.1: Legend for plots of linear fit of $E(\sqrt{t})$

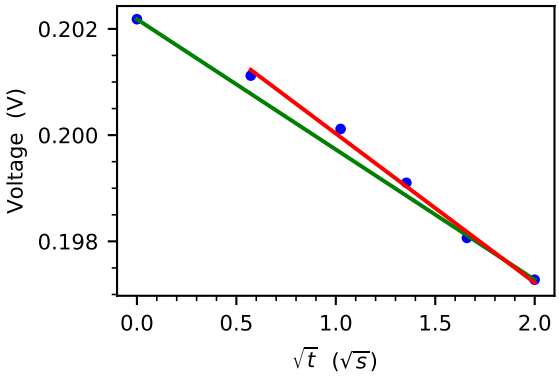

(a) 80 nm, discharge, τ = 4 s

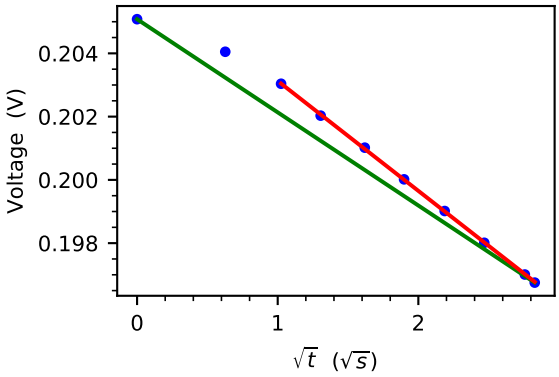

(b) 80 nm, discharge, τ = 8 s

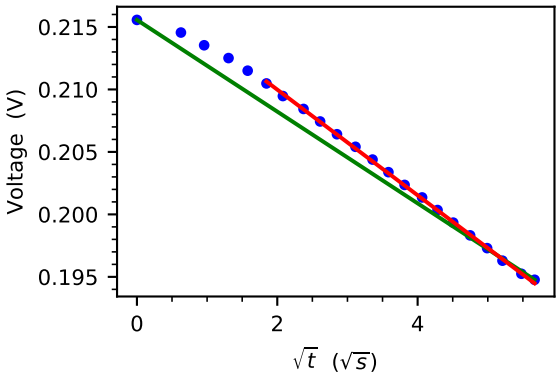

(c) 80 nm, discharge, τ = 32 s

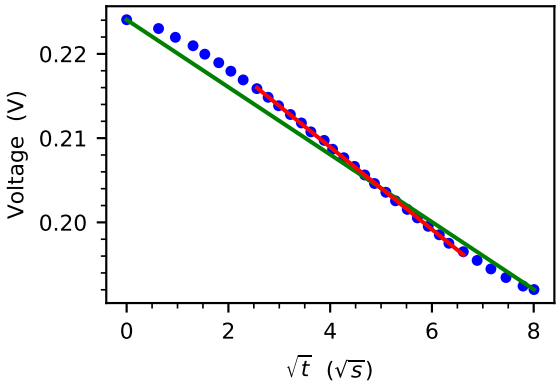

(d) 80 nm, discharge, τ = 64 s

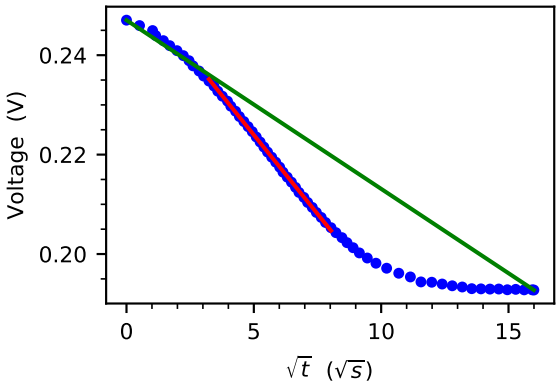

(e) 80 nm, discharge, τ = 256 s

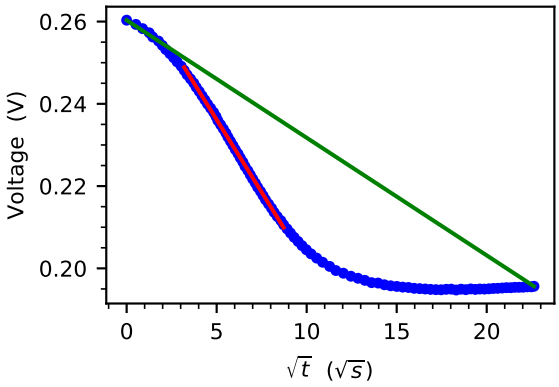

(f) 80 nm, discharge, τ = 512 s

Figure G.2: Linear fit of the linear area on the E versus square root of t curve for four different pulse lengths, C/10. The blue dots are the experimental data points and the red line is the linear fit.

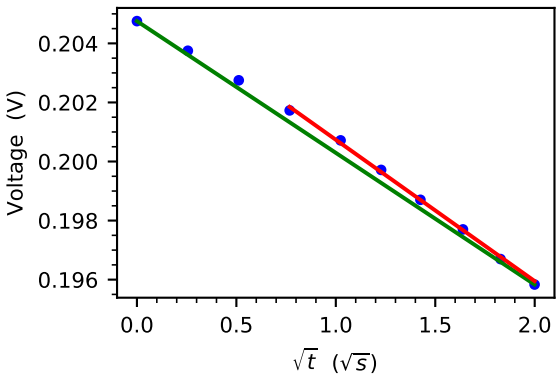

(a) 80 nm, discharge, τ = 4 s

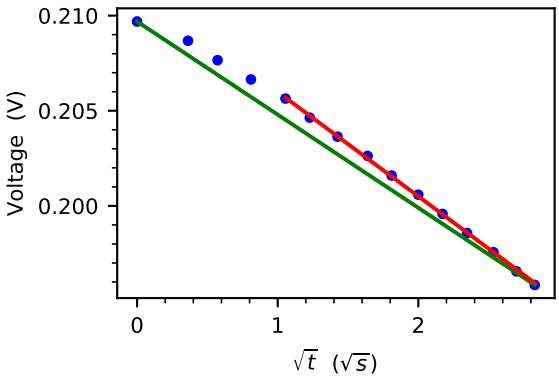

(b) 80 nm, discharge, τ = 8 s

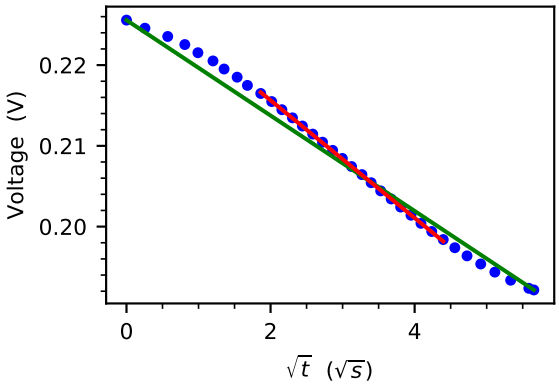

(c) 80 nm, discharge, τ = 32 s

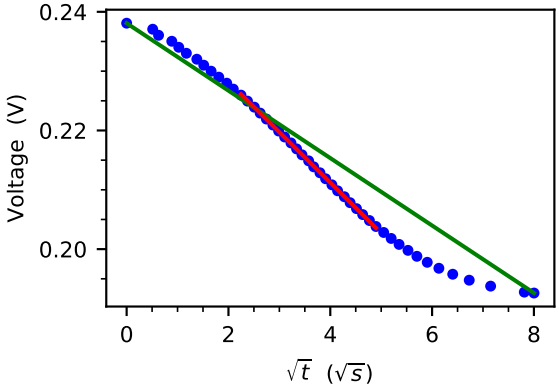

(d) 80 nm, discharge, τ = 64 s

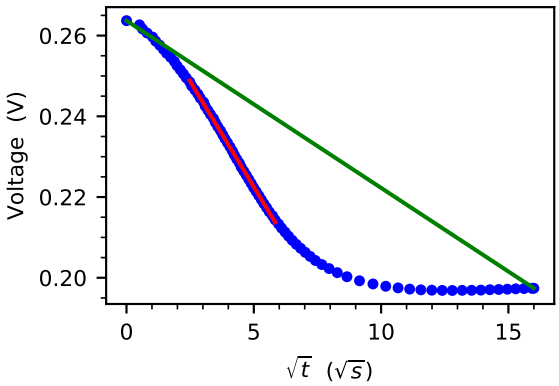

(e) 80 nm, discharge, τ = 256 s

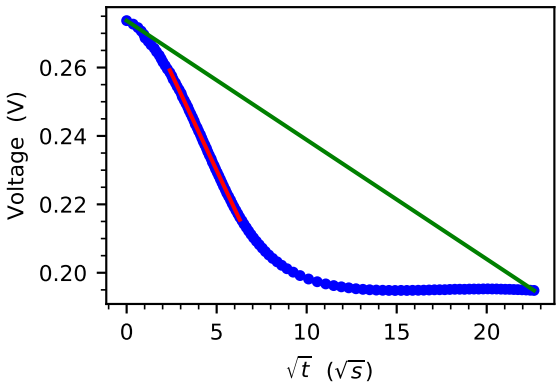

(f) 80 nm, discharge, τ = 512 s

Figure G.3: Linear fit of the linear area on the E versus square root of t curve for four different pulse lengths, C/5. The blue dots are the experimental data points and the red line is the linear fit.

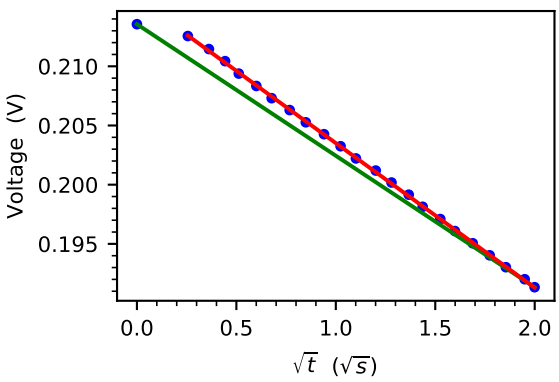

(a) 80 nm, discharge, τ = 4 s

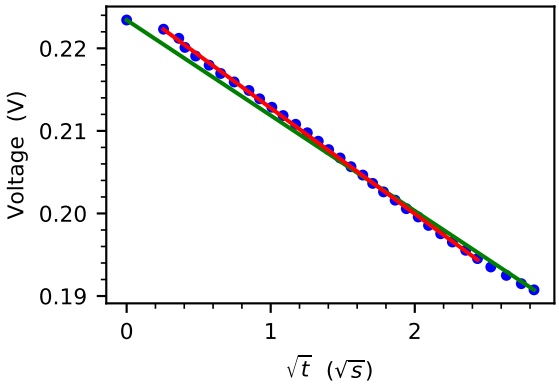

(b) 80 nm, discharge, τ = 8 s

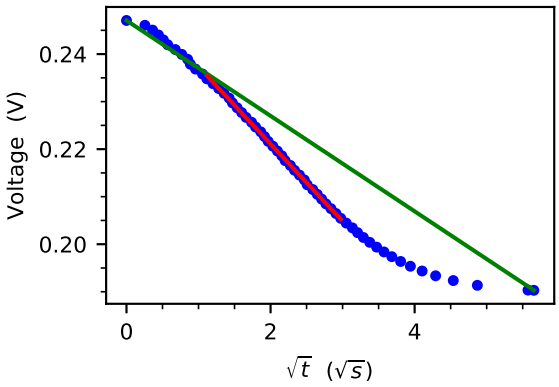

(c) 80 nm, discharge, τ = 32 s

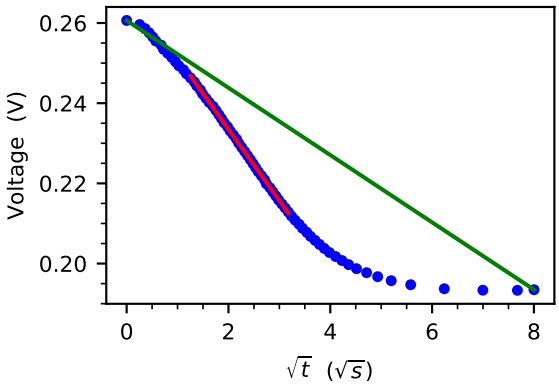

(d) 80 nm, discharge, τ = 64 s

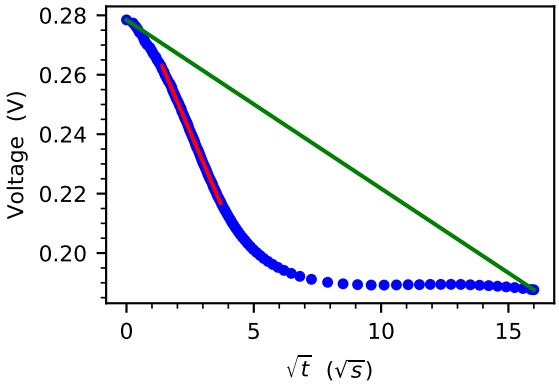

(e) 80 nm, discharge, τ = 256 s

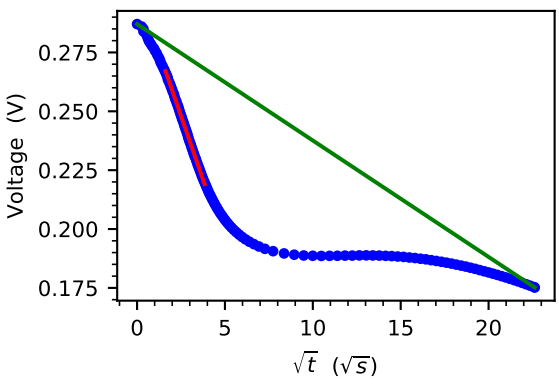

(f) 80 nm, discharge, τ = 512 s

Figure G.4: Linear fit of the linear area on the E versus square root of t curve for four different pulse lengths, C/2. The blue dots are the experimental data points and the red line is the linear fit.

Appendix H

GITT Using $\frac{dE}{d\sqrt{t}}$ vs GITT Using $\frac{\Delta E}{\Delta\sqrt{t}}$

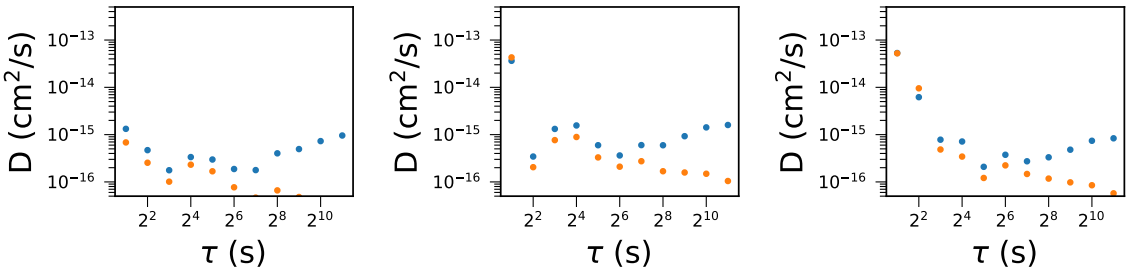

(a) 60 nm, C/10, 0.25 SOC *(b) 60 nm, C/10, 0.5 SOC* *(c) 60 nm, C/10, 0.75 SOC*

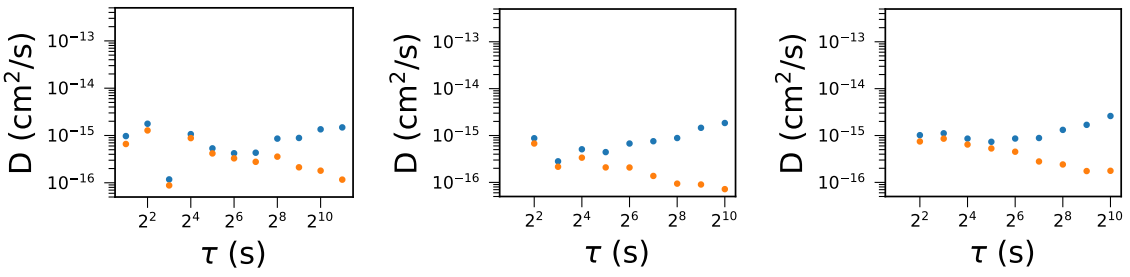

(d) 60 nm, C/5, 0.25 SOC *(e) 60 nm, C/5, 0.5 SOC* *(f) 60 nm, C/5, 0.75 SOC*

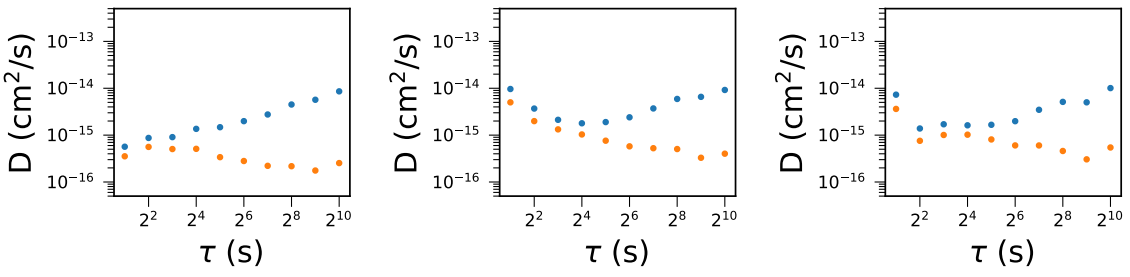

(g) 60 nm, C/2, 0.25 SOC *(h) 60 nm, C/2, 0.5 SOC* *(i) 60 nm, C/2, 0.75 SOC*

Figure H.1: Diffusion coefficients calculated using the normal GITT equation (eq. (2.25)), shown as blue dots, together with the diffusion coefficients calculated using eq. (2.22), shown as orange dots.

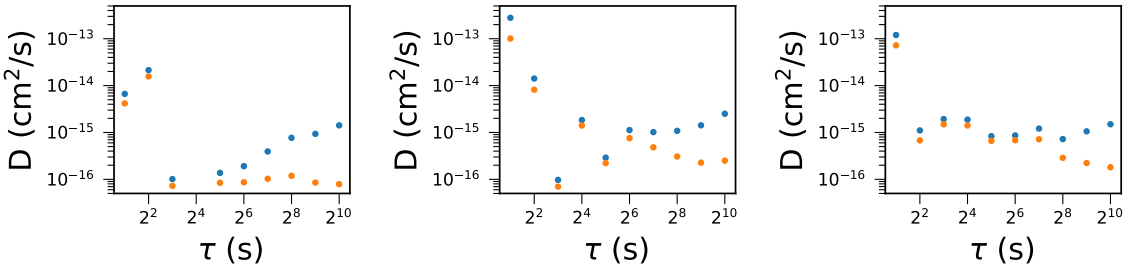

(a) 80 nm, C/10, 0.25 SOC *(b) 80 nm, C/10, 0.5 SOC* *(c) 80 nm, C/10, 0.75 SOC*

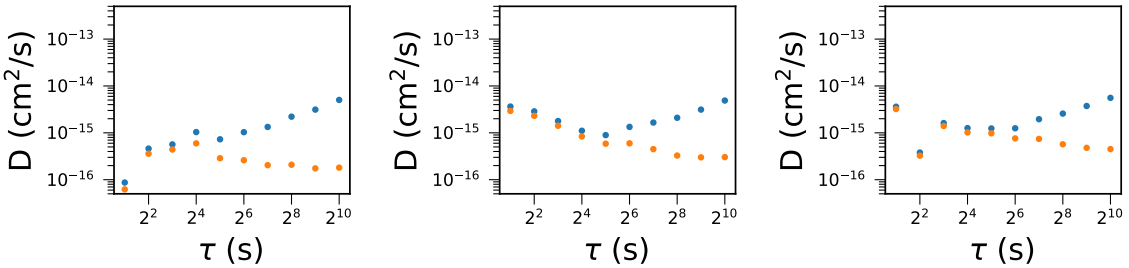

(d) 80 nm, C/5, 0.25 SOC *(e) 80 nm, C/5, 0.5 SOC* *(f) 80 nm, C/5, 0.75 SOC*

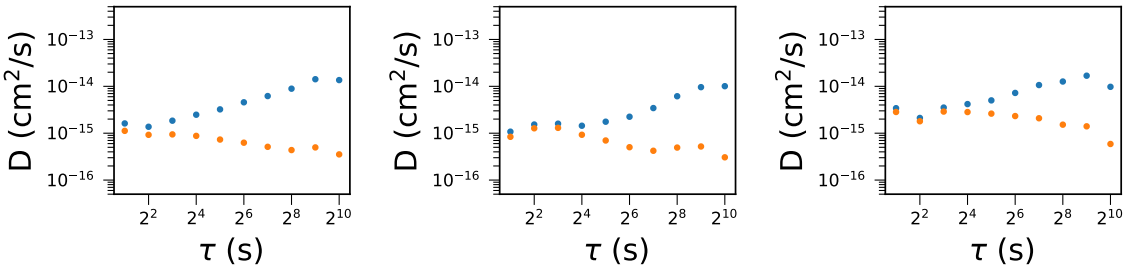

(g) 80 nm, C/2, 0.25 SOC *(h) 80 nm, C/2, 0.5 SOC* *(i) 80 nm, C/2, 0.75 SOC*

Figure H.2: Diffusion coefficients calculated using the normal GITT equation (eq. (2.25)), shown as blue dots, together with the diffusion coefficients calculated using eq. (2.22), shown as orange dots.

Appendix I

GITT Using $\frac{dE}{d\delta}$ vs GITT Using $\frac{\Delta E}{\Delta\delta}$

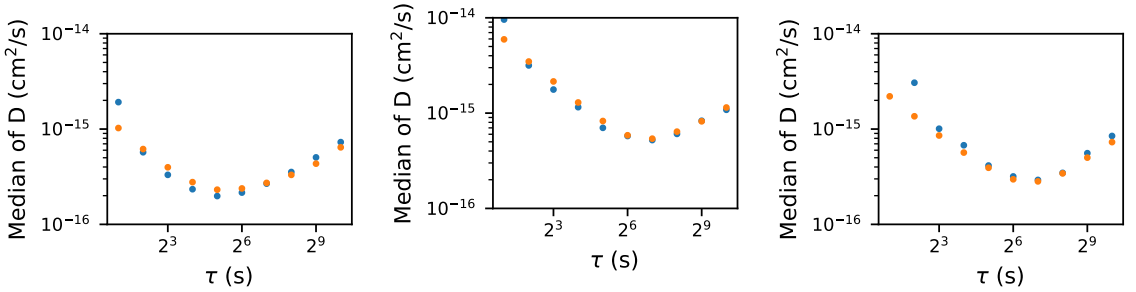

(a) 60 nm, C/10, 0.2 - 0.3 SOC

(b) 60 nm, C/10, 0.45 - 0.55 SOC

(c) 60 nm, C/10, 0.7 - 0.8 SOC

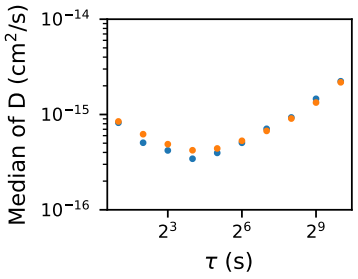

(d) 60 nm, C/5, 0.2 - 0.3 SOC

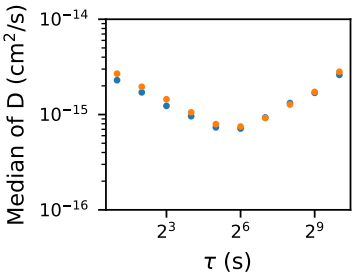

(e) 60 nm, C/5, 0.45 - 0.55 SOC

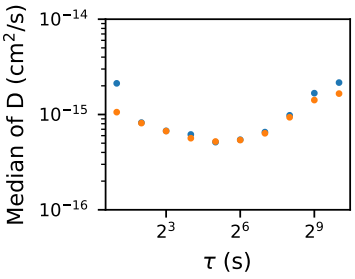

(f) 60 nm, C/5, 0.7 - 0.8 SOC

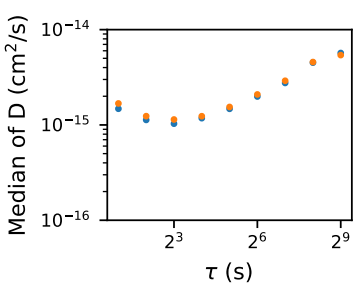

(g) 60 nm, C/2, 0.2 - 0.3 SOC

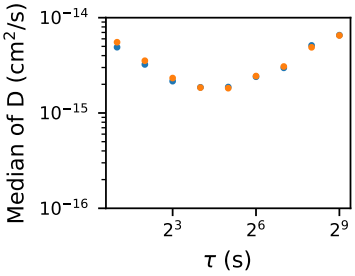

(h) 60 nm, C/2, 0.45 - 0.55 SOC

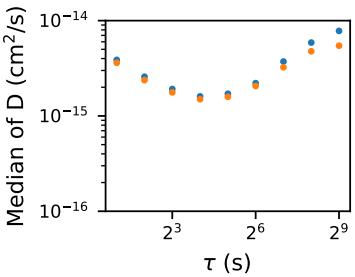

(i) 60 nm, C/2, 0.7 - 0.8 SOC

Figure I.1: Diffusion coefficients calculated from the normal GITT equation (eq. (2.25), as blue dots, together with the diffusion coefficients calculated from the curve fit version (eq. (2.23)), as orange dots. 60 nm thin films.

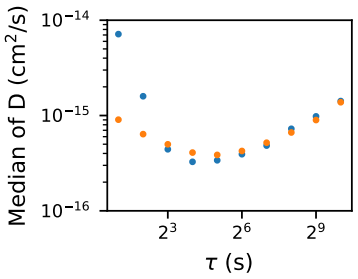

(a) 80 nm, C/10, 0.2 - 0.3 SOC

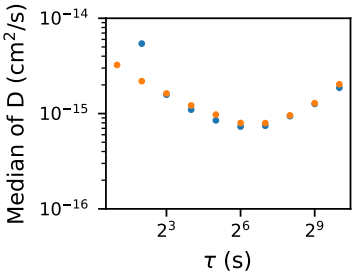

(b) 80 nm, C/10, 0.45 - 0.55 SOC

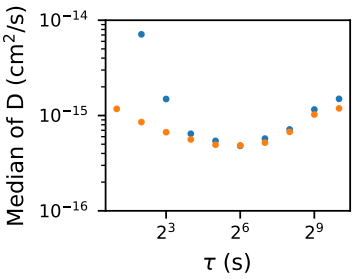

(c) 80 nm, C/10, 0.7 - 0.8 SOC

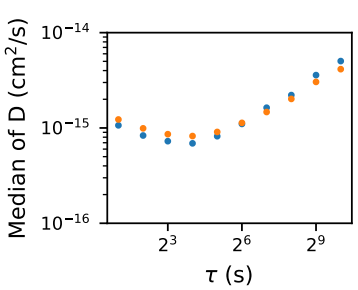

(d) 80 nm, C/5, 0.2 - 0.3 SOC

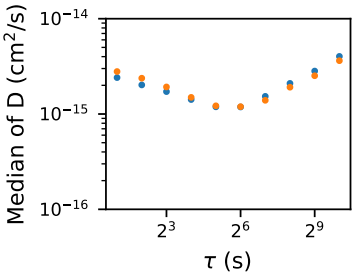

(e) 80 nm, C/5, 0.45 - 0.55 SOC

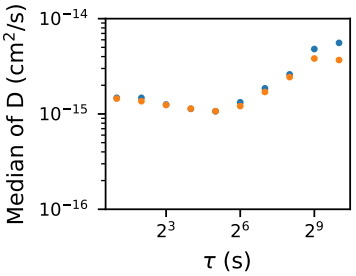

(f) 80 nm, C/5, 0.7 - 0.8 SOC

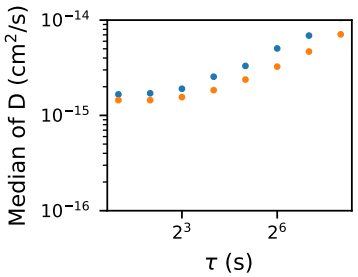

(g) 80 nm, C/2, 0.2 - 0.3 SOC

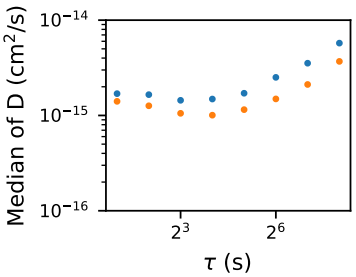

(h) 80 nm, C/2, 0.45 - 0.55 SOC

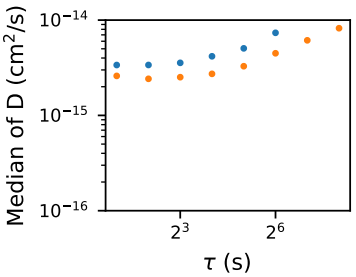

(i) 80 nm, C/2, 0.7 - 0.8 SOC

Figure I.2: Diffusion coefficients calculated from the normal GITT equation (eq. (2.25), as blue dots, together with the diffusion coefficients calculated from the curve fit version (eq. (2.23)), as orange dots. 80 nm thin films.

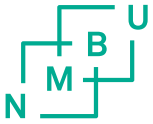

Norges miljø- og biovitenskapelige universitet
Noregs miljø- og biovitskapelege universitet
Norwegian University of Life Sciences

Postboks 5003
NO-1432 Ås
Norway